A SCALING METHODOLOGY FOR DYNAMIC SYSTEMS: QUANTIFICATION OF APPROXIMATE SIMILITUDE AND USE IN MULTIOBJECTIVE DESIGN

by

Burit Kittirungsi

A dissertation submitted in partial fulfillment
of the requirements for the degree of
Doctor of Philosophy
(Mechanical Engineering)
in The University of Michigan
2008

Doctoral Committee:

Professor Jeffrey L. Stein, Co-Chair
Assistant Research Scientist Hosam K. Fathy, Co-Chair
Professor Anna G. Stefanopoulou
Professor Erdogan Gulari
Research Associate Professor Zoran S. Filipi

To My Beloved Family

ACKNOWLEDGEMENTS

First and foremost, I would like to thank Prof. Jeffrey Stein and express my sincere gratitude for his and invaluable guidance, encouragement, patience that he has kindly given me throughout my study here in Ann Arbor.

I am very deeply indebted to Dr. Hosam Fathy for his mentorship that plays an essential role in leading me academically to be the person that I am today. I will perpetually be thankful for his willingness to help as well as all the time that he had spent teaching, guiding, challenging and encouraging me to become a better researcher.

I am also appreciative of Prof. Anna Stefanopoulou's insightful advice which has also been instrumental in the fuel cell air supply system study. I would also like express my gratitude to other committee members, Prof. Filipi and Prof. Gulari, for their helpful input and comments.

At the University of Michigan, I feel very fortunate to have the opportunity to work alongside many talented individuals. Most importantly, I am thankful for Tulga Ersal's help and efforts in developing the vehicle model in the last case study. Without his help, I would probably have taken forever to complete the study. I am also grateful to my first mentor, Dr. Loucas Louca, for his guidance and kind patience in the early days of my graduate study. Several thanks are also due to many other students whom I have collaborated with over the years especially Jay Tawee Pukrushpan, Geoff Rideout, Rob Hoffman, Dongsoo Kang, Kangwon Lee, and Gayathri Seenumani.

My deepest gratitude goes to my parents, Boonchai and Sivalee, in bringing me up to be a decent person in this world. I am forever thankful for their constant support and hard work since the day that I was born. I want to also extend my appreciation to my wonderful sister, Busaya, who has been a great help to the family while I have been away. Lastly, I feel very fortunate and thankful to have met Sirimon whose understanding, companionship, and encouragement has been tremendous in providing me with a great support throughout my graduate career.

TABLE OF CONTENTS

LIST OF FIGURES

Figure

LIST OF TABLES

Table

LIST OF APPENDICES

Appendix

LIST OF SYMBOLS

English Symbol

$A_{t,i}$	Nozzle's cross-sectional area
A_i	Activity value
AI_i	Activity Index
B	Damping variable category
B_s	Suspension damping coefficient
B_t	Tire damping coefficient
C_a	Lateral stiffness, Lateral stiffness variable category
C_D	Discharge coefficient
C_p	Specific heat capacity at constant pressure
C_v	Specific heat capacity at constant volume
D	Blower impellor diameter, Blower size
e	Effort of an energetic element
E	Energy
f	Flow of an energetic element
F	Input force
F	Objective function
F_d	Design objective

F_s	Similitude objective
g_i	Optimization constraint
H_i	Enthalpy
I	Inertia variable category
K	Stiffness variable category
K_s	Suspension stiffness
K_t	Tire stiffness
k_i	Index indicating the number of associated variables
L	Unit of length
L_b	Design variable lower bounds
M	Unit of mass, Mass variable category
M_{added}	Added roof-top mass
M_s	Sprung mass
M_{us}	Unsprung mass
m	Mass
$\dot{m}_{required}$	Desired mass flow rate at steady state
$\dot{m}_{steady}$	Mass flow rate at steady state
N	Blower map's rotational speed
N_a	Number of assumptions
N_s	Number of scaling laws
N_v	Number of variables
p	Pressure
P	Power

Δp	Blower map's Pressure rise
Q	Blower map's volume flow rate
R	Gas constant
R_a	Gas constant of air
S	Scaling factor
T	Unit of time
T_a	Duration over which an element's activity is calculated
T_j	Temperature
t	Time, Time variable category
U_b	Design variable upper bounds
V	Voltage, Volume
v	Linear velocity variable category
W	Preference weight on design objective
X_{CG}	Vehicle CG height
ΔX_{CG}	Change in CG height due to added mass
X_{roof}	Vehicle roof height with respect to nominal CG
x	Design variables, Displacement variable category
x_1	Vertical displacement of the sprung mass
x_{1ss}	Steady state value of x_1
x_2	Vertical displacement of the unsprung mass

Greek Symbol

$\eta_{BW,Opr}$	Blower operational efficiency
λ_i	Ratio of a quantity's scaled value over its original value
γ	Ratio of specific heats
ρ	Fluid density
ρ_{BW}	Density factor of blower size
τ_s	Response time
ω	Angular velocity variable category
π_i	Dimensionless parameter
θ	Angle variable category

Subscript

atm	Atmosphere
BW	Blower
F	Front
LA	Lower arm
nom	Nominal value
R	Rear
rm	Return manifold
sm	Supply manifold
susp	Suspension
UA	Upper arm

ABSTRACT

A SCALING METHODOLOGY FOR DYNAMIC SYSTEMS: QUANTIFICATION OF APPROXIMATE SIMILITUDE AND USE IN MULTIOBJECTIVE DESIGN

by

Burit Kittirungsi

Co-Chairs: Jeffrey L. Stein and Hosam K. Fathy

A design technique that adapts or scales a system design to meet new requirements is developed. This scaling technique is potentially useful because it focuses on retaining existing desirable characteristics (e.g., efficiency, stability) of the original design through minimal modifications. Previous work in the literature explored this notion by developing scaling techniques based on the *dynamic similitude* principle. However, such similitude-based scaling is often found too restrictive because it may not be feasible to satisfy all of the scaling laws designated by the similitude principle exactly. Moreover, the literature only defines such similitude discretely in terms of whether the scaled design satisfies these scaling laws. This definition then makes it impossible to assess the degree to which two designs are close to satisfy similitude. The work in this dissertation mitigates these difficulties as follows:

First, it uses a novel combination of activity-based model reduction and dimensional analysis to assess the relative importance of each scaling law and permit

neglecting the least important ones, thereby providing more freedom than strict similitude-based scaling. Next, a metric is developed to cope with the situation in which the most important scaling law(s) cannot be followed due to other conflicting requirements and constraints. This metric allows one to quantify *approximate similitude*, that is, the degree to which the scaled design is close to satisfying the discrete definition of exact similitude. Then, this quantification is utilized in a multiobjective scaling framework that trades off approximate similitude versus the conflicting requirements and constraints.

The applicability of the methodology is demonstrated through three case studies. The first study applies the methodology to a linear quarter-car system to scale the chassis vibrations. The second study scales a fuel cell's nonlinear air supply system subject to different power requirements. The last case study represents a scaling design study of a complex multi-body dynamic vehicle design to maintain rollover safety properties when subject to extra roof-top loads. These examples demonstrate that the proposed method does provide a systematic, computationally efficient approach to redesign as compared with casting the redesign as an optimization problem.

CHAPTER I

INTRODUCTION

1.1 MOTIVATION

Modeling and simulation techniques have widely become instrumental in the design and development stage of many advanced technology programs. They play an essential part in allowing a great variety of design concepts to be generated and tested without having to rely on physical prototypes. Therefore, they help companies maintain their competitiveness by expediting the design and redesign processes of their engineered products to efficiently keep up with the frequently changing, and stringent needs in the market [1].

In the initial design process, engineers often make use of modeling and simulation techniques along with their hands-on experience to evolve their product into its optimum, subject to possibly many specifications. Some of these specifications inevitably have to be later modified according to such stringent market needs. While these modifications render the optimal original design no longer optimal for the new application, some desirable properties of the original design may still have to be sustained and then migrated to the new design. For instance, a vehicle powertrain engineer might wish to redesign an existing automatic transmission optimized for one engine to use in conjunction with a more powerful engine [2], while still maintaining the original design's

desirable characteristics (e.g., gear-shift response time). As another example, a vehicle designer may wish to scale a fuel cell optimally designed for one vehicle to propel a more or less power-demanding vehicle, while retaining its operational efficiency and dynamic responses [3]. These cases demonstrate the fact that engineers often seek new product designs which require *scaling* the magnitudes of existing proven designs' outputs (e.g., torque, power, displacement, etc.) while also *maintaining* their salient design properties (e.g., efficiency, stability). It is this context that the word "scaling" will be used in this dissertation.

As contemporary engineering systems are generally multidisciplinary, redesigning such systems typically requires the solution of a large-scale complex problem involving multiple domains with complex couplings among them [4]. Therefore, it is advantageous to have an efficient design scaling technique which can provide a shortcut by carefully evolving existing design solutions instead of seeking completely new ones. Such a scaling paradigm can be quite attractive because it would allow the engineers to optimize a scalable system design once, then resize it for different application needs [5, 6] . This also implies that one can take a design that has been tuned to perform well, through trial-and-error, and scale it to perform as well under new circumstances, without having to repeatedly go through the complex and expensive trial-and-error process.

Scaling differs from traditional engineering system design optimization in its strong emphasis on minimal modifications. In scaling an internal combustion engine to meet higher power demands, for instance, one typically seeks to change only a few engine parameters (e.g., number of cylinders or displacement per cylinder) to meet the new power demands while retaining the remaining desirable engine characteristics. This

can only be possible if such desirable characteristics are invariant with respect to the parameter or combination of parameters used for scaling. From a conceptual standpoint, therefore, scaling is essentially a search for invariance, and every scaling algorithm should be based on *a principle of invariance* (a.k.a., a *similarity principle*).

Many different similarity principles exist in the literature, each of which can be interpreted as a metric quantifying whether or not two systems are similar. First, *geometric similarity* [7, 8] defines the conditions under which two objects are similar in shape. Further, *kinematic and dynamic similarities* [7-9] define the conditions under which the two objects undergo similar motions, and experience similar forces during those motions, respectively. In particular, these similarity conditions designate the values at which the properties (e.g., length, density, pressure, etc.) associated with one object has to be with respect to the other object. This notion of *dynamic similarity* or *dynamic similitude* (these two terms will be used interchangeably in this dissertation) is applicable to any energetic system in any domain (e.g., mechanical, thermofluidic, electromagnetic, etc.) because the notions of force and motion are equivalent to those of the power variables (i.e., effort and flow) in system dynamics [10]. In spite of the long history of these similarity principles, they still remain very useful especially when the basic laws of governing systems are known, but their solutions are difficult to obtain [11].

Due to the wide applicability mentioned above, several scaling approaches appear in the literature have utilized these similitude principles, especially dynamic similitude (e.g., [8, 9, 12-14]). Nevertheless, such similitude-based scaling approaches still have the following shortcomings. First, similitude-based scaling often turns out to be too restrictive because it may be infeasible to follow all of the conditions designated by a

given similitude principle exactly (e.g., [9, 14-17]). This infeasibility can be, for instance, due to some physical constraints present in the scaling problem (e.g., material constraints in structural testing). Second of all, dynamic similitude is a discrete principle of invariance, that is, two system designs either satisfy the conditions of similitude or not at all (this will be explained in more detail in Chapters 2 and 4). As a result, whenever similitude is not feasible, one cannot assess the degree to which the two designs are "close" to satisfying the discrete definition of exact dynamic similitude. Toward this end, the work in this dissertation is intended to provide a methodology which can help mitigate the effects of these shortcomings.

1.2 RESEARCH OBJECTIVE

The objective of this research is to develop a method to scale the outputs of an existing proven system to meet new desired specifications, while retaining its desirable properties. Whenever it is feasible, the developed technique should ensure dynamic similitude between the original and scaled designs, thereby propagating the desirable dynamic properties from the original design to the scaled one. For this methodology to be efficient, it should also provide a technique to assess the relative importance of different similitude conditions. This should allow engineers to neglect the least important conditions, thereby gaining more flexibility in scaling.

It is further proposed that, when the similitude conditions deemed important cannot be followed exactly due to other conflicting requirements, the developed technique should be equipped with a metric to quantify the degree of deviation from similitude on a continuous basis. This then makes it possible to assess the degree to

which two systems are “close” in the sense of dynamic similarity. Finally, the technique should enable multiobjective system scaling, where this degree of dynamic similitude can be traded off against competing scaling requirements which allows one to explore and benchmark the performance of possible scaled designs.

1.3 THESIS SUMMARY

Chapter 1 presents the motivation as well as objectives of this thesis. Then, previous work by other researchers along with its advantages and limitations are given and discussed in Chapter 2.

Chapter 3 presents a novel combination of dimensional analysis and the activity-based model reduction technique. Dimensional analysis permits the derivation of a set of conditions which, if strictly followed in scaling, assures dynamic similarity between any two systems. Activity is an energy-based metric which was originally developed for the purpose of model reduction. It is however employed in this research to find the relative importance of each scaling condition derived from dimensional analysis; thereby helping the system designers select to follow only the important ones. The viability of this innovative combination is highlighted by two examples. The first example represents the scaling of a simple two-degree-of-freedom mass-spring-damper system and the second example considers the scaling of a fuel cell stack’s air supply system design for a new set of fuel cell system power requirements.

Chapter 4 then extends the findings in Chapter 3 by considering the situation in which the most important scaling condition(s) cannot be followed or, in other words, dynamic similitude is not entirely feasible to achieve. This brings forward the discussion

of approximate similitude and the development of a metric which quantifies the degree of approximate similitude. As a result, this metric permits the construction of a design scaling tool whose solutions represent design trade-offs reconciling design requirement satisfaction and dynamic similitude achievement. The viability of this tool is shown through the same two systems introduced in Chapter 3.

Chapter 5 shows the applicability of the scaling methodology developed in this research to a complex multi-body dynamic vehicle system. Finally, the thesis concludes with Chapter 6 summarizing the research, discusses the major contributions as well as limitations. Some directions for future research pertaining to this area are also given in this final chapter.

CHAPTER II

BACKGROUND

As previously described in Chapter 1, a motivation of this research stemmed from the need to redesign or scale the output(s) of existing designs (e.g., fuel cell air supply system) to accommodate new requirements (e.g., power output) while maintaining its desirable properties (e.g., efficiency). This chapter reviews relevant scaling techniques that have been developed previously and concurrently by other researchers. These scaling techniques from the literature can be broadly classified into two groups: application-specific and generalized scaling techniques.

2.1 APPLICATION-SPECIFIC SCALING TECHNIQUES

This first family of scaling techniques described below relies upon the use of some specialized tools or theories existing within their problem domains. These techniques, therefore, by their nature cannot be readily extended to other domains. Some of these existing techniques which are closely related to the application areas of this dissertation are summarized as follows:

Cuddy and Wipke [18] investigated an engine scaling problem in a vehicle performance simulator. A linear scaling strategy with respect to the engine's maximum

torque curve and operating speed range was used to determine proper engine sizing based on existing baseline models. They observed that this type of scaling is, however, valid only within relatively small departures from the baseline models. Delagrammatikas [19, 20] then described that a number of limitations that exist when engine maps are scaled by such a linear method. To alleviate these limitations, he coupled a high-fidelity engine simulation tool (which is capable of producing engine maps on the fly) with the vehicle simulator. However, this approach has a drawback in that it depends upon the use of such specialized simulation tools and using such high-fidelity tools to produce engine maps usually incurs a high computational cost.

Wei and Rizzoni [6, 21] proposed a scaling approach for ICE engines using the *Willians line* approximation method [22] which is used to determine the scaling of swept volume and piston stroke of the engines when more/less power is required. This approach is validated through an example which shows that it gives a good estimation when compared with the actual data. This powerful concept unfortunately turns out to be restricted to only ICE engines. An extension of this approach to another energy-converter system (e.g., battery, fuel cell) requires validations through experimentation [6]. Further, the technique does not indicate how other physical parameters (e.g., bore diameter, connecting-rod length) should be scaled (or kept the same).

Aside from the engine scaling techniques above, attempts to develop efficient scaling approaches have appeared in other applications as well. Cho and Rajamani [5] for example, derived a physics-based dynamic model of an elevator's vertical motion and used it for scaling. In order to utilize this model in predicting the high-rise elevator systems, they started by constructing a low-rise elevator model which is more conducive

to validation. Then, this model was scaled based on the scaling laws of rope and damping stiffness to predict the responses of the high-rise system. The scaling laws in this case were, however, derived from the specific understanding in rope physics which are not readily applicable to other physical systems.

Power sizing of the fuel cell and battery in a hybrid-vehicle configuration was studied by Boettner *et al.* [23]. Power management strategies were developed in these studies to determine optimal load sharing among the battery and fuel cell units. The sizing of fuel cell power was, however, achieved only by increasing/decreasing the number of cells and the work focuses only on steady-state operation. More recently, Han *et al.* [24] also utilized an optimization technique to find optimal sizing and achieve maximum power output of a quasi-steady state fuel cell model whose scaled design variables are the number of the stack's cells and compressor size. Again, these studies do not determine how other parameters in the system should be scaled; neither does it address how the fuel cell power changes during the transient operation. In analogous research, Ohl *et al.* [25] considered a fuel cell's reformer scaling problem by developing a model of sufficient detail to be useful in identifying the design parameters that dominate the dynamic behavior. This specific model allows one to select or scale appropriate design parameters in order to minimize the response time and satisfy the specified output hydrogen flow rate.

2.2 GENERALIZED SCALING TECHNIQUES

The techniques in this category are developed using the invariance principles (previously explained in Chapter 1) which are widely applicable to different system

domains. As a result, in contrast to those in the previous section, these techniques are not application-dependant and, therefore, have been used across many different application areas. Specifically, the notion of dynamic invariance or dynamic similitude has gained tremendous popularity as a definition of similarity in engineering, where it is often formally expressed in terms of "The Method of Dimensions", more commonly known as "Buckingham's Pi Theorem" [9, 12].

2.2.1 BUCKINGHAM'S PI THEOREM AND ITS USE IN SYSTEM SCALING

The notion of similitude first entered into the field of engineering mechanics probably by Euler and then it is extended into the field of heat transfer in the early 1800s by Fourier [11]. It is not until fifty years afterwards that a generalized framework of the study of similitude was developed by Lord Rayleigh and named as "The Method of Dimensions" [8, 11]. Shortly after that, Carvallo and Vaschy independently formulated the method of dimensions as a formal mathematical theorem [11]. The theorem was believed to be forgotten until Buckingham wrote a series of papers on the subject starting in 1914 which made this theorem significantly more well-known to the scientific community [11]. This explains why the theorem is nowadays recognized as "Buckingham's Pi Theorem".

Buckingham's Pi Theorem[1] states that for every system completely described by N variables and parameters in M fundamental dimensions, there exist N-M independent dimensionless "Pi" parameters that must be kept invariant during scaling in order to maintain dynamic similitude [9, 12]. In other words, Buckingham's Pi Theorem provides a systematic method for determining the minimum set of dimensionless Pi parameters

[1] See Appendix A for a formal statement of Buckingham's Pi Theorem

which characterize the dynamics of a system. The selection of these Pi parameters is not unique, but keeping them constant guarantees that all other dimensionless combinations of the original *N* system variables and parameters will also remain constant. This type of analysis is oftentimes referred to as *Dimensional Analysis*. This definition of dynamic invariance is interesting not only from a physical perspective, but also from a mathematical one. Specifically, it is well recognized that dynamic invariance is a special case of group invariance. In particular, one can deem two systems of equations similar if their solution manifolds are related through a group transformation applied to their input parameters. This powerful observation has spawned several generalizations on Buckingham's Pi Theorem based on mathematical group theory [26, 27].

In the context of system scaling, Buckingham's Pi Theorem permits the derivation of *design scaling laws*, i.e., mathematical relationships that relate design variables of the original and scaled systems. These scaling laws, then, designate a set of conditions which, if followed exactly, assure complete similarity between the two systems. For this reason, similitude-based scaling has long been utilized in testing of engineering scaled physical prototypes. These prototypes usually consist of pieces of hardware scaled after certain physical systems to preserve and represent their original phenomena. This allows engineers to test one component, at one particular size, and then generalize the results to a broad range of sizes without a need for re-experimentation. Initial work in this regard dates back to the 1880's. As summarized in [13], A.L. Cauchy, a French mathematician, investigated small scale prototype models of vibrating rods and plates in 1829. Next, W. Froude made the first water-basin model for designing watercraft in 1869. Then, O. Reynolds published his classic model experiments on fluid motion in pipes in 1883. And

not many years after that, the famous Wright brothers built a wind tunnel to test wing models.

More recent work using similitude-based scaling is also ubiquitous in the literature, some of which are summarized as follows: Wu *et al.* [28] utilize a 1/10 scaled laboratory model to predict the three-dimensional structural vibrations of a full-size gantry crane. Wu [29] presented scaling laws for vibration characteristics of a plate-typed structure subjected to moving loads. Vassalos [14] studied the modeling and similitude of marine structures. Goldfarb [30] defined a set of necessary and sufficient conditions to preserve dynamic similarity in a bilateral manipulation problem. Poiley and Alleyne [31] demonstrated that certain non-linear tire characteristics can be expressed in a non-dimensional framework and shown to be dynamically similar to full-sized tires.

It is also interesting to note an implication of the dynamic invariance principle in linear systems theory. That is, it has been shown that dynamic similitude guarantees that the pole and zero locations of the original and scaled systems are identical [32, 33]. As a result, this implies that any control scheme that is compatible with the original model also remain so with the scaled model. For this reason, dimensional analysis can also be employed to help design a controller that remains valid among systems that are dynamically similar. For example, Ghanekar *et al.* [32, 34-36] designed controllers for a robotic manipulator system based on its dimensionless groups. Brennan and Alleyne [37] developed a framework based on dimensional analysis that allows parameter-based comparisons between different vehicles. Then, a state-feedback controller was designed based on this information to robustly stabilize all vehicles encompassed by the normal

distribution of vehicle parameters. This framework also allows them to utilize a scale vehicle testbed to emulate full-sized vehicles on a highway [37].

2.2.2 LIMITATIONS OF INVRIANCE PRINCIPLES AND NEED FOR APPOXIMATE SIMILITUDE

In spite of its popularity and various important strengths, the notion of dynamic invariance suffers from one key limitation. Specifically, dynamic similitude is a *discrete* principle of invariance, in the sense that either the set of scaling laws derived from Buckingham's Pi Theorem is exactly satisfied or not at all. Consider, for example, two simple linear and time-invariant mass-spring-damper systems (as will be shown in Chapter 3). In this case, dynamic similitude deems these two systems similar if and only if the scaling laws are completely satisfied. That is, the ratios of their masses and dampers have to equal the ratio of their stiffnesses exactly. Any failure to comply with any of the scaling laws, regardless of which scaling law and no matter how minor the failure is, violates the discrete definition of dynamic similitude. In practice, such discrete definition of dynamic similitude can clearly be quite restrictive: a fact recognized in both the biological and engineering sciences.

In the life sciences, species are known to retain significant similarities to their ancestry during the course of evolution, but these similarities often disobey strict dynamic invariance. This creates a need for alternative definitions of similitude that capture the fact that two species can be *approximately* similar, despite differing in potentially important ways. *Allometry* is a biological principle of invariance that deems two species similar if their characteristics are related through any monomial scaling law (see Appendix A for a definition of monomial functions), even if this scaling law does

not comply with Buckingham's Pi Theorem. In addition, many mathematical models and laws have been proposed to explain the intriguing emergences of the biological quantities that remain invariant for all living organisms (e.g., the number of heart-beats, total energy to support an organism per unit mass) [38, 39]. Similarly, *morphometry* is a biological principle of invariance that examines the similarities in shape between different animal species (especially in skull structure) while allowing for important and significant localized differences [40]. Both allometry and morphometry are quite useful for understanding the evolution of species [38-41], but are limited in their applicability to engineering system scaling.

The discrete nature and resulting limitations of dynamic similitude as a principle of invariance are well recognized not just in the biological literature, but in several engineering literatures as well. It is widely recognized in experimental fluid mechanics, for example, that building a scaled prototype of a marine vessel (where the inertial and viscous fluid forces are deemed dominant) such that both Reynold's and Froude's dimensionless numbers remain invariant may be difficult [9, 12, 13]. Instead, experimental fluid mechanicists often judiciously choose to keep only one of these two dimensionless parameters constant and allow the other to vary based on the relative dominance of skin friction versus body drag. Similarly, it is well-known that exact similitude analysis of fluid flow problems (e.g. flow through pipes) is physically impossible because of the complex paths followed by the fluid [9]. Further, researchers in the thin shell vibrations literature have long recognized that scaling the thicknesses of thin shells in accordance with exact similitude may be physically impossible, and that a notion of *approximate similitude* may be necessary instead [17]. In the structural testing

discipline, researchers [15, 16] have also recognized that, due to material constraints preventing absolute similitude, the experimental results obtained from scaled prototypes often do not perfectly translate to those of the actual-sized counterparts. This then necessitates the use of correction factors as part of scaling the experimental results and applying them to the full structures [9]. Finally, the difficulty inherent in scaling intensive properties (those that do not depend on system size, e.g., density, color, etc.) in accordance with exact dynamic similitude is also evident from the bilateral manipulator design problem [30]. To sum up, the engineering literature has long recognized that scaling a dynamic system *exactly* may be difficult or impossible to achieve, and there is, therefore, a strong need from *approximate* scaling.

In an attempt to address the above need for approximate scaling, Rezaeepazhand and Simtses [42] proposed to use sensitivity analysis for evaluating the relative importance of the design scaling laws of shell vibration models. Such relative importance becomes useful in allowing engineers to neglect the least important scaling laws and, therefore, helping to make the discrete definition of dynamic similitude less restrictive. However, this technique has a drawback in the computational cost incurred as a result of using sensitivity analysis. Such a cost becomes more severely expensive especially when more variables have to enter into the analysis. In addition, sensitivity analysis sometimes entails evaluating function derivatives which can become problematic if the function of interest does not lend it itself to differentiability.

Despite the flexibility which can be gained from quantifying the relative importance of scaling laws, difficulties can still arise when the scaling law(s) deemed important cannot be followed exactly due to other, conflicting scaling requirements and

constraints. Such requirements may include, for instance, maximizing system efficiency, minimizing packaging needs, or minimizing cost, and may be as critical to achieve in the scaling problem at hand as similitude. As a result, dynamic similitude cannot be attained in scaling and, therefore, needs to be compromised. Under this scenario, the existing techniques in the literature do not yet present a formal way to determine the extent to which dynamic similitude can be achieved. More importantly, whenever dynamic similitude cannot be satisfied, it is not clear how and which parameters one should change to allow the scaled design to be closer to satisfying similitude.

Given the above assessment, the proposed research in this dissertation strives to verify the following hypotheses:

1) The relative importance of scaling laws can be captured by a more computationally efficient metric.
2) The degree to which two designs are close to satisfying similitude can be quantified or approximated. It is also important that this quantification take advantage of the relative importance found in 1).
3) Given the quantification in 2), the degree of similitude can then be traded off versus other conflicting design requirements and constraints.

2.3 CHAPTER SUMMARY

This chapter summarizes the existing design scaling methodologies appearing in the literature. One group of these methodologies is developed specifically based on the problems at hand and cannot be easily generalized to systems in other domains. On the other hand, there exists another group of scaling techniques which relies on the similitude

principle. These similitude-based techniques not only prove to be applicable to a wide variety of system domains, but also allow engineers to resize some or all of the system's parameters while maintaining its desirable properties. Nevertheless, these similitude-based scaling strategies are often found inefficient because of the discrete nature of the similitude principle, that is, the resulting scaling laws have to be either satisfied exactly or not at all.

CHAPTER III

EFFICIENT SCALING METHODOLOGY USING DIMENSIONAL AND ACTIVITY ANALYSES

As described in Chapter 2, previous work in the literature developed similitude-based design scaling techniques that make it possible to take a proven system design and scale it to meet new desired dynamic characteristics. However, such similitude-based scaling is often too restrictive because it may not be feasible to satisfy all of the resulting scaling laws exactly. The work in this chapter proposes, for the first time, to use a novel combination of an energy-based model reduction technique [43] and dimensional analysis to mitigate this restriction. This results in a computationally efficient method to assess the relative importance of scaling laws. As a result, this allows us to scale only the important components of a given dynamic system, thereby providing more freedom than pure similitude-based scaling.

The viability of this proposed method is highlighted in this chapter by two examples. The first example demonstrates the proposed efficient scaling technique on a two-degree-of-freedom mass spring damper system. The second example uses the developed methodology to scale a fuel cell stack's air supply system design for a new set of fuel cell power requirements and compares the resulting design with that obtained from traditional design optimization.

3.1 OVERVIEW OF THE USE OF BUCKINGHAM'S PI THEOREM TO DERIVE SYSTEM SCALING LAWS

This section gives an overview of Buckingham's Pi theorem (or dimensional analysis) focusing on its use in scaling a dynamical system to attain similarity as well as deriving the system's scaling laws as follows:

(i) Identify the governing physical laws of the system of interest: As explained in Chapter 1, the scaling techniques developed in this dissertation are considered as a re-design tool to evolve an existing design to satisfy new requirements. Therefore, the work herein assumes that the governing physical laws (or equations) of these existing system designs are previously derived and given. This assumption assures that scaling laws obtained from dimensional analysis are complete and sufficient for scaling [13].

(ii) Identify variables and parameters that appear in the governing equations and identify their fundamental units: A system of units is classified as a set of fundamental units when it is both necessary and sufficient for measuring the quantities (i.e., variables and parameters) of a certain phenomena. The determination of the number of fundamental units needed for any problem was also investigated in [44] based on mathematical group theory (its connections to Buckingham's Pi theorem are given in Appendix A). In Newtonian mechanics, for example, there are three fundamental units and the units of other physical quantities are called derived units. These three fundamental units are usually taken as mass, length, and time [8], although there also exist other possibilities (e.g., force/length/time).

(iii) Identify the dimensional formula associated with each variable (or parameter): Dimensional formula is the relation that shows the fundamental units for any quantity raised to appropriate powers and enclosed in square brackets. For instance, the dimensional formula of a force in a Newtonian mechanical system based on the mass/length/time fundamental unit system is $[MLT^{-2}]$.

(iv) Determine the number of dimensionless Pi parameters: Buckingham's Pi theorem determines the number of Pi parameters as follows (see Appendix A for a complete formal statement of the theorem):

"If there are M physical quantities defined in terms of N independent fundamental units, there are M – N independent dimensionless parameters."

Each of the resulting M – N dimensionless parameter is always a monomial function[2] of the original M variables [12] (a formal definition of a monomial function is also given in Appendix A).

(v) Derive Pi parameters: This is done by, first, selecting a *core* group of N variables which must contain, among them, all of the fundamental units of the system. Then, we form a set of $M - N$ product groups with each product group consisting of all of the core variables and one of those $M - N$ variables which were excluded from the core group. Next, we assume arbitrary exponents for each of the variables in each product group. By requiring each product group to be dimensionless, it is then possible to solve for these arbitrary exponents and, therefore, the Pi parameters.

[2] A monomial function is a special kind of polynomial which has only one term and each of the variables in this term is raised to a certain power. In addition, the power has to be a rational number. For instance, given several variables (e.g., x, y, and z) and rational numbers (e.g., a, b, and c), a monomial function based on these variables and numbers can be $f(x) = x^a y^b z^c$.

(vi) Derive scaling laws: Define $\lambda_Q = \frac{Q_{scaled}}{Q_{original}}$ as a scaling factor corresponding to any arbitrary system variable or parameter Q. Then, by similitude principle, dynamic characteristics of the original design is maintained by keeping the dimensionless Pi parameters of the original and scaled systems invariant [9, 29]. Using this principle as well as the definition of the scaling factor above results in the system's scaling laws.

The remaining of this section presents how the procedure described above can be applied to derive scaling laws of the following two-degree-of-freedom (2-DOF) mass-spring-damper system:

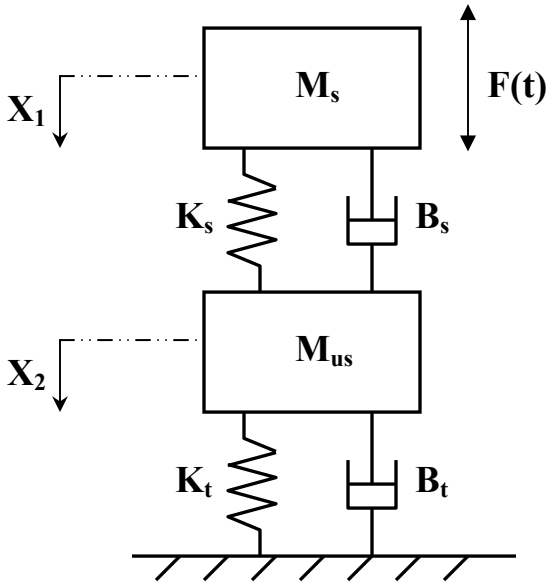

Figure 3.1: Quarter-car Model

This is the well-known quarter-car suspension model, where M_s and M_{us} are the sprung and unsprung masses, K_s and K_t are the suspension and tire stiffnesses, B_s and B_t are the suspension's shock absorber and the tire's damping coefficients, and x_1 and x_2 are the vertical displacements of the sprung and unsprung masses. The input of the system is

the vertical force, *F(t)*, applied to the sprung mass and the outputs of interest are displacements of the masses. The quarter-car model is widely used to study the ride quality of ground vehicles. Physically, the sprung mass (M_s) represents the mass of the body of a vehicle while the unsprung mass (M_{us}) includes the masses associated with the wheels and suspension components. The tire stiffness (K_t) is used to represent the visco-elastic nature of the tire and its inherent damping is represented by the tire damping coefficient (B_t). This setup allows us to investigate, for example, the effect of engine vibration forces when the vehicle is idling. The governing equations of motion in this case are as follows:

$$\begin{aligned} M_s\ddot{x}_1 + B_s(\dot{x}_1 - \dot{x}_2) + K_s(x_1 - x_2) &= F(t) \\ M_{us}\ddot{x}_2 + B_s(\dot{x}_2 - \dot{x}_1) + K_s(x_2 - x_1) + B_t\dot{x}_2 + K_t x_2 &= 0 \end{aligned} \tag{3.1}$$

For simplicity, it is assumed that both of the springs and dampers in this system have linear characteristics. Now, dimensional analysis starts by identifying the set of relevant variables which can be extracted from Equation 3.1 and shown below:

$\{M_s, M_{us}, K_s, B_s, K_t, B_t, F, x_1, x_2, t\}$, Number of relevant quantities = **10**

The next step is to find *dimensional formulae* of the listed variables based on the *fundamental units*. Given the set of quantities at hand, the dimensional formula for each quantity is:

$$\begin{aligned} &M_s, M_{us} = [M] \qquad K_s, K_t = [MT^{-2}] \quad B_s, B_t = [MT^{-1}] \\ &F = [MLT^{-2}] \qquad x_1, x_2 = [L] \qquad t = [T] \end{aligned} \tag{3.2}$$

It follows that the number of fundamental units being used in this problem = **3**. Next, by Buckingham's Pi theorem, we have the following result:

Number of dimensionless (π) groups = **10 – 3 = 7**

These Pi groups are derived and shown below. The details of the derivation these groups are omitted here but explained in detail in Appendix B. Note that these groups are not unique [28] but one potential selection is as follows:

$$\pi_1 = \frac{M_{us}}{M_s} \qquad \pi_2 = \frac{x_2}{x_1} \qquad \pi_3 = \frac{k_t}{k_s} \qquad \pi_4 = \frac{B_s}{M_s^{1/2} k_s^{1/2}}$$
$$\pi_5 = \frac{B_t}{M_s^{1/2} k_s^{1/2}} \qquad \pi_6 = \frac{F}{k_s x_1} \qquad \pi_7 = \frac{k_s^{1/2} t}{M_s^{1/2}} \tag{3.3}$$

Substituting the definition of a scale factor into Equation 3.3 and complying with the similitude principle yields the following scaling laws for the system's various scale factors as follows. It is important to note that even though the Pi groups given in Equation 3.3 are not unique, any other choices will result in the same set of scaling laws [28] as indicated in Equations 3.4 and 3.5 below:

$$\begin{aligned}
&\lambda_{M_s} = \lambda_{M_{us}} \\
&\lambda_{K_t} = \lambda_{K_s} \\
&\lambda_{M_s}^{1/2} \lambda_{K_s}^{1/2} = \lambda_{B_s} \\
&\lambda_{M_s}^{1/2} \lambda_{K_s}^{1/2} = \lambda_{B_t} \\
&\lambda_t \lambda_{K_s}^{1/2} = \lambda_{M_s}^{1/2}
\end{aligned} \tag{3.4}$$

$$\begin{aligned}
&\lambda_{x_1} \lambda_{K_s} = \lambda_F \\
&\lambda_{x_1} = \lambda_{x_2}
\end{aligned} \tag{3.5}$$

The first group of scaling laws (Equation 3.4) is associated with the system's parameters, while the second group (Equation 3.5) is pertinent to the input and outputs of the quarter-car system.

At this point, to determine how the parameters should be adjusted to satisfy new design requirements, it is assumed that the following requirements are to be satisfied in the re-design stage of this quarter-car system:

1) The time scale is to remain invariant (i.e., $\lambda_t = 1$).
2) The input force also remains the same (i.e., $\lambda_F = 1$).
3) The response of the sprung mass displacement is to be reduced by half (i.e., $\lambda_{x1} = 0.5$)

These requirements simplify the scaling laws in Equations 3.4 and 3.5 and result in the following *scaling factor*:

$$\lambda_{M_{us}} = \lambda_{K_s} = \lambda_{K_t} = \lambda_{B_t} = \lambda_{B_s} = \lambda_{M_s} = 2 \tag{3.6}$$

The scaling factor above indicates that if every parameter in this system is scaled up by a factor of two, then not only the requirements given above are satisfied but also dynamic similitude between the original and scaled systems is achieved. The latter achievement implies (as will be seen shortly) that properties of the original design are propagated to the scaled design. To demonstrate the interesting implications of this result, suppose that the every scaling law in Equation 3.6 is followed and the input force, *F(t)*, is an impulse-like function. Then, the time responses of the original and similitude scaled systems are as shown in Figure 3.2. The values of the system's parameters are given in Table 3.1. Interestingly, the figure below shows that dynamic characteristics of the original design (e.g., stability, settling time, peak time) are successfully maintained and carried over to the scaled design. This result clearly demonstrates and attests to the practicability of Buckingham's Pi Theorem and dimensional analysis as a tool in system scaling.

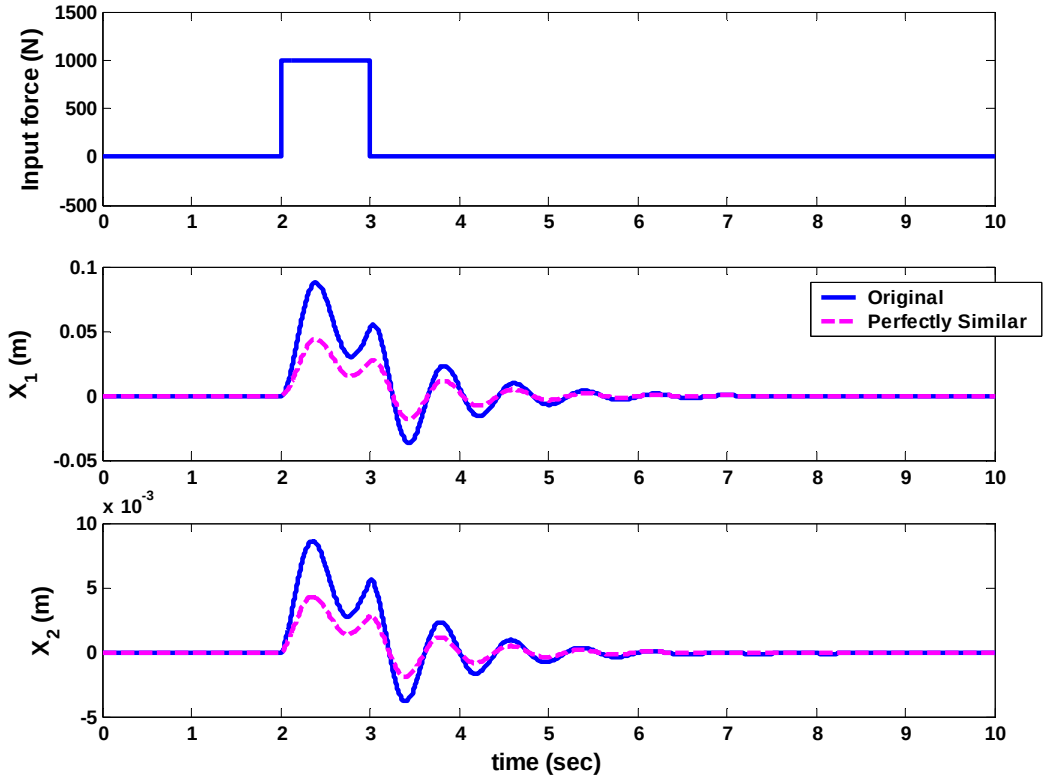

Figure 3.2: Perfect similitude responses

3.2 QUANTIFYING THE RELATIVE IMPORTANCE OF SCALING LAWS

As described in Chapter 2, while pure similitude-based scaling approaches appear to be a very tractable tool in system scaling, it is unfortunately often found to be too restrictive. This restriction is usually a result of the fact that some other physical constraints have to also be taken into consideration. For instance, the suspension design team might be less reluctant to modify the suspension spring rate (K_s) in this quarter-car system design problem because doing so might interfere with other packaging constraints. Then, a critical question arises, that is, can one still achieve adequate

similitude and simultaneously reduce the displacements by half without changing the suspension stiffness (K_s)?

In an attempt to answer this type of question, researchers proposed to conduct physical experiments [13] (or use sensitivity analyses [42]) to determine the influence of each scaling law of a physical system (or simulation model), thereby achieving more flexibility in scaling. However, such approaches can inevitably become time consuming (or computationally expensive), when the complexity of the model becomes more burdensome which entails more variables to be involved in the analysis.

To alleviate this drawback, using an energy-based metric, named "activity" [43] is proposed as an innovative and computationally efficient tool to determine the relative importance of each scaling law. Activity was originally developed as a metric for automated model-reduction and justified as an efficient assessment of elements' relative importance [43, 45]. This metric is applicable to both linear and non-linear systems. In particular, the activity of a particular energetic element is defined as the L_1 norm of the power flow into and out of the element over the course of a particular system state and input trajectory, multiplied by the length of the time window used for computing the norm. For example, if the effort of a generalized scalar energetic element is *e(t)* and the flow through it is *f(t)*, the its activity is mathematically defined as:

$$\text{Activity} = \int_0^{T_a} \left| e(t) f(t) \right| dt \tag{3.7}$$

where T_a is the duration over which this activity is calculated.

In the context of this research, we conjecture that *scaling laws associated with low-activity elements are less important to system dynamics than ones associated with high-activity elements*, and demonstrate this conjecture numerically. A clear advantage

gained by using activity analysis is the fact that, for a given input, activities of elements in a dynamic model can be calculated from *only one* run of the simulation.

The following figure explains how dimensional and activity analyses are incorporated into the scaling technique developed in this chapter.

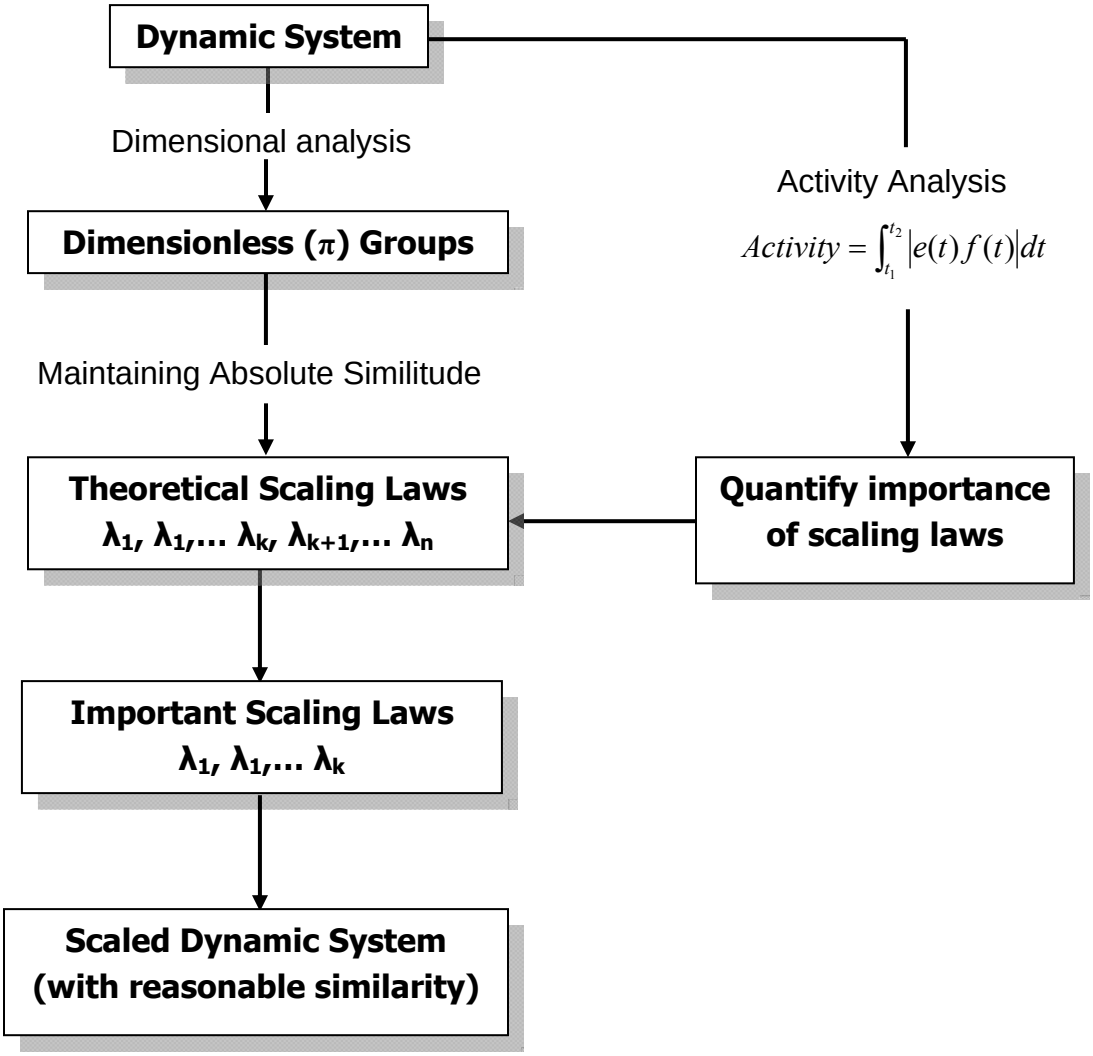

Figure 3.3: Scaling Methodology Using Dimensional and Activity Analyses

The scheme above indicates that activity analysis is used to quantify the relative importance of scaling laws. This information allows us to choose to scale only the more important parameters (denoted by the first k scaling laws in Figure 3.3) and neglect the less important ones without significantly compromising similitude. To illustrate the use of this notion on the quarter-car system, we first calculate the activities of all energetic and dissipative elements of the original 2-DOF system during the time window over which the simulation in Figure 3.2 was run and they are shown in Table 3.1 below. The values in the right-most column represent the activity index of each element which is the ratio of each element's activity over the sum of all activities. The mathematical definition of Activity Index (*AI*) is given below:

$$AI_i = \frac{\int_0^{Ta} |e_i(t) f_i(t)| dt}{\sum_{i=1}^{k} \int_0^{Ta} |e_i(t) f_i(t)| dt} \tag{3.8}$$

where k denotes the number of elements in the model under consideration. This index can be thought of as the portion of the total system energy flowing through a specific element in the system [43].

Element	**Value**	**Activity** [Joules]	**Activity Index** [%]
$\mathbf{K_s}$	187620 N/m	226.762	50.49
$\mathbf{M_s}$	267 kg	139.566	31.08
$\mathbf{B_s}$	700 N.s/m	58.504	13.02
$\mathbf{K_t}$	193950 N/m	23.887	5.31
$\mathbf{M_{us}}$	36.6 kg	0.1968	0.044
$\mathbf{B_t}$	200 N.s/m	0.1776	0.040

Table 3.1: Element activities of quarter-car system

According to our conjecture, the activity values in Table 3.1 suggest that the scaling laws associated with M_{us} and B_t should be the least important to the scaling of the system, so they can be discarded in scaling. In addition, this implies that if other

parameters (K_s, M_s, B_s, and K_t) are still scaled according to Equation 3.6, the dynamic similarity between the two systems should still be reasonably maintained. This is clearly justified by the result shown in Figure 3.4 in which the two responses match very well. In fact, the summed squares of residuals between the two responses over the entire trajectories, with the time step of 0.001 seconds, are only 1.69E-06 m^2 and 4.63E-07 m^2 for x_1 and x_2 respectively.

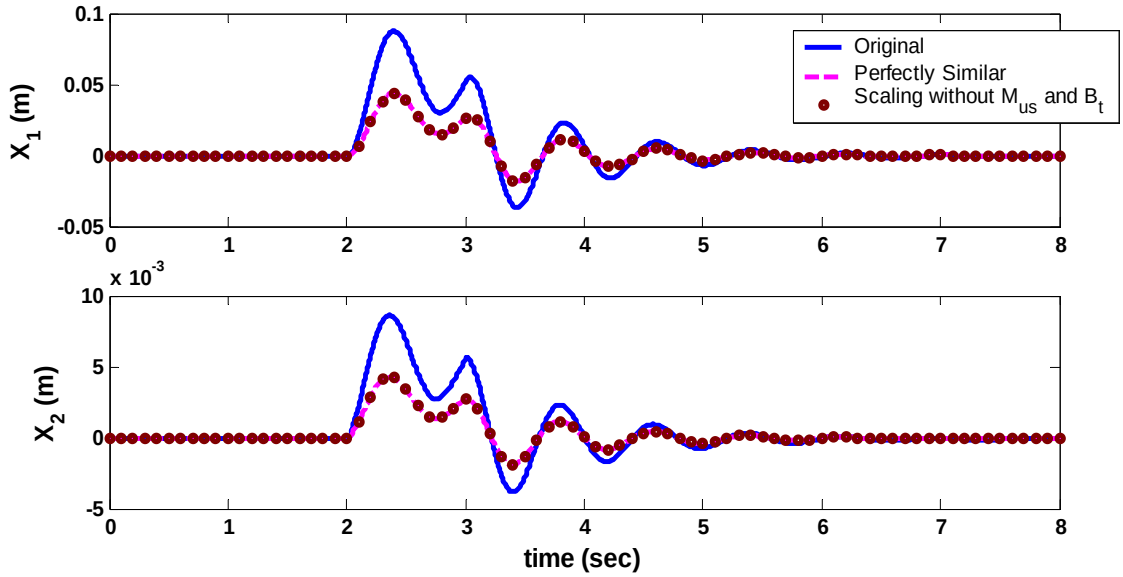

Figure 3.4: Responses when M_{us} and B_t are not scaled

On the other hand, if the most active element, K_s, is discarded from the scaling, our conjecture predicts that dynamic similarity should no longer be well maintained, and this turns out to be the case as shown in Figure 3.5 below:

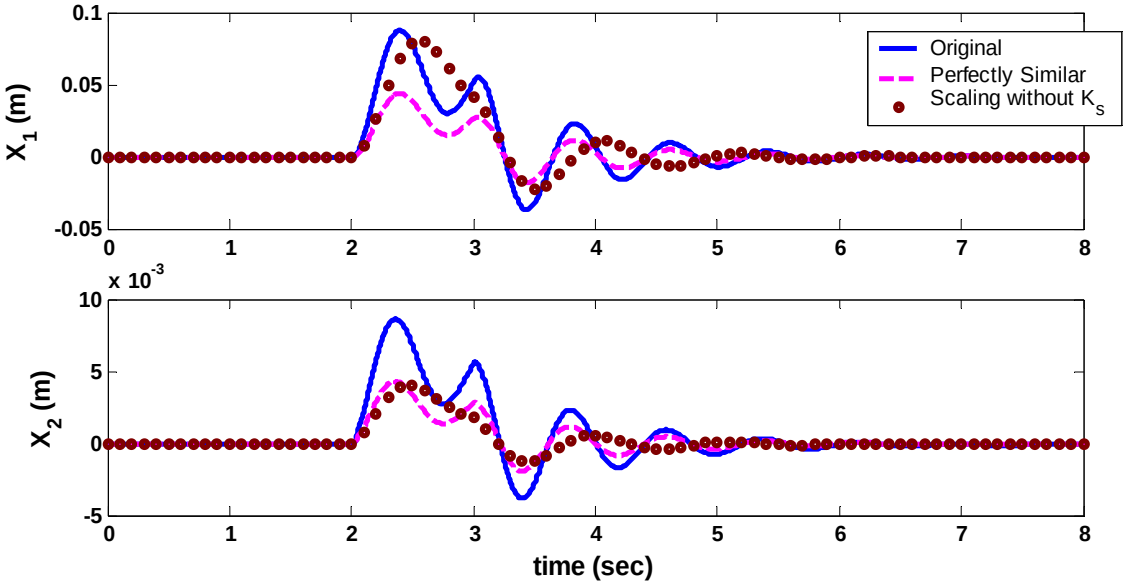

Figure 3.5: Responses when K_s is not scaled

It is possible to rationalize the above results as follows. First, if dynamic similarity is maintained in scaling, then activities will scale in proportion to each other.[3] Accordingly, the ranking of activities will remain the same. It follows that in both the original and perfectly scaled models, the least active elements remain unchanged. Next, based on this premise, if the less important scaling laws which are associated with low-activity elements cannot be scaled, one can infer that the activities of these elements will remain the smallest over some range of scaling of other elements. Therefore, over this range, discarding the scaling laws of these lower-activity elements will most likely not significantly penalize dynamic similarity. While this is not a rigorous proof, it does provide an initial and appealing justification for the approach taken in this section.

[3] Recall that activity is defined as $\int_0^{T_a} |e(t)f(t)|\,dt$. Because the effort and flow of every element in a system have (or can be converted to) the same units, whatever scaling factors that are imposed to the pair will be applicable to other elements' efforts and flows. As a result, all activities are scaled with the same factor.

At this point, one can answer the question raised in the beginning of this section as follows: It is not feasible to retain the same suspension spring design and, at the same time, achieve dynamic similarity as well as reduce the displacements by half. Instead, the results above attest to the possibility of keeping the same tire stiffness (K_t) and damping and (B_t) still closely achieving such requirements.

3.3 FUEL CELL AIR SUPPLY SYSTEM SCALING

In this section, the air supply system of the Polymer Electrolyte Membrane (PEM) fuel cell dynamic model developed in [3] is investigated. The goal of the scaling is to increase/decrease the air mass flow rate going through this air supply system, while maintaining desirable characteristics of the original system (e.g., minimum power consumption, rise time, etc.). This section demonstrates that the scaling technique developed so far in this section has the potential to become a great aid in designing the air supply system to satisfy different air flow rates while still maintaining such desirable characteristics. More specifically, a traditional optimization-based design approach is implemented to scale the system and its results are compared with those obtained from the scaling approach proposed in this dissertation.

First, details of the air supply system's models employed in this study are given in the following sub-section.

3.3.1 Air Supply System Modeling

The system considered herein is a simplified model of the fuel cell stack's air supply system. The simplifications consist of (i) removing chemical reactions in the cathode and (ii) using a blower as the flow device, instead of a compressor [46] (which renders this system a low-pressure system). To facilitate the calculation of element

activities, the system is modeled using bond graphs [10] as shown in the Figure 3.6. The main function of this air supply system is to regulate the amount of air flow going through the fuel cell stack system subject to the stack's power output demand.

Blower

The blower model represents a centrifugal blower modeled as a four-port transformer defined by two static maps. One of the maps represents flow rate ($\dot{m}_{BW}$) as a function of pressure ratio and rotational speed (ω) and the other designates the blower operational efficiency ($\eta_{BW,Opr}$) as a function of its flow rate and rotational speed (the associated map and data are given in Appendix C) The air-compressing process is assumed to be isentropic and the ideal gas assumptions also hold. The model's main inputs include the supply manifold's pressure (P_{sm}) and the motor's rotational speed (ω_m) and the main outputs are motor torque (τ_m) and mass flow rate out of the blower ($\dot{m}_{BW}$). The power consumed and temperature rise in the blower can be derived using basic thermodynamic principles [47] and given by:

$$\begin{aligned} P_{BW} &= \frac{\dot{m}_{BW} C_P T_{atm}}{\eta_{BW,Opr}} \left(\left(\frac{p_{sm}}{p_{atm}} \right)^{\frac{\gamma-1}{\gamma}} - 1 \right) \\ T_{BW} &= T_{atm} + \frac{T_{sm}}{\eta_{BW,Opr}} \left(\left(\frac{p_{sm}}{p_{atm}} \right)^{\frac{\gamma-1}{\gamma}} - 1 \right) \end{aligned} \tag{3.9}$$

It is important to note here that the entire air supply system has to be carefully designed (or sized) in such a way that the pressure ratio across the blower and the rotational speed (required to achieve a desired flow rate) allow the system to operate at its maximum possible blower operational efficiencies. This, then, implies that the power needed to achieve such a desired flow rate is at its minimum.

The dynamics associated with the blower inertia (I_{BW}) is governed by the following equation, where P_{in} represents power input to the blower.

$$I_{BW}\frac{d\omega}{dt} = \frac{1}{\omega}(P_{in} - P_{BW}) \tag{3.10}$$

Supply Manifold

According to the observation made in [3], it is expected that the air temperature can vary somewhat inside the supply manifold. The supply manifold is, therefore, modeled by a 2-port capacitor which represents changes in mass flow and associated enthalpy. In addition, it is assumed that the manifold is adiabatic with respect to its surroundings. The governing equations are:

$$\begin{aligned} \frac{dm_{sm}}{dt} &= \dot{m}_{in,sm} - \dot{m}_{out,sm} \\ \frac{dE_{sm}}{dt} &= \dot{H}_{in,sm} - \dot{H}_{out,sm} \end{aligned} \tag{3.11}$$

Furthermore, if we assume that the air can be modeled as perfect gases, the constitutive laws of the capacitor become:

$$\begin{aligned} T_{sm} &= E_{sm} \big/ m_{sm} C_v \\ p_{sm} &= m_{sm} R\, T_{sm} \big/ V_{sm} \end{aligned} \tag{3.12}$$

The inputs of this model are its mass flow rate ($\dot{m}_{sm}$) and the rate of change in energy ($\dot{E}_{sm}$) and the outputs are its pressure (p_{sm}) and temperature(T_{sm}).

Return Manifold

Due to the fact that the air temperature leaving the fuel stack is relatively low when compared to the air leaving the flow device, the return manifold is assumed to be isothermal. The manifold is hence modeled as a 1-port capacitor. The governing equation and constitutive law are as follows:

$$\begin{aligned} \frac{dp_{rm}}{dt} &= \frac{RT_{rm}}{V_{rm}}(\dot{m}_{in,rm} - \dot{m}_{out,rm}) \\ p_{rm} &= \frac{m_{rm}R_aT_{rm}}{V_{rm}} \end{aligned} \tag{3.13}$$

The input of this model is the mass flow rate ($\dot{m}_{rm}$) and the output is represented by the pressure (p_{rm}).

Nonlinear Nozzle

The air flow passing through these nozzles is assumed to behave isentropically. In bond-graphs, each of the nozzles can hence be represented as a multi-port resistor where all bonds have "effort-in" causality [10]. As a result, the mass flow rate across the nozzle is described by:

$$\dot{m}_{A_t} = \frac{C_D A_t \, p_{in,A_t}}{\sqrt{RT_{in,A_t}}} \begin{cases} 1/\sqrt{2} & for \quad P_{out,A_t}/P_{in,A_t} \le 0.5 \\ \sqrt{2\frac{P_{out,A_t}}{P_{in,A_t}}\left(1-\frac{P_{out,A_t}}{P_{in,A_t}}\right)} & for \quad P_{out,A_t}/P_{in,A_t} > 0.5 \end{cases} \tag{3.14}$$

The energy associated with this mass flow is given by:

$$\dot{E}_{A_t} = c_p T_{in,A_t} \dot{m}_{A_t} \tag{3.15}$$

The inputs of the model are pressures and temperatures of the incoming and outgoing flows. The outputs are denoted by mass flow rates and rates of change in energy of the flows.

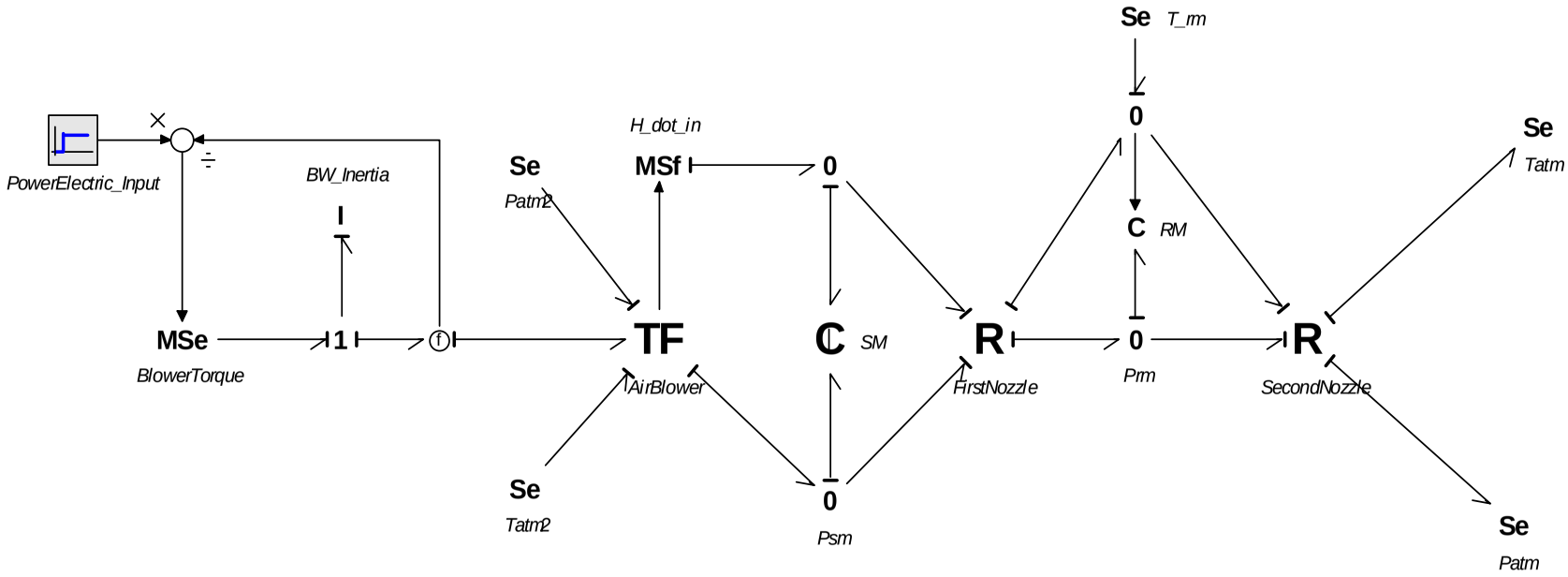

Figure 3.6: Simplified Air Supply System

3.3.2 Traditional Approach: Optimization Problem Formulation

The scaling objective in the context of fuel cell stack systems is to scale the air flow rates going through this air supply system which ultimately controls the overall fuel cell stack power output levels. It has been shown in [3] that adjusting these air flow rates directly relate to changing the levels of the fuel cell stack's power output. As described in Section 3.3.1, the air supply system utilizes power supplied to the blower (P_{in}) in order to compress the atmospheric air to satisfy certain desirable flow rates. For this reason, it is beneficial, from an energy savings standpoint, to design the air supply system in such a way that it consumes the least possible amount of power in the blower while still satisfying designated desired flow rates. Such power consumption is determined by the locations of operational points on the blower's efficiency map. This gives an explanation why the system's parameters (e.g., manifold sizes, blower size, etc.) have to be carefully designed to achieve the operational points that result in optimal efficiencies which translate into minimum power consumed by the blower to satisfy such desired flow rates.

Due to the design requirements realized above, the following list summarizes the goals and assumptions which are accounted for in the scaling study of this air supply system:

1) Scaling the levels of air flow rates in order to increase/decrease the fuel cell power output levels. It is assumed that each air supply system design has to operate at two different desired flow rates. For example, the original design is assumed to operate at flow rates of 0.01 and 0.02 kg/s. Changing the flow rate from 0.01 kg/s to 0.02 kg/s is done by supplying a step input in power supplied to the blower (P_{in}).

2) Maintaining the optimality in operational efficiency ($\eta_{BW,Opr}$) at the blower. This means that, for instance, if the original design is designed to operate at the point where the blower efficiency reaches its optimum (say, $\eta_{BW,Opr,Original} = 40\%$), the scaled design's operational efficiency should be the same as (or close to) 40%. This assures that the power consumed by the blower of the scaled system is minimal while still satisfying the increased (or decreased) desirable flow rates.

3) Maintaining reasonable dynamic characteristics of the original system (e.g., good response time, and no back flow). A reasonable response time is required so that the scaled design also has reasonable open-loop dynamic characteristics. The back-flow requirement is imposed because control authority will be lost if back flow occurs and the fuel cell will be damaged.

Given the goals above, an optimization problem can be formulated and described mathematically as follows:

$$
\begin{aligned}
&\text{Maximize} && f(\boldsymbol{x}) = P_{in} \\
&\text{with respect to}^{4} && \boldsymbol{x} = \{V_{sm}, V_{rm}, A_{t,1}, A_{t,2}, D\} \\
&\text{subject to} && g_1 \coloneqq 0.08\ m^3 \leq V_{sm} \leq 0.03\ m^3 \\
& && g_2 \coloneqq 0.002\ m^3 \leq V_{rm} \leq 0.02\ m^3 \\
& && g_3 \coloneqq 0.01\ m^2 \leq A_{t,1} \leq 0.06\ m^2 \\
& && g_4 \coloneqq 0.02\ m^2 \leq A_{t,2} \leq 0.12\ m^2 \\
& && g_5 \coloneqq 0.5\ \leq D \leq 3.0 \\
& && g_6 \coloneqq \tau_{s,original} - 1\ \text{sec}\ \leq \tau_s \leq \tau_{s,original} + 1\ sec^{5}
\end{aligned}
\qquad (3.16)
$$

[4] The significance of the design variable D will be explained in Section 3.3.3.

$$g_7 \coloneqq p_{sm,in} - p_{sm,out} \geq 0$$

$$g_8 \coloneqq p_{rm,in} - p_{rm,out} \geq 0$$

$$g_9 \coloneqq p_{sm,out} - p_{rm,in} \geq 0$$

$$g_{10} \coloneqq \dot{m}_{steady} = \dot{m}_{desired}$$

$$g_{11} \coloneqq I_{BW} = I_{BW,original}\left(\frac{D}{D_{original}}\right)^5$$

where the first five constraints (g_1, g_2, g_3, g_4, and g_5) denote bounds on the design variables. Constraint g_6 represents the bounds on the response time (τ_s) to a step input in power supplied to the blower (P_{in}). Moreover, Constraints g_7, g_8, and g_9 prevent the design from having back flow. Constraint g_{10} then reflects the requirement in which the air mass flow rate of the scaled design needs to satisfy the given desired flow rates. Moreover, the last constraint (g_{11}) represents the physical coupling between the changes in the blower size (D) and its rotational inertia (I_{BW}). In the optimization problem, the system is assumed to operate in the same environment; thereby making the atmospheric pressure (P_{atm}) and temperature (T_{atm}) as well as the return manifold temperature remain at the original values. The parameter values corresponding to the original design of this air supply system are given in Appendix C.

To demonstrate the applicability of the scaling technique developed in this dissertation to this air supply system, the original design (which was originally designed for $\dot{m}_{steady}$ = 0.01 to 0.02 kg/s) is re-optimized using the optimization formulation described above in Equation 3.16 to satisfy the new and increased desirable flow rates. Then, the scaled design obtained from this optimization formulation is compared to that obtained from the scaling technique explained in the next section (the underlying

[5] The response time is defined as the time until the response reaches 99% of its steady state value

motivation and justification for us to attempt to use the scaling technique will become more obvious in the next section). This comparison scheme can also be described by the following diagram:

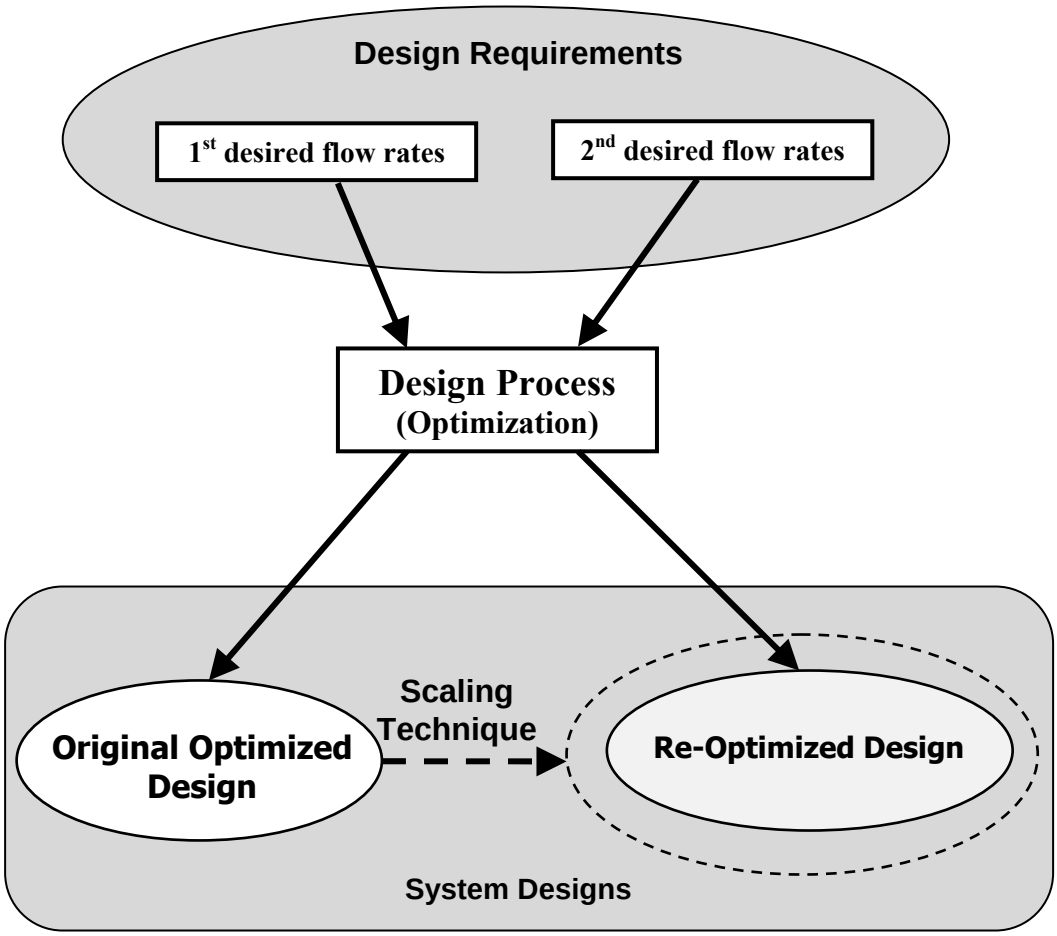

Figure 3.7: Optimization and Scaling

Note that the design scaling problem of the air supply system in this chapter is set up in such a way that some physical constraints that one may encounter in practice are omitted. These constraints can be, for example, a packaging constraint placing bounds on the sizing of some of the variables. The effect of these practical constraints will be taken into consideration in Chapter 4 in this dissertation.

3.3.3 Scaling Approach: Scaling Problem Formulation

Upon using the scaling notion developed thus far in this dissertation, scaling laws of the air supply system are first derived as follows: The following represents a set of variables sufficient for describing the physics of the air supply system indicated by Equations 3.9 - 3.15:

$$\left\{ \begin{matrix} t, m_{sm}, m_{rm}, m_{BW}, p_{sm}, p_{rm}, p_{atm}, V_{sm}, V_{rm}, T_{BW}, T_{sm}, T_{rm}, T_{atm} \\ A_{t,1}, A_{t,2}, R, \gamma, C_{D,1}, C_{D,2}, C_P, P_{BW}, P_{in}, I_{BW}, \eta_{BW,Opr} \end{matrix} \right\} \tag{3.17}$$

which indicates that the number of variables = **24.** The meanings of these symbols in the above set are given in nomenclature section of this dissertation. Care should be taken to distinguish that a lowercase letter "p" denotes a pressure, while an uppercase letter "P" represents a power. Next, the dimensional formulae of these variables are:

$$\begin{matrix} t = [T] & m_{sm}, m_{rm}, m_{BW} = [M] & p_{sm}, p_{rm}, p_{atm} = [ML^{-1}T^{-2}] & V_{sm}, V_{rm} = [L^3] \\ T_{sm}, T_{rm}, T_{BW}, T_{atm} = [\theta] & A_{t,1}, A_{t,2} = [L^2] & C_P, R = [L^2T^{-2}\theta^{-1}] & \\ \gamma, C_{D,1}, C_{D,2}, \eta_{BW,Opr} = [] & P_{BW}, P_{in} = [ML^2T^{-3}] & I_{BW} = [ML^2] & \end{matrix} \tag{3.18}$$

where M,L,T, and θ denotes the fundamental units of mass, length, time, and temperature respectively. By Buckingham's Pi theorem, the number of dimensionless (π) groups is = **24 – 4** = **20**. These groups were derived and shown below.

$$\begin{matrix} \pi_1 = \frac{m_{sm}}{m_{BW}} & \pi_2 = \frac{m_{rm}}{m_{BW}} & \pi_3 = \frac{p_{sm}A_{t,1}^{1/2}t^2}{m_{BW}} & \pi_4 = \frac{p_{rm}A_{t,1}^{1/2}t^2}{m_{BW}} \\ \pi_5 = \frac{p_{atm}A_{t,1}^{1/2}t^2}{m_{BW}} & \pi_6 = \frac{V_{sm}}{A_{t,1}^{3/2}} & \pi_7 = \frac{V_{rm}}{A_{t,1}^{3/2}} & \pi_8 = \frac{A_{t,2}}{A_{t,1}} \\ \pi_9 = \frac{T_{BW}}{T_{rm}} & \pi_{10} = \frac{T_{sm}}{T_{rm}} & \pi_{11} = \frac{T_{atm}}{T_{rm}} & \pi_{12} = \frac{T_{rm}t^2R}{A_1} \\ \pi_{13} = \frac{C_Pt^2T_{rm}}{A_{t,1}} & \pi_{14} = \frac{P_{BW}t^3}{m_{BW}A_{t,1}} & \pi_{15} = \frac{P_{in}t^3}{m_{BW}A_{t,1}} & \pi_{16} = \frac{I_{BW}}{m_{BW}A_{t,1}} \\ \pi_{17} = \gamma & \pi_{18} = C_{D,1} & \pi_{19} = C_{D,2} & \pi_{20} = \eta_{BW,Opr} \end{matrix} \tag{3.19}$$

The scaling laws can then be derived using these dimensionless parameters as well as the definition of a scaling factor indicated previously in Section 3.1. The derivation assumes that the gas constants (R), specific heat capacity (C_P), discharge coefficients of the nozzles ($C_{D,1}$,$C_{D,2}$), and time remain (t) invariant:

$$
\begin{aligned}
&(i) \quad \lambda_{m_{sm}} = \lambda_{m_{rm}} = \lambda_{m_{BW}} \\
&(ii) \quad \lambda_{p_{sm}} = \lambda_{p_{rm}} = \lambda_{m_{BW}} \Big/ \lambda_{T_{atm}}^{1/2} \\
&(iii) \quad \lambda_{P_{BW}} = \lambda_{P_{in}} = \lambda_{m_{BW}} \lambda_{T_{atm}} \\
&(iv) \quad \lambda_{\eta_{BW,Opr}} = 1
\end{aligned}
\tag{3.20}
$$

$$
\begin{aligned}
&(v) \quad \lambda_{V_{sm}} = \lambda_{V_{rm}} = \lambda_{A_{t,1}}^{3/2} = \lambda_{A_{t,2}}^{3/2} = \lambda_{T_{rm}}^{3/2} \\
&(vi) \quad \lambda_{T_{sm}} = \lambda_{T_{rm}} = \lambda_{T_{BW}} = \lambda_{T_{atm}} \\
&(vii) \quad \lambda_{I_{BW}} = \lambda_{m_{BW}} \lambda_{T_{atm}} \\
&(viii) \quad \lambda_{p_{atm}} = \lambda_{m_{BW}} \Big/ \lambda_{T_{atm}}^{1/2}
\end{aligned}
$$

The first four scaling laws in Equation 3.20 above indicate how system inputs/outputs are scaled, while the rest designate how the parameters in the system should be scaled to achieve similitude scaling.

To vary the size of the blower to accommodate larger flow rates, Wright [48] describes that the performance of an incompressible flow device (e.g., blower) in relation to its size can be represented by the following dimensionless groups:

$$
\pi_{21} = \frac{\Delta p}{\rho N^2 D^2} \quad and \quad \pi_{22} = \frac{Q}{ND^3} \tag{3.21}
$$

where Δp denote the pressure rise in the blower, Q represents the volume flow rate, N is the rotational speed of the blower, and ρ is the fluid density. The variable D can be considered as the size (or diameter) ratio of the impellers of any two blower designs. These relationships result in the scaling laws below which can be used to scale the blower maps with respect to its size (D):

$$\lambda_{\Delta p} = \lambda_D^2 \lambda_N^2 \quad and \quad \lambda_Q = \lambda_D^3 \lambda_N \tag{3.22}$$

Then, to account for the effect of changing the blower size on its inertia, the rotational inertia of the blower (I_{BW}) is assumed to be related to the size of the blower (D) through the following relationship:

$$\lambda_{I_{BW}} = \lambda_{\rho_{BW}} \lambda_D^5 \tag{3.23}$$

where ρ_{BW} represents a density factor that converts the blower size into its associated rotational inertia.

At this point, it is rather interesting to note that the fourth scaling law in Equation 3.20 has the following implication: If the scaling laws associated with the parameters of the air supply system (as shown in Equations 3.20, 3.22, and 3.23) are followed exactly, then operating points of the scaled design on the blower's efficiency map should result in the same operational efficiencies as those of the original design. In other words, if the original design operates at the points where the least possible amount of power is consumed to satisfy the original desired flow rates (i.e., $\dot{m}_{desired,original}$ = 0.01 to 0.02 kg/s), then any scaled design that achieves similitude will also consume the least possible amount of power to satisfy the increased desired flow rates (e.g., $\dot{m}_{desired,new}$ = 0.02 to 0.04 kg/s). This provides an initial justification of why our scaling technique can

potentially be used as a design tool to achieve the same goals as those of the optimization formulation described in the Section 3.3.2.

3.3.4 Comparison of Results

Based on the optimization formulation in Equation 3.16, the re-optimized air supply system design is assumed to be subject to desired flow rates of 0.02 to 0.04 kg/s (doubled of the original designated flow rates). The resulting optimal design is given in Table 3.3. It should be noted here that the objective function value (i.e., maximizing the blower operational efficiency) is insensitive to the ranges of values within the lower and upper bounds where the supply (V_{sm}) and return manifold (V_{rm}) volumes are varied (this is confirmed by the plots in Figure 3.8 below). For this reason, these two design variables, as shown in Table 3.3, can be set any values within their lower and upper bounds.

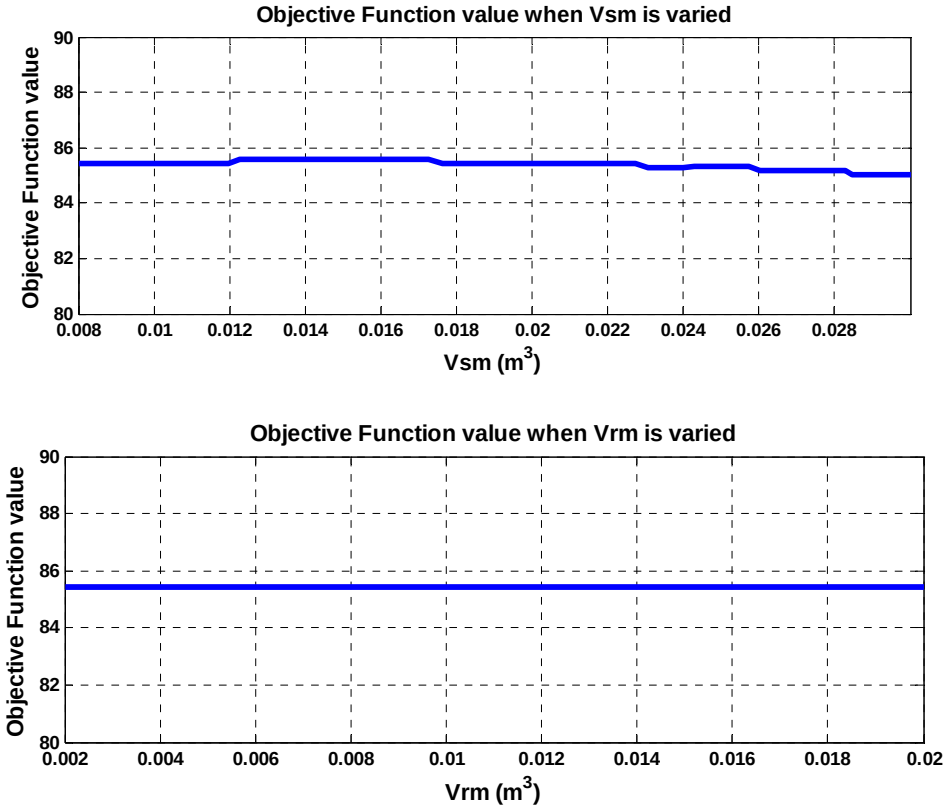

Figure 3.8: Objective function value with respect to variations in V_{sm} and V_{rm}

To compare with the optimization results, the scaling technique is implemented and explained in detail as follows: The procedure starts by assessing the importance of scaling laws which were already derived in Section 3.3.3. In doing so, the activity of each bond-graph element (as shown in Figure 3.6) is calculated. Unlike the quarter-car problem, the resulting activity values, however, cannot all be directly associated with the parameters of the system since some of these activities do not hold a one-to-one relationship with any of the parameters. For instance, the atmospheric temperature (T_{atm}) and pressure (P_{atm}) each shows up in two bond-graph elements. This then raises the following question: which bond-graph element should one associate the importance of the atmospheric temperature's scaling law with? To address this question, an ad-hoc, but rather intuitive, approach is employed to associate these activities with the parameters. This approach is explained in detail in Appendix D. The resulting relative importance indices are given in Table 3.2 below.

Parameter	Activity Index [%]
First Nozzle: $A_{t,2}$	26.46
Second Nozzle: $A_{t,1}$	26.64
Blower: D	16.66
Atmospheric Temperature: T_{atm}	9.92
Power Input: P_{in}	8.60
Blower Inertia: I_{BW}	8.35
Atmospheric Pressure: p_{atm}	3.28
Return Manifold Temperature: T_{rm}	0.047
Supply Manifold Volume: V_{sm}	0.011
Return Manifold Volume: V_{rm}	0.0006

Table 3.2: Element activities of original *optimized* design

Next, the scaling laws in Equation 3.20, 3.22, and 3.23 are used in the following steps in order to adjust the parameters (as listed in Table 3.2) so that the resulting scaled design satisfies the new desired flow rates (0.02 to 0.04 kg/s):

(i) According to Table 3.2, our conjecture (stated in Section 3.2) suggests that the scaling laws associated with the supply and return manifolds are not important since their activities are the least in the ranking. Interestingly, this is also in agreement with the information found from the sensitivity analysis previously shown in Figure 3.8 which accentuates the use of activity to gain more flexibility in scaling. For this reason, the supply and return manifolds (V_{sm} and V_{rm}) do not need to be scaled, hence $\lambda_{V_{sm}} = 1$, and $\lambda_{V_{rm}} = 1$.

(ii) Since it is judicious to assume that the atmospheric condition remains invariant, the atmospheric temperature (T_{atm}) and pressure (P_{atm}) as well as the return manifold temperature (T_{rm}) are kept constant. Therefore, this results in $\lambda_{T_{atm}} = 1, \lambda_{p_{atm}} = 1,$ and $\lambda_{T_{rm}} = 1$.

(iii) Doubling the desired mass flow rates results in $\lambda_{m_{BW}} = 2$. This scaling factor together with those obtained from (ii) allow us to use the third scaling law in Equation 3.19 to scale the levels of power input supplied to the blower (P_{in}), this gives $\lambda_{P_{in}} = 2$.

(iv) The scaling of the cross-sectional area of the first and second nozzles ($A_{t,1}$ and $A_{t,2}$) relies on the concept of Monotonicity Principle [49]. That is, the objective function value (represented by blower power consumption) is found to be decreasing monotonically with respect to $A_{t,1}$ and $A_{t,2}$ (see Fig

C.2 in Appendix C), and the upper bounds on $A_{t,1}$ and $A_{t,2}$ turn out to be the only increasing constraints with respect to these two parameters. Therefore, these upper bounds are said to be *critical* [49]. As a result, to maintain the operational points at which the least possible amount of power is consumed in the blower while still satisfying new desirable flow rates, $A_{t,1}$ and $A_{t,2}$ need to be set at their corresponding upper bounds. As indicated in Constraints g_3 and g_4 of Equation 3.16, the upper bounds in this problem are set at two times larger than the original design's parameter values, therefore the associated scaling factors of these two parameters become $\lambda_{A_{t,1}} = 2$, and $\lambda_{A_{t,2}} = 2$

(v) Finally, by designating that $\lambda_{\Delta p} = 1$ (as a result of $\lambda_{p_{atm}} = 1$) and $\lambda_{\mathrm{Q}} = 2$ (as a result of $\lambda_{m_{BW}} = 2$ and assuming that air density does not vary), the blower size (D) of the scaled designs can be determined using the first two scaling laws in Equation 3.22. Then, the rotational inertia (I_{BW}) can be calculated according to Equation 3.23.

Using these steps above gives the scaled design shown in the right-most column of Table 3.3:

	Original Design	Re-optimized Design	Scaled Design
Desired Flow Rates: $\dot{m}_{required}$ [kg/s]	0.01 to 0.02	0.02 to 0.04	0.02 to 0.04
Supply Manifold Volume: V_{sm} [m^3]	0.02	Any value (within bounds)	0.02
Return Manifold Volume: V_{sm} [m^3]	0.05	Any value (within bounds)	0.05
First Nozzle's Area: $A_{t,1}$ [m^2]	0.03	0.06	0.06
Second Nozzle's Area: $A_{t,2}$ [m^2]	0.06	0.12	0.12
Blower Size: D (Multiple of original)	1	1.30	1.41
Blower Power Consumption: P_{in} [Watt]	444 to 1709	886 to 3419	888 to 3418

Table 3.3: Optimization and scaling results

At this point, it is important to realize that even though the parameters in the system are scaled according to the five steps just described above, it is inevitable that some of the scaling laws associated with the system's parameters (the last four scaling laws in Equation 3.20) are still violated. This is due to, for example, the coupling between the blower's inertia (I_{BW}) and its size (D) which causes the seventh scaling law in Equation 3.20 to fail. In addition, the eight scaling law in Equation 3.20 also fails as a result of the invariance in both the return manifold temperature (T_{rm}) and atmospheric pressure (P_{atm}). This failure to comply with the scaling laws (hence violation of similitude) is then expected to produce some deviation in the resulting scaled designs from similitude because the activity of the elements associated with the atmospheric pressure (P_{atm}) and blower inertia (I_{BW}) are deemed somewhat important as shown in Table 3.2. As a consequence, this should mean that some (or all) of the scaled design's properties (or outputs) do not perfectly meet the scaling factors designated by the first

four scaling laws in Equation 3.20. This speculation, in fact, turns out to be true. Figure 3.9 below clearly shows, for instance, that the scaled design's mass flow rates at steady state deviate slightly from 0.02 and 0.04 kg/s, while the re-optimized design does meet this requirement exactly (because satisfaction in mass flow rate is incorporated as a hard constraint in the formulation). Despite this deviation, the time responses shown in Figure 3.9 still attest to the fact that the design obtained from the scaling technique is somewhat comparable to that from optimization. Moreover, it should be worth noting that the scaling technique implemented herein does not entail intensive computation while this does not hold true when the optimization is employed. In particular, it takes approximately 10 minutes[6] to obtain an optimal solution. On the other hand, the scaling solution requires only algebraic manipulations once the scaling laws are derived.

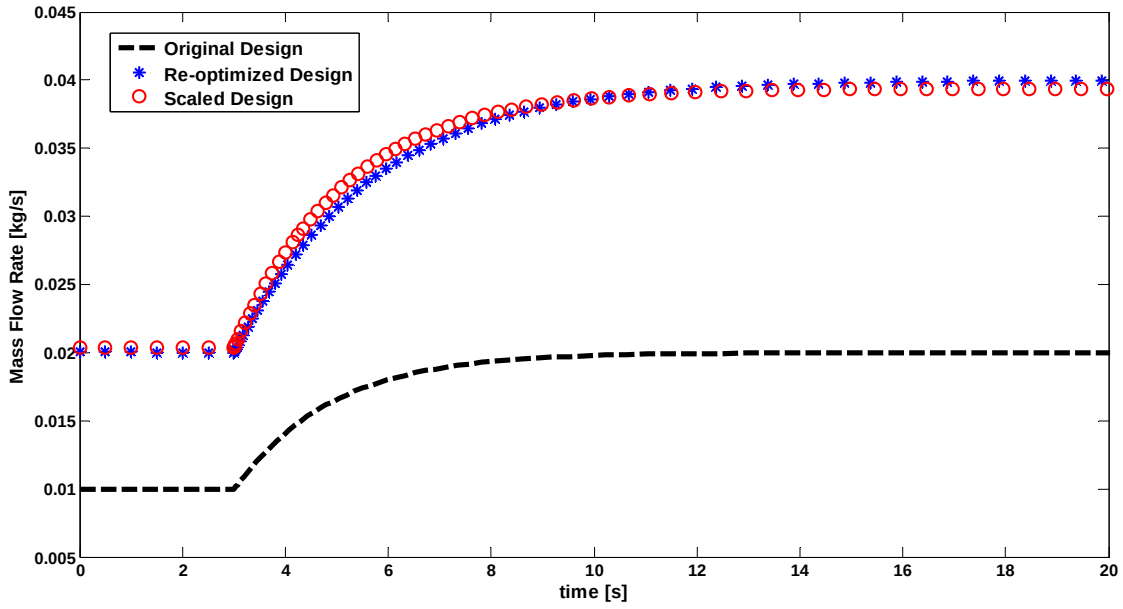

Figure 3.9: Time responses of the original, re-optimized, and scaled designs

It is also very important to note here that the scaled design presented in Table 3.3 and Figure 3.9 is a result of only one of the many ways to scale the parameters using the

[6] This number is based on a dual core 2.0 GHz machine with a 2 GB ram memory.

scaling laws in Equations 3.20, 3.22 and 3.23. It is possible to argue that, for example, even though the size of the blower (D) is determined based on the assumption that the scaling factor associated with the mass flow rate is $\lambda_{\dot{Q}} = 2$, it is clearly shown in Figure 3.9 that the resulting scaled design's mass flow rates are not exactly at 0.02 and 0.04 kg/s and therefore do not meet this scaling factor exactly. This possibly makes that scaled value of D previously calculated not legitimate. Then, the following interesting question arises: Is there a better (or more quantitative) way to change D (and other parameters) to better achieve the design requirement (i.e., desired mass flow rates) as well as similitude? Or, more generally stated, when similitude is not possible to achieve, how should the parameters be adjusted so that the resulting scaled design stays close to similitude while still closely satisfying other design requirements?

To this end, it is obvious that, while one can readily quantify the extent to which the design requirement is achieved (e.g., the mass flow rate is X percent off the desired value), it is more difficult to quantify the extent to which a scaled design satisfies similitude. Therefore, in order to answer the above questions as well as to make the scaling technique developed herein more efficient, a metric which can quantify the degree to which a scaled design is "close" to satisfying similitude should be developed. Once this metric is developed and justified, it should help us tradeoff the ability to achieve similitude against the ability to satisfy design requirements. In the context of the air supply system scaling, this tradeoff can be interpreted as the ability to maintain the blower operational efficiency versus the ability to satisfy the desired flow rates. This gives us the motivation to investigate into a way to quantify such *closeness* which will be addressed in the succeeding chapters in this dissertation.

3.4 CHAPTER SUMMARY

This chapter presents a unique combination of an element activity metric and dimensional analysis to assess the relative importance of scaling laws and selectively scale only the important components. This method is shown to provide more freedom than the pure similitude-based scaling and attain more computational efficiency than sensitivity analysis. The examples in the chapter demonstrate that the developed technique is applicable to both linear and nonlinear systems, and also prove that it can be implemented to multi-domain problems. Furthermore, the findings in this chapter can assist engineers to modify only the influential components, thereby avoid any needless adjustments to the system that could happen otherwise.

The air supply system case study also carries an interesting idea, that is, the presented technique can become a powerful aid to optimization in scaling system designs. However, for more complicated systems with more stringent constraints or requirements, one can expect that the current technique can become rather limited because it might not even be feasible to scale those important components, thereby heavily jeopardizing the similarity between the original and scaled systems. Due to this limitation, the succeeding chapter focuses on trying to create a metric are capable of assessing the degree to which two systems are “close” to satisfy similitude. This metric will also help us build a tool that enables multiobjective system scaling where the degree of similitude can be traded off against other competing design requirements.

CHAPTER IV

APPROXIMATE SIMILITUDE: QUANTIFICATION AND USE IN MULTIOBJECTIVE SCALING

As demonstrated in Chapter 3, when scaling laws deemed important cannot be followed exactly, not only the design requirement is not met perfectly, but also the resulting scaled designs' characteristics deviate from those of the original design. With this in mind, this chapter aims at formulating a metric quantifying such a degree of deviation in similitude. In particular, this chapter addresses two limitations of the dynamic similitude literature through two original fundamental contributions. It presents the first quantification of *approximate similitude* on a continuous – rather that discrete – basis. It also incorporates this quantification within a multiobjective system scaling framework for the first time. The chapter is organized as follows. The first section presents a simple motivating example that highlights the definition of exact dynamic similitude as well as its key limitations. The second section then defines a new continuous metric that quantifies the degree to which two systems are approximately similar. This section also presents a multiobjective optimization framework to trade the resulting approximate similitude metric off against other system scaling requirements and constraints. Finally, the third and fourth sections demonstrate the resulting flexible multiobjective scaling algorithm using two case studies. The first case study examines the

scaling of the quarter-car system, while the second examines the scaling of a fuel cell air supply system, both of which were previously introduced in Chapter 3. The results of these studies and contributions of this work are discussed in Section 4.5.

4.1 MOTIVATING EXAMPLE: LIMITATIONS OF EXACT SIMILITUDE

Consider the quarter-car system previously introduced in Chapter 3. It has been shown that any system scaling that obeys the scaling laws given in Equations 3.4 and 3.5 exactly satisfies Buckingham's Pi Theorem, and its outputs will be dynamically similar to the original system design. For instance, suppose again that one seeks a new system design complying with the following specifications: *(i)* $\lambda_t = 1$, i.e., the time scale is not changed; *(ii)* $\lambda_F = 1$, i.e., the input force remains the same; *(iii)* $\lambda_{x_1} = 0.5$, i.e., we wish to reduce the magnitude of the sprung mass displacement by half. Then, the scaling laws of this system reduce to the following:

$$\lambda_{M_{us}} = \lambda_{K_s} = \lambda_{K_t} = \lambda_{B_t} = \lambda_{B_s} = \lambda_{M_s} = 2 \tag{4.1}$$

To visualize these scaling laws, consider the relationship between only two scale factors, namely, $\lambda_{M_{us}}$ and λ_{K_s} . This relationship is plotted below, ignoring all other scale factors for simplicity:

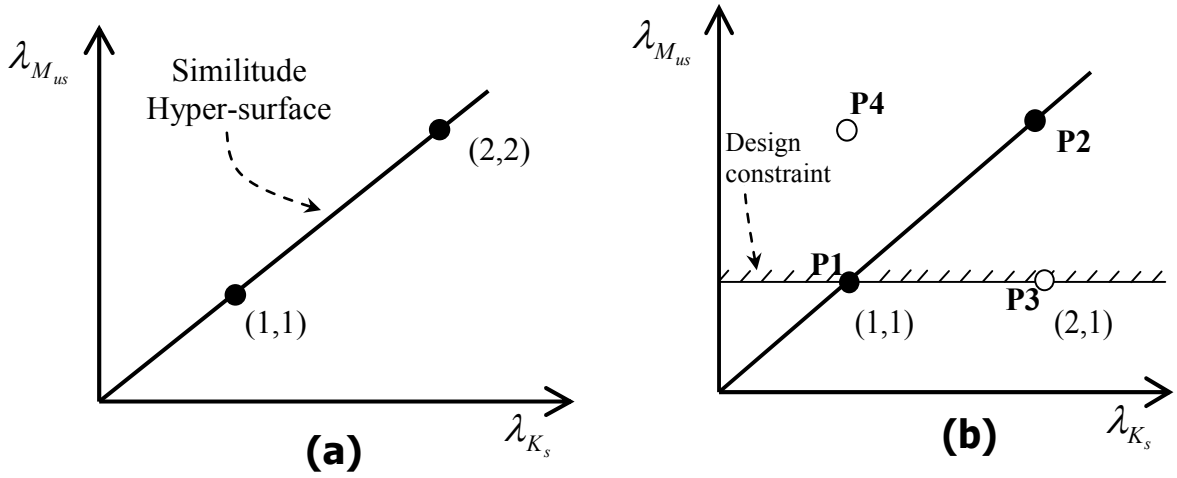

Figure 4.1: Scaling law coordinate system: (a) unconstrained, (b) constrained

Figure 4.1a above shows the relationship between $\lambda_{M_{us}}$ and λ_{K_s} if the quarter-car system is scaled in exact compliance with dynamic similitude. In this case, the original and scaled system designs are represented by the points (1,1) and (2,2), respectively. The line segment in the first quadrant that contains these two points enumerates the pairs of all unsprung mass and suspension stiffness values complying with dynamic similitude. We refer to this line segment as a *similitude line*, and alternatively refer to it as a *similitude hyperplane* in more than two dimensions. In general, this hyperplane may be a nonlinear *similitude hypersurface*, and according to Buckingham's Pi Theorem, this hypersurface will always be monomial [12]. Any design lying on this monomial similitude hypersurface satisfies dynamic similitude exactly, and any design not lying on it does not satisfy dynamic similitude. This highlights the discrete nature of dynamic similitude: it is either satisfied exactly or not at all.

Consider the problem of scaling the above quarter-car suspension system to meet the above scaling requirements (namely, $\lambda_t = 1$, $\lambda_F = 1$, $\lambda_{x_1} = 0.5$) and retain as many desirable suspension characteristics as possible, subject to the constraint that the

unsprung mass cannot be changed (i.e., $\lambda_{M_{us}} = 1$). This scenario is depicted in Figure 4.1b, where the additional constraint is represented by a line plus dashes. Perfect dynamic similitude is impossible in such a constrained scenario, but one may still choose to satisfy the scaling laws for all system design variables except the unsprung mass. This gives the point (2,1) in Figure 4.1b. In other words, point (2,1) denotes the design whose all parameters (also including those four parameters omitted from the figure, i.e., M_s, K_t, B_s, B_t) are increased by a factor of two except the unsprung mass which is constrained at the original value. Given this point, one may legitimately ask: to what extent is it *approximately similar* to the original design? Furthermore, if this new scaled design is, indeed, approximately similar to the original, can one devise a new scaling algorithm that *attempts to retain dynamic similarity as much as possible, but allows for some deviations from the similitude hypersurface*? These questions are impossible to answer with a discrete definition of dynamic similitude. To address them, the next section presents the first continuous quantification of dynamic similitude in the literature. Furthermore, Sections 4.3 and 4.4 utilize this quantification as part of a multiobjective scaling formulation that trades similitude off against other scaling requirements, for the first time. The contributions in Sections 4.2 to 4.4 also leverage the findings discovered in the previous chapter, that is, different scale parameters and scaling laws do not affect a given system's behavior equally. Therefore, any quantification of *approximate similitude* must not only account for the deviation of a scaled design from the corresponding similitude hypersurface, but also weigh this deviation by the importance of the parameters in which it occurs.

4.2 APPROXIMATE SIMILITUDE METRIC AND MULTIOBJECTIVE SCALING METHOD

To quantify approximate similitude, consider the similitude hyperplane corresponding to the scale factors $\lambda_{M_{us}}$ and λ_{K_s} of the quarter-car system. Furthermore, consider four points on this similitude hyperplane: a point P1 (1,1) corresponding to the original design, a point P2 (2,2) corresponding to a perfectly scaled design, and two points P3 (2,1) and P4 (1,2) corresponding to non-similitude designs[7]. Noting that P3 and P4 are equidistant from the similitude hyperplane, one may argue that they deviate equally from similitude, but this is not confirmed by Figure 4.2 as follows.

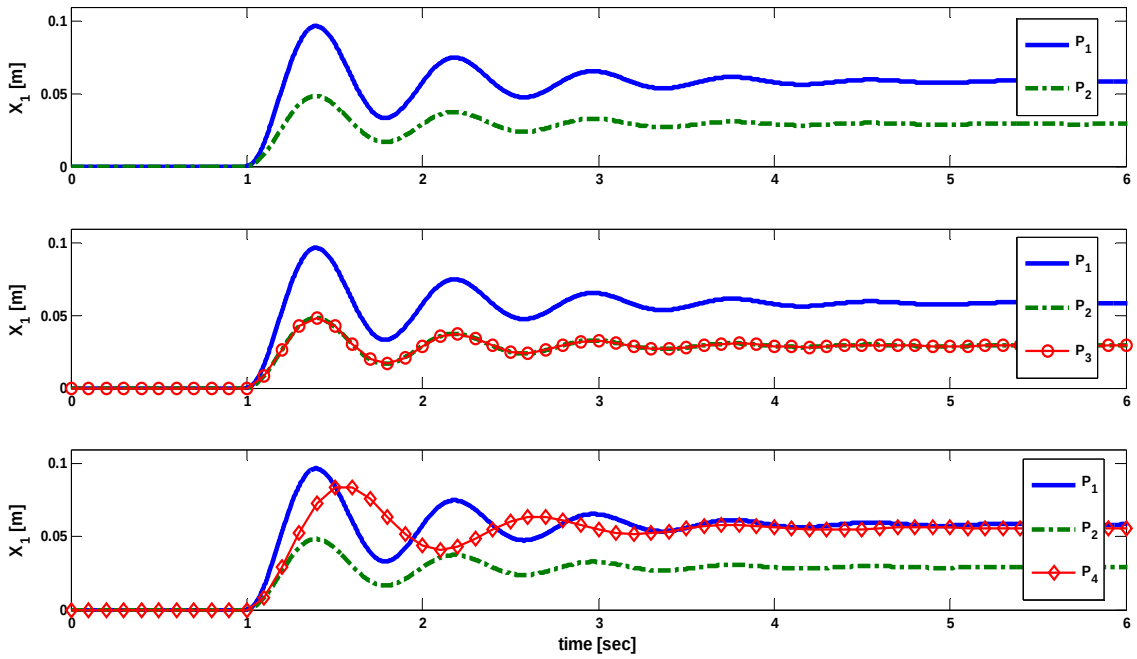

Figure 4.2: Time responses of designs P_1, P_2, P_3, and P_4

Figure 4.2 plots the sprung mass displacements corresponding to the points P1-P4. As asserted by Buckingham's Pi Theorem, the sprung mass displacement

[7] Note that, at Point P2 (2,2), the other four parameters absent from the scaling law coordinates (i.e., M_s, K_t, B_s, B_t) are also scaled by a factor of two according to similitude. Similarly, at Point P3 (2,1), since these four parameters are not constrained, they are still scaled by a factor of two.

corresponding to P2 is exactly half that corresponding to P1. Interestingly, the sprung mass displacement corresponding to P3 is almost identical to the displacement corresponding to P2. Intuitively, this implies that P3 is *approximately similar* to P2, and therefore also approximately similar to P1. This is not true for P4, whose sprung mass displacement deviates significantly from P2, thereby indicating poor approximate similitude between P4 on the one hand and P1 and P2 on the other. An important conclusion of this simple example is that *distance from the similitude hypersurface alone does not constitute a satisfactory quantification of approximate similitude*. Points that are equidistant from the similitude hypersurface may, in fact, differ significantly in their compliance with approximate similitude. To quantify approximate similitude, one must therefore capture not only a design's deviation from the corresponding similitude hyperplane, but also the degree to which this deviation penalizes approximate similitude.

To capture such a degree, we consider the activities corresponding to the different quarter-car system parameters for the original system design, P1 (as listed in Table 3.1 in the previous chapter). It shows that the most active suspension element is the spring (K_s), and that the unsprung mass (M_{us}) is orders of magnitude lower in activity. It has been previously shown in Chapter 3 that scaling the suspension stiffness correctly is significantly more important than scaling the unsprung mass correctly if one seeks dynamic similitude. This explains the significant differences between points P3 and P4 in terms of similitude, despite their equal distance from P2. In one case, namely, P3, the deviation occurs in a less important parameter, and similitude is not affected significantly. In the other case, namely, P4, the deviation occurs in a more important parameter, and similitude is affected much more. In summary, we observe that deviations

from scaling laws corresponding to more active parameters penalize similitude significantly more than deviations from scaling laws corresponding to less active parameters.

The above discussion lays the foundations for the approximate similitude metric proposed herein. In particular, we propose to quantify approximate similitude in terms of the *activity-weighted distance* between a non-similitude design and a corresponding design on the similitude hypersurface. Consider, for instance, a non-similitude quarter-car suspension design given by scale factors λ_{M_s}, $\lambda_{M_{us}}$, λ_{K_s}, λ_{K_t}, λ_{B_s} and λ_{B_t}. Furthermore, let (*S,S,S,S,S,S*) be an arbitrary point on the six-dimensional similitude hypersurface corresponding to these scale factors. This arbitrary point satisfies the scaling laws for the given system as indicated by Equation 4.1, and is therefore a perfectly scaled design. Denote the activities corresponding to the above scale factors by A_{M_s}, $A_{M_{us}}$, A_{K_s}, A_{K_t}, A_{B_s} and A_{B_t}, respectively. Then we propose to use the following metric to quantify approximate similitude in the quarter-car system case:

$$\begin{aligned} F_s = {} & A_{M_s}(\lambda_{M_s} - S)^2 + A_{M_{us}}(\lambda_{M_{us}} - S)^2 + \\ & A_{K_s}(\lambda_{K_s} - S)^2 + A_{K_t}(\lambda_{K_t} - S)^2 + \\ & A_{B_s}(\lambda_{B_s} - S)^2 + A_{B_t}(\lambda_{B_t} - S)^2 \end{aligned} \tag{4.2}$$

The above metric captures not only a given design's deviation from the similitude hypersurface, but also the degree to which this deviation corresponds to highly active parameters. It also has an interesting graphical interpretation, as shown in Figure 4.3 below.

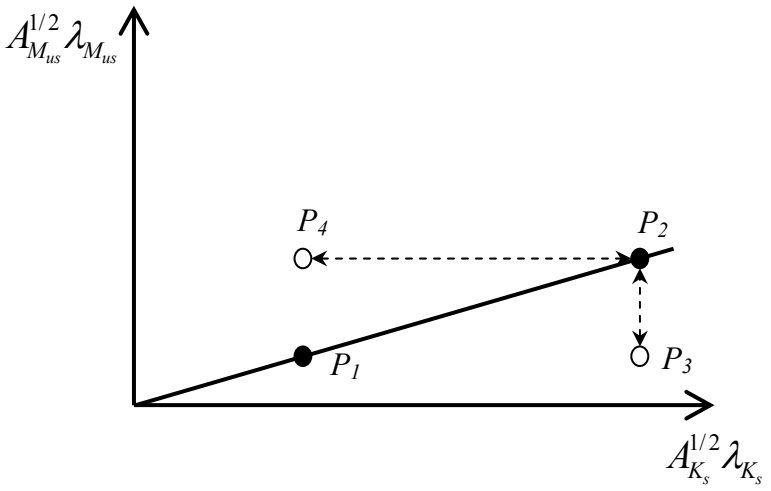

Figure 4.3: Modified scaling law coordinate system

Figure 4.3 plots the similitude hypersurface for the quarter-car example, again focusing only on the scale factors $\lambda_{M_{us}}$ and λ_{K_s} for simplicity. Unlike previous similitude hypersurface plots, however, it multiplies the axis corresponding to each scale factor by the square root of the activity corresponding to that scale factor. This tilts the similitude hypersurface to the right significantly, since the suspension stiffness is much more active than the unsprung mass[8]. Points P3 and P4 are no longer equidistant from P2. In fact, point P3 is much closer to P2 than P4 is. Furthermore, denoting point P2 by (S,S) rather than (2,2), we note that the distance between an arbitrary point on this new plot and point P2 is given by (a two-parameter version of) the approximate similitude objective in Equation 4.2. In other words, the proposed approximate similitude objective still equals the distance between a scaled design and a chosen point on the similitude hypersurface, but on a plot where each axis is scaled by the square root of the corresponding activity.

The above *continuous* quantification of approximate similitude allows designers to trade similitude off against other requirements in a multiobjective scaling framework,

[8] Note that, solely for the sake of effective illustration, Figure 4 is not drawn exactly to scale.

for the first time. Designs furnished by such a framework represent compromises between one's ability to attain similitude and one's need to satisfy other important scaling objectives and constraints. In this dissertation, we formulate the multiobjective scaling problem as follows:

$$\begin{aligned} \min_x F(x) &= F_s(x) + F_d(x) \\ \text{subject to: } & L_b \le x \le U_b \end{aligned} \tag{4.3}$$

where x, F, L_b, and U_b denote the design variables, overall objective function, and design variable lower and upper bounds, respectively. The vector of design variables x includes both the scale factors (i.e., the λ's) and the corresponding ideal scale factors (i.e., the S's) from Equation 4.2. Furthermore, the overall objective function contains two terms: a *"design objective"* F_d representing scaling specifications (e.g., desired steady state response, peak response, etc.), and an *"approximate similitude objective"* F_s capturing deviation from exact similitude. Case studies in the succeeding sections use this multiobjective formulation to scale a quarter-car system and a fuel cell air supply system approximately.

4.3 APPROXIMATE SIMILITUDE DESIGN OF A QUARTER-CAR SYSTEM

To illustrate the above approximate similitude scaling approach, consider the quarter-car scaling example considered in the previous chapter. Table 4.1 presents typical parameter values for this problem. It also presents some hypothetical upper and lower bounds on each parameter. Consider the problem of scaling this suspension to minimize the following design objective:

$$F_d \quad = \quad W\left(\frac{(x_1 - x_2)_{\max,actual}}{(x_1 - x_2)_{\max,spec}} - 1\right)^2 \qquad (4.4)$$

In this design objective, W is a *preference parameter* weighing the importance of the design objective compared to the similitude objective (F_s). Furthermore, the intent of the design objective is to achieve a certain desired *maximum suspension travel*, defined as the maximum difference between the displacements of the sprung and unsprung masses, i.e., $(x_1\text{-}x_2)_{\max}$. Minimizing such travel reduces the likelihood of "bottoming", and is thus a common suspension design objective [50, 51]. Suppose we seek to cut suspension travel exactly in half, while maintaining exact dynamic similitude. Table 4.1 lists the resulting scaled suspension parameter values, based on the scaling laws from Equation 4.1. These scaled parameters violate the upper bounds on both the sprung mass and the suspension stiffness. Furthermore, since these two particular parameters correspond to the highest activities in Table 3.1 (in the previous chapter), we conclude that scaling based on exact similitude is infeasible under this scenario. Instead, we combine the design scaling objective in Equation 4.4, the similitude objective in Equation 4.2, the parameter bounds from Table 2, and the multi-objective scaling formulation in Equation 4.3 to scale the suspension *approximately*. The resulting scaled designs are presented in Table 4.2 for different values of the weight W.

Parameter	Original	Exact Similitude Scaling	Lower Bound (L_B)	Upper Bound (U_B)
M_s [kg]	267	534	200	**400**
M_{us} [kg]	36.6	73.2	30	80
K_s [N/m]	18760	37520	15000	**35500**
K_t [N/m]	193950	387900	150000	500000
B_s [N.s/m]	700	1400	200	1500
B_t [N.s/m]	200	400	50	600

Table 4.1: Quarter-car system parameters and bounds

Preference Weight (W)	**Pareto Optimal Design**								
	M_s [kg]	M_{us} [kg]	K_s [N/m]	K_t [N/m]	B_s [N.s/m]	B_t [N.s/m]	S [-]	F_s^* [-]	F_d^* [-]
0.1	400	54.8	28144	290910	1050	300	1.499	0.00007	0.111
1	400	55.1	28467	293750	1063	304	1.513	0.0058	0.100
10	400	63.4	0362	310450	1144	324	1.595	0.2276	0.0507
100	400	67.5	34102	344030	1306	362	1.758	1.611	0.0058
500	400	68.0	34979	352000	1344	375	1.796	2.119	0.0021

Table 4.2: Quarter-car Pareto optimal designs

Figure 4.4 presents the various optima listed in Table 4.2 for different values of the weight W as a Pareto frontier. As this frontier shows, increasing the value of W furnishes suspensions that come closer to meeting the design goal of cutting suspension travel in half. This comes at the expense of similitude, which is increasingly sacrificed as W increases. To gain physical insight into this loss of similitude, recall that the perfectly scaled design in Table 4.1 assumes that the time scale is fixed. It follows, based on

Buckingham's Pi Theorem, that perfect similitude also implies that the frequency scale is fixed. In other words, the perfectly scaled suspension must have the same natural frequencies as the original design. Furthermore, note that perfect similitude must also preserve the system's suspension damping ratios, since they are dimensionless (see Appendix D for a derivation showing natural frequency and damping ratio expressed in terms of dimensionless parameters). These facts are evident in Figure 4.4b and Figure 4.4c, which show that the system's first natural frequency (sprung mass natural frequency) and damping ratio remain unaltered when similitude is perfectly attained (see Appendix D for plots showing correlations of F_s vs. damping ratio and natural frequency). As the weight W increases, however, similitude is gradually sacrificed, and this causes a shift in system natural frequencies and damping ratios.

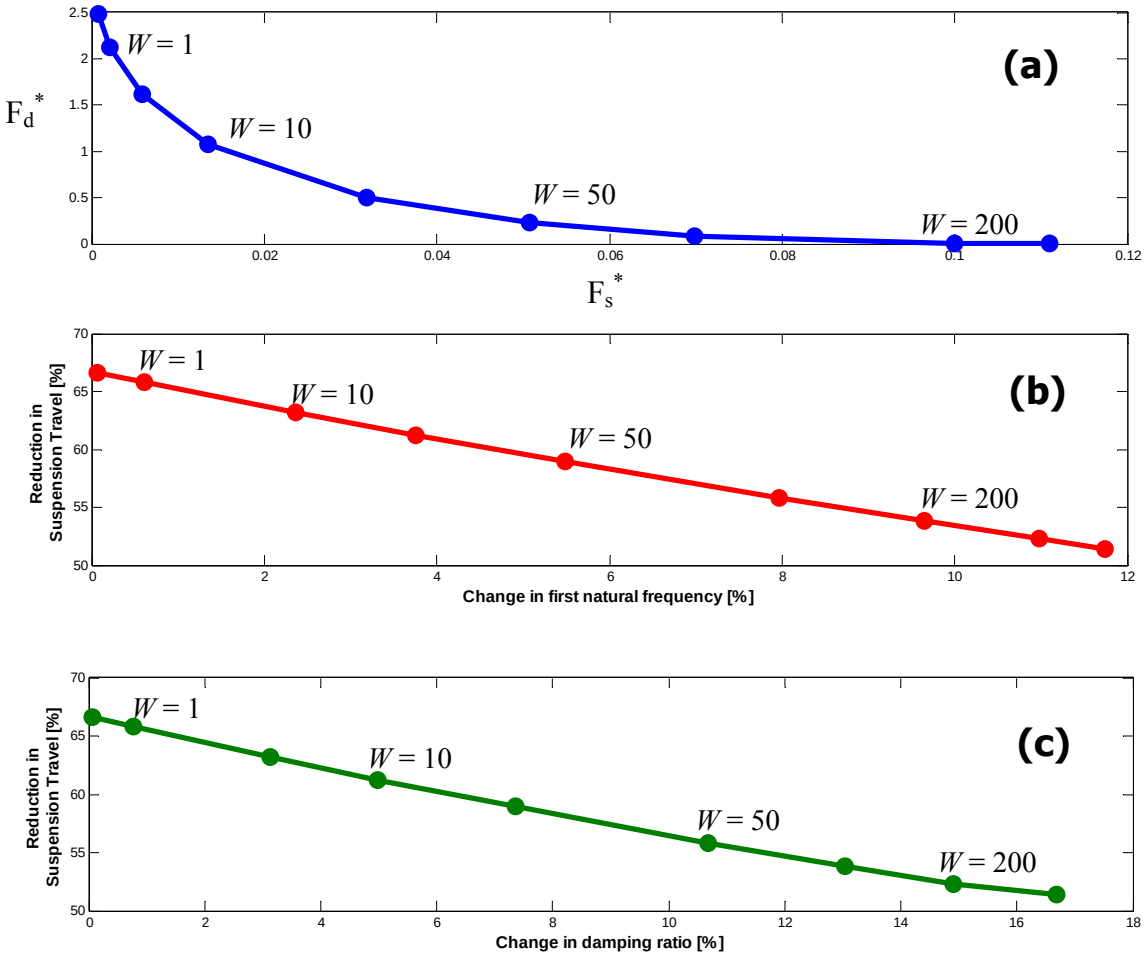

Figure 4.4: Quarter-car design trade-offs

The above results highlight two main strengths of the proposed approximate similitude metric and scaling method. First, the metric and scaling method extend similitude beyond its traditional discrete definition, hence enabling inexact system scaling. Secondly, tradeoffs between similitude and competing scaling requirements can be addressed explicitly.

4.4 APPROXIMATE SIMILITUDE DESIGN OF A FUEL CELL AIR SUPPLY SYSTEM

This section examines the scaling of a Polymer Electrolyte Membrane (PEM) fuel cell's air supply system (as introduced earlier in Chapter 3) to meet new power requirements. The governing equations describing this system are already given in Chapter 3 by Equations 3.9 – 3.15. The primary function of this air supply system is to regulate the amount of oxygen in the fuel cell's cathode during power generation. Such regulation is important, because the fuel cell's power output depends directly on the air flow rate through the air supply system, as shown in [3]. The goal of this case study is to investigate the scaling of the air supply system to provide different air flow rates, thereby meeting new fuel cell power demands.

Upon approximate scaling, we begin by deriving ideal scaling laws for the air supply system. We then compute the activity associated with each scaling law, and combine the resulting activities with the scaling laws to furnish an approximate similitude metric (these activities were calculated and previously given in Table 3.2 in the previous chapter). Finally, we formulate a design metric, and explicitly trade it off against the similitude metric to achieve approximate scaling. Scaling laws for the above air supply system are explained in Chapter 3 and replicated again below:

$$\lambda_{m_{sm}} = \lambda_{m_{rm}} = \lambda_{m_{BW}} \quad , \quad \lambda_{p_{sm}} = \lambda_{p_{rm}} = \lambda_{m_{BW}} \Big/ \lambda_{T_{atm}}^{1/2}$$

$$\lambda_{P_{BW}} = \lambda_{P_{in}} = \lambda_{m_{BW}} \lambda_{T_{atm}} \quad , \quad \lambda_{V_{sm}} = \lambda_{V_{rm}} = \lambda_{A_{t,1}}^{3/2} = \lambda_{A_{t,2}}^{3/2} = \lambda_{T_{rm}}^{3/2} \tag{4.5}$$

$$\lambda_{T_{sm}} = \lambda_{T_{rm}} = \lambda_{T_{BW}} = \lambda_{T_{atm}} \quad , \quad \lambda_{I_{BW}} = \lambda_{m_{BW}} \lambda_{T_{atm}} \quad , \quad \lambda_{p_{atm}} = \lambda_{m_{BW}} \Big/ \lambda_{T_{atm}}^{1/2}$$

$$\lambda_{\Delta p} = \lambda_D^2 \lambda_N^2 \quad , \quad \lambda_Q = \lambda_D^3 \lambda_N \quad and \quad \lambda_{\eta_{BW,Opr}} = 1$$

It is also worth mentioning again that the very last scaling law in Equation 4.5 suggests that perfect similitude scaling results in the ability to maintain the same operating points on the blower's efficiency map. This implies that if the original design's operating points are optimized (which means that the blower consumes the least amount of power possible to satisfy some certain desired flow rates), the optimality will also exist in the perfect similitude design. This clearly represents a desirable feature in the scaling of a fuel cell system, especially from an energy savings standpoint.

The design scaling problem for this air supply system is set up to reflect the situation in which the system engineer wishes to, firstly, scale the air flow rates to twice their original values and, secondly, maintain the original design's desirable properties (e.g., blower efficiency, rise time, etc.). Towards these broad goals, we consider the following two scenarios:

(i) The first scenario assumes the blower to be fixed

(ii) The second scenario allows the blower size parameter D to vary.

In both scenarios, the following parameters in Table 3.2 (i.e., $A_{t,1}$, $A_{t,2}$, P_{in}, V_{sm}, and V_{rm}) still remain design variables and, therefore, are allowed to vary. Again, we assume that the scaled air supply systems operate in the same environment as the original

system, i.e., $\lambda_{P_{atm}} = 1$, $\lambda_{T_{atm}} = 1$, and $\lambda_{T_{rm}} = 1$. As explained in Chapter 3, combining these requirements with the assumptions that the gas constant, time, and blower density factor do not change (i.e., $\lambda_R = 1$, $\lambda_t = 1$, and $\lambda_{\rho_{BW}} = 1$) makes it difficult to scale this air supply system in accordance with the exact similitude scaling laws in Equation 4.5 while doubling its air flow. Therefore, we pursue an approximate similitude solution instead.

We begin the approximate similitude scaling problem formulation by formulating the following approximate similitude objective function:

$$\begin{aligned} F_S = \; & A_{V_{sm}}(\lambda_{V_{sm}} - S_2^{3/2})^2 + A_{V_{rm}}(\lambda_{V_{rm}} - S_2^{3/2})^2 + A_{A_{t,1}}(\lambda_{A_{t,1}} - S_2)^2 + \\ & A_{A_{t,2}}(\lambda_{A_{t,2}} - S_2)^2 + A_{T_{rm}}(\lambda_{T_{rm}} - S_2)^2 + A_{T_{atm}}(\lambda_{T_{atm}} - S_2)^2 + \\ & A_{p_{atm}}(\lambda_{p_{atm}} - \frac{S_1}{S_2^{1/2}})^2 + A_D(\lambda_D - S_1^{1/4}S_1^{1/8})^2 + \\ & A_{P_{in}}(\lambda_{P_{in}} - S_1S_2)^2 + A_{I_{BW}}(\lambda_{I_{BW}} - \frac{S_2}{S_1})^2 \end{aligned} \tag{4.6}$$

Substituting the assumptions and requirements described earlier as well as the blower inertia-size relationship in Equation 3.23 into the above objective function gives us the following:

$$\begin{aligned} F_S' = \; & A_{V_{sm}}(\lambda_{V_{sm}} - S_2^{3/2})^2 + A_{V_{rm}}(\lambda_{V_{rm}} - S_2^{3/2})^2 + A_{A_{t,1}}(\lambda_{A_{t,1}} - S_2)^2 + \\ & A_{A_{t,2}}(\lambda_{A_{t,2}} - S_2)^2 + A_{T_{rm}}(1 - S_2)^2 + A_{T_{atm}}(1 - S_2)^2 + \\ & A_{p_{atm}}(1 - \frac{S_1}{S_2^{1/2}})^2 + A_D(\lambda_D - S_1^{1/4}S_1^{1/8})^2 + \\ & A_{P_{in}}(\lambda_{P_{in}} - S_1S_2)^2 + A_{I_{BW}}(\lambda_D^5 - \frac{S_2}{S_1})^2 \end{aligned} \tag{4.7}$$

A clear distinction between this similitude objective and the quarter car similitude objective is that the present similitude objective contains two ideal scaling variables, S_1 and S_2. This reflects the fact that the similitude hypersurface for the fuel cell air supply system is two-dimensional, while the similitude hypersurface for the quarter-car system is one-dimensional (i.e., a line). The dimension of the similitude hypersurface depends on *(i)* the number of physical variables and parameters used in scaling, N_v, *(ii)* the number of scaling laws, N_s, and *(iii)* the number of assumed requirements on scaling, N_a.

To determine the dimension of the similitude hypersurface for the quarter-car system, note that the system is described by 10 variables given in Equation 3.1. Therefore, N_v=10. Furthermore, note that for these variables to satisfy exact similitude, they must satisfy 7 scaling laws listed in Equations 3.4 and 3.5. Therefore, N_s=7. Finally, note that we scale the quarter-car system subject to the requirements that neither time nor the input force are variant. This introduces two additional scaling requirements (which are independent of one another), i.e., N_a=2. Taking all of these facts into account, we conclude that for the quarter-car scaling problem, one can freely vary $N_v - N_s - N_a$ variables without sacrificing exact similitude. In other words, the dimension of the exact similitude surface is 10-7-2=1.

In a similar fashion, the fuel cell air supply system's governing equations which are described in Section 3.3.1 consist of a total of 24 variables, i.e., N_v = 24. Next, to satisfy similitude, 20 scaling laws in Equation 3.20 have to be followed, therefore, N_s = 20. Note that although there are 3 requirements assumed in the scaling of this system ($\lambda_t = 1, \lambda_{C_P} = 1, \lambda_R = 1$), and the last two requirements are dependent of one another. As a result, N_a = 2. Therefore, we conclude that the dimension of the exact similitude

surface is 24-20-2 = 2, hence the need for 2 perfect scaling variables, S_1 and S_2.

Returning to the air supply system scaling problem, given the approximate similitude objective in Equation 4.7, we now formulate the design objective as follows:

$$F_d = W \ \left(\dot{m}_{steady} \Big/ \dot{m}_{desired} - 1\right)^2 \tag{4.8}$$

This design objective above represents the requirement of doubling the flow rate of supplied air. In other words, $\dot{m}_{desired}$ is chosen to be twice the air flow rate of the original air supply system. Recall from the previous chapter that the original system was designed for $\dot{m}_{desired}$ at 0.01 to 0.02 kg/s and the scaled design wants to achieve 0.02 to 0.04 kg/s. The original system design parameter values and upper and lower bounds are identical to those in Equation 3.16 and Appendix C.

The similitude objective (Equation 4.7) and design objective (Equation 4.8) are then incorporated into the multiobjective formulation (as indicated in Equation 4.3). The results of approximate similitude-based scaling are presented below. Specifically, Figure 4.5 shows the different air flow rates corresponding to a step change in power consumed by the blower (P_{in}) for different Pareto-optimal scaled system designs, assuming a fixed blower (D is fixed). These responses demonstrate how the mass flow rates of the scaled designs gradually approaches the design specifications as preference parameter W increases.

Increasing the preference parameter W may result in better attainment of the design goal of doubling the fuel cell air supply system's flow capacity, but this comes at a penalty in similitude. One way to visualize this penalty is to plot deviations from the desired air flow rates versus decline in operational blower efficiency ($\eta_{BW,Opr}$) for

different optimal scaled design[9], as shown in Figure 4.6. Operational blower efficiency is not explicitly incorporated in the air supply system scaling problem. However, as noted earlier, perfect similitude-based scaling of the air supply system guarantees constant blower efficiency. More specifically, the ability to maintain similitude results in the same operation points on the blower's efficiency map. As a result, the corresponding amount of power (P_{in}) consumed by the blower will be at its minimum (while still satisfying the increased desired flow rates). A decline in blower efficiency, therefore, can be used as one heuristic and intuitive measure of deviation from similitude. The results in Figure 4.6 show that blower efficiency does decline significantly as the preference parameter W is increased. This is particularly pronounced in the scenario where the blower is fixed, rather than resized.

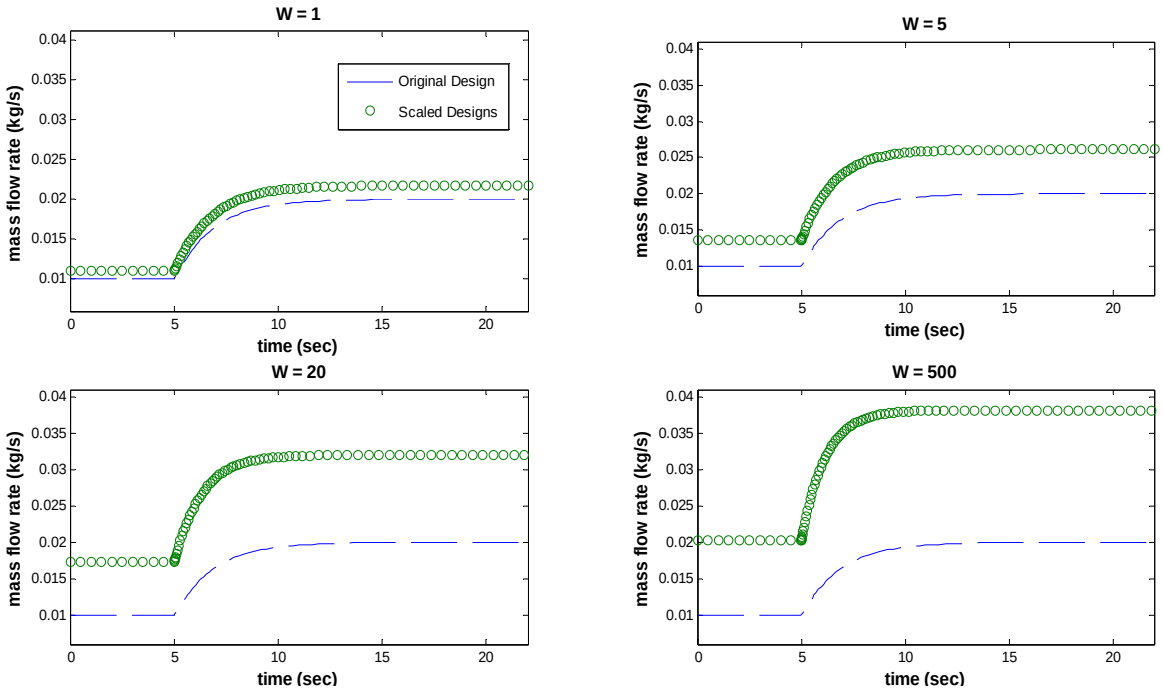

Figure 4.5: Mass flow rates of optimal scaled designs (fixed blower size)

[9] Because there are two levels of desired flow rates (i.e., 0.02 to 0.04 kg/s) which then give two values of blower operational efficiencies, the tradeoffs shown in Figure 4.6 are averages of the two efficiencies.

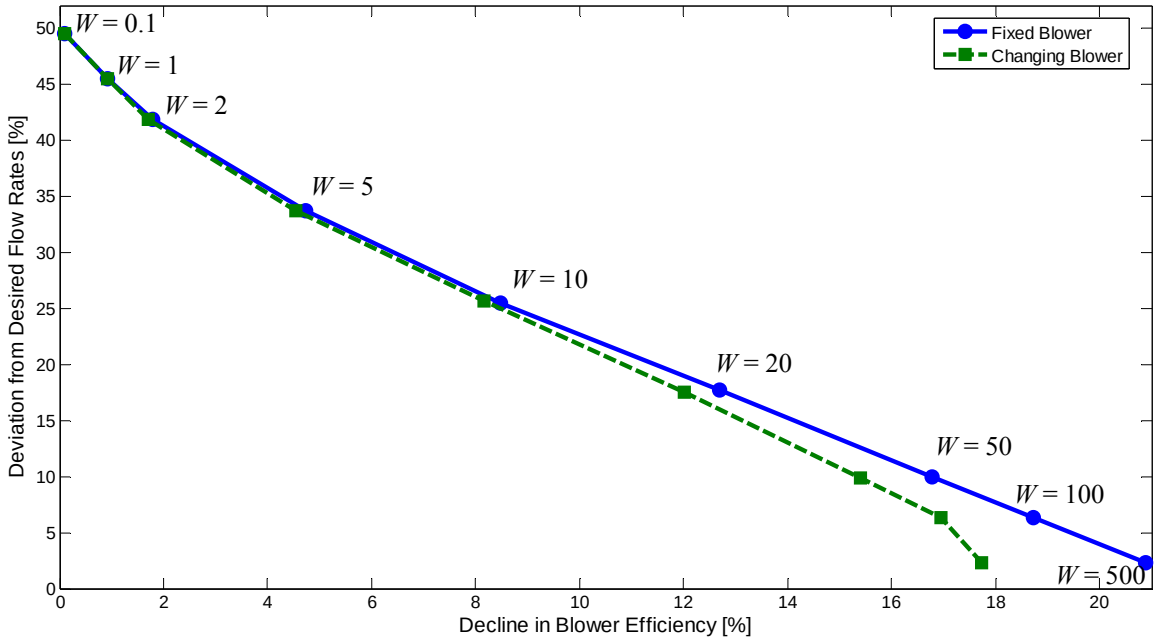

Figure 4.6: Design tradeoffs in air supply system scaling

The above results can be quite useful in determining the extent to which competing scaling criteria, such as the need for efficiency versus the need for increased air flow, can be accommodated. This is particularly true when other physical constraints are present, such as packaging constraints. Such constraints can render the scaling of a low-pressure system infeasible, and necessitate a high-pressure system instead. For instance, because the air supply system used in this work is based on the Ford P2000 fuel cell prototype vehicle [3] and low-pressure systems are commonly composed of components whose sizes are larger than those of the high-pressure systems [46] , the packaging constraint becomes the most critical one for this application. In particular, the size of the first nozzle's cross-sectional area ($A_{t,1}$) determines the diameter of the supply pipe installed underneath the vehicle. The size of this pipe must be carefully designed to allow for safe ground clearance. Based on the vehicle's dimensions specified in [52], the maximum allowable size of the first nozzle's area should remain below 0.045 m^2,

approximately. In both cases of the scaling problem considered herein (i.e., fixed blower and variable blower size), this packaging constraint places a limit which in turn causes the designs corresponding to $W \geq 50$ to be no longer feasible. This is shown in Figure 4.7 below which plots the first nozzle's cross sectional area ($A_{t,1}$) as a function of preference parameter (W).

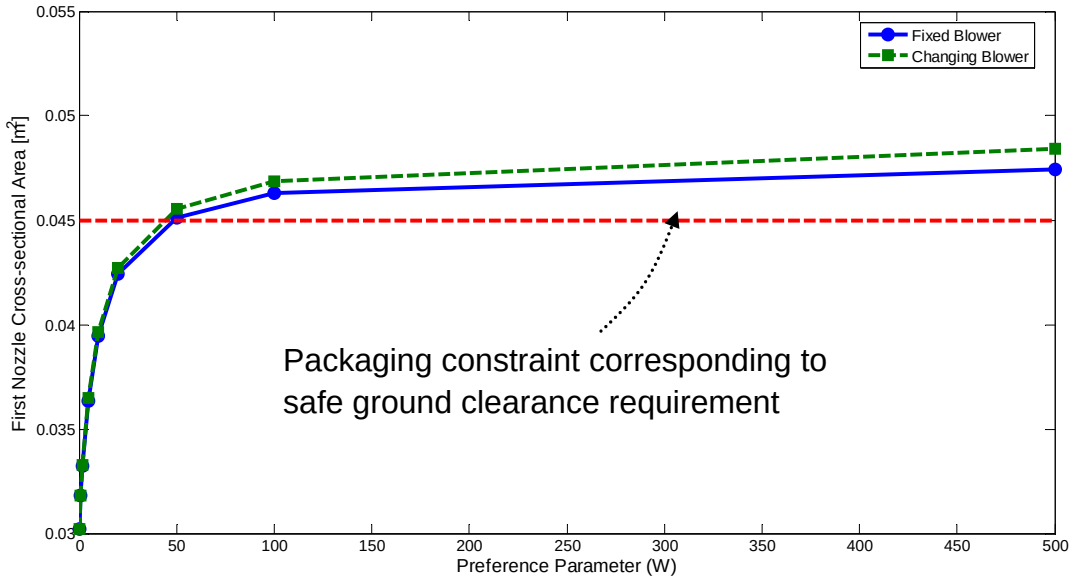

Figure 4.7: Influence of packaging constraints on scaling feasibility

With this finding, the following important conclusion can then be drawn from this scaling study: the low pressure system can only be *scaled* (as can be seen from Figure 4.6) to reach nearly *a twenty percent deviation* from the desired flow rates. This then implies that if larger flow rates (i.e., larger fuel cell power levels) are necessary, we might need to resort to the high-pressure system instead. Insights like this are difficult to obtain using a *discrete* definition of similitude: a fact which underscores the viability of the method proposed herein.

4.5 CHAPTER SUMMARY

This chapter extends the scaling technique developed in the previous chapters. In particular, it has been described that the literature proposes *similitude* as a technique for solving the problem of scaling a proven dynamic system to meet new design requirements. However, difficulties arise when some of the important scaling laws identified via similitude cannot be satisfied exactly. This often results from constraints on design properties such as space and packaging, and prevents the attainment of exact similitude. Difficulties also arise when one seeks to achieve multiple competing objectives, rather than just similitude, in scaling: a scenario not explicitly addressed by dynamic similitude-based scaling. To address these problems, this chapter develops the first *continuous* metric that can quantify the *proximity* of a given system to exact similitude. The metric combines dimensional and activity analyses to determine not only which scaling laws are violated by a given design, but also to what degree this violation may be important. The metric also has interesting graphical interpretations presented earlier in this paper. Using this *approximate similitude* metric, one can explicitly trade off the attainment of similitude versus the satisfaction of other scaling requirements and constraints. Thus, this chapter adds two key contributions to the literature. It quantifies approximate similitude for the first time, and it presents a multiobjective formulation of the approximate scaling problem, also for the first time. The viability of these contributions is demonstrated using two case studies, one focusing on quarter-car suspension system scaling and the other focusing on fuel cell air supply system scaling.

CHAPTER V

APPROXIMATE SIMILITUDE SCALING OF HMMWV

This chapter demonstrates the applicability of the scaling techniques developed in this dissertation to a complex nonlinear multibody dynamic model of the High Mobility Multipurpose Wheeled Vehicle (HMMWV or "Humvee"). In particular, the problem of scaling the HMMWV to enable it to carry additional rooftop loads will be investigated. Even though the HMMWV was originally designed to have exceptional maneuverability [53], the rollover propensity of the vehicle can significantly deteriorate due to these extra loads which increase the vehicle's C.G. height. It is shown that the approximate similitude scaling technique can used to determine how different components of the system should be redesigned in order to satisfy the load specification while simultaneously maintaining the critical dynamic performance of the vehicle. More specifically, the scaling study in this chapter focuses on making minimal design modifications to the vehicle to improve its rollover stability without involving major design changes, e.g., suspension mechanism redesign. The chapter's first section gives a brief introduction to the HMMWV dynamic model used in the study. Then, the scaling laws are summarized in Section 2. The chapter concludes by presenting the design trade-offs established from the scaling study as well as discussing insights that can be gained from these results.

5.1 MULTIBODY DYNAMIC HMMWV MODEL

The HMMWV is a four-wheel dual-use vehicle designed to provide combat, and service support roles. There are many different variants of this vehicle which are capable of accepting various body configurations to accommodate, for example, weapon systems and ambulance roles. Therefore, a high degree of mobility is necessary in both off-road and on-road situations [53]. The HMMWV model developed in this study utilizes bond-graphs as the modeling technique of choice [54]. This modeling paradigm (which can generally be categorized as a physical component-based technique) not only facilitates the use of our scaling technique, but is also known to promote commonality, reusability, hierarchical modeling as well as offer better physical insight into our system of interest [10, 55].

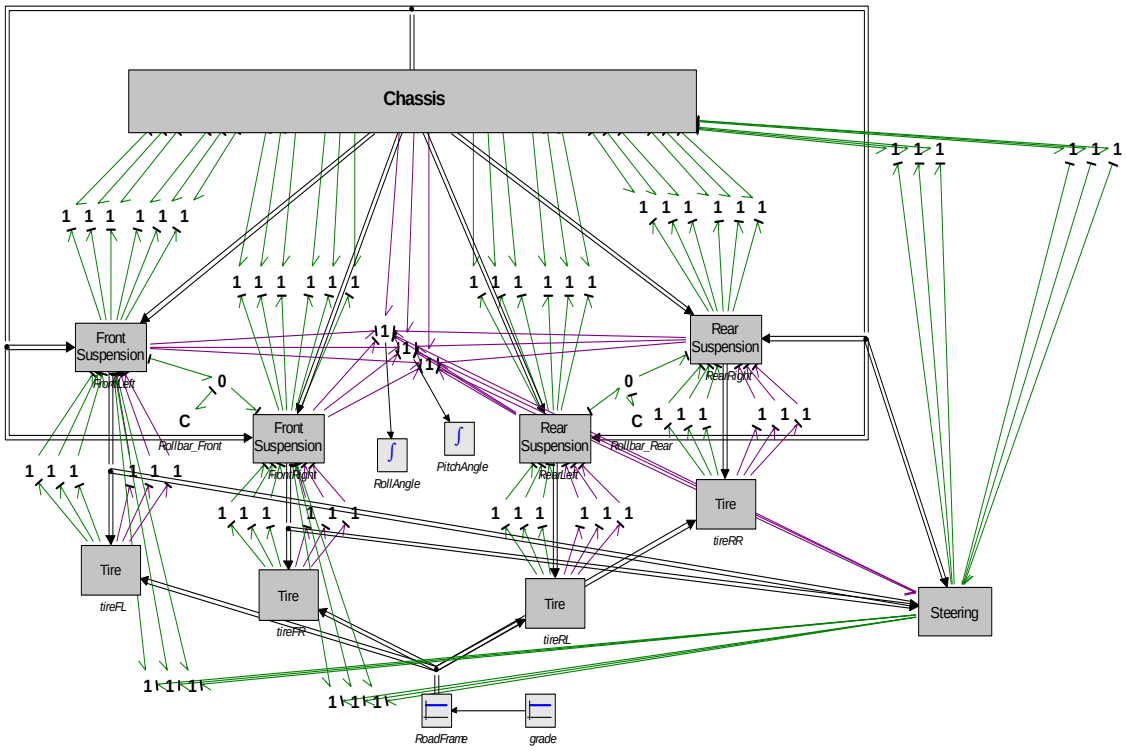

Figure 5.1: HMMWV model's main components

The main components included in the model are the chassis, front and rear A-arm suspensions, front and rear tires, steering system, and anti-roll bar effects. These sub-systems are shown in the top-level part of the model as illustrated in Figure 5.1 above (pictures showing implementation details of these sub-systems are given in Appendix C). The chassis body and suspension arms are represented by rigid bodies. These rigid bodies are assumed to be constrained through different types of joints and forces/moments. These connections also rely on the use of coordinate transformations and generation of position and orientation variables [10, 54]. The vehicle model, however, does not include the engine and powertrain systems. The inputs of the model are the steering angle input applied to the steering system's Pitman arm and rotational velocity inputs applied to the front wheels of the vehicle. A picture describing the configuration of the steering system in the model is also given in Appendix C.

The suspension stiffnesses and damping coefficients are assumed to be constant over the range of simulation, and so are the rollbar stiffnesses. The tire models implemented replicate a simple tire model used in the simulation software DADS [52] (see Appendix E for details of the tire slip models). The entire HMMWV model has 360 states and 605 parameters. The nonlinearities in the model come from the nonlinear constraining forces, the three-dimensional rigid body kinematics, etc. The key parameters of the original model are given in Table 5.1.

The vehicle-fixed coordinate frame of the HMMWV model is defined with reference to a right-hand orthogonal coordinate system as follows:

- The positive x-axis points forward on the longitudinal plane of symmetry
- The positive y-axis goes out the left side of the vehicle

- The positive z-axis goes out upward with respect to the vehicle
- Roll, pitch, and yaw constitute rotations around x, y, and z axis respectively.

Parameter	Value
Chassis Mass	3514 kg
Chassis Inertia [I_{xx},I_{yy},I_{zz}]	[1504, 5950, 6357] kg.m^2
CG Height	1.16 m
Wheelbase	3.20 m
Track Width	1.80 m
Front Spring Rate	250 kN/m
Rear Spring Rate	300 kN/m
Wheel Radius	0.461 m
Vertical Tire Stiffness	1.3 x 10^5 N/m
Cornering Tire Stiffness	1.0 x 10^5 N/rad

Table 5.1: Default HMMWV key parameters

The driving scenario characterized by the two inputs, i.e., steering and wheel rotational velocity inputs, is shown in Figure 5.2 and Figure 5.3 below. The steering profiles are chosen such that the driving aggressiveness continuously increases over the maneuver. This driving pattern has been extracted from statistical data and deemed sufficiently realistic to represent a human driver's aggressiveness [56]. This renders these profiles suitable for a rollover type of study.

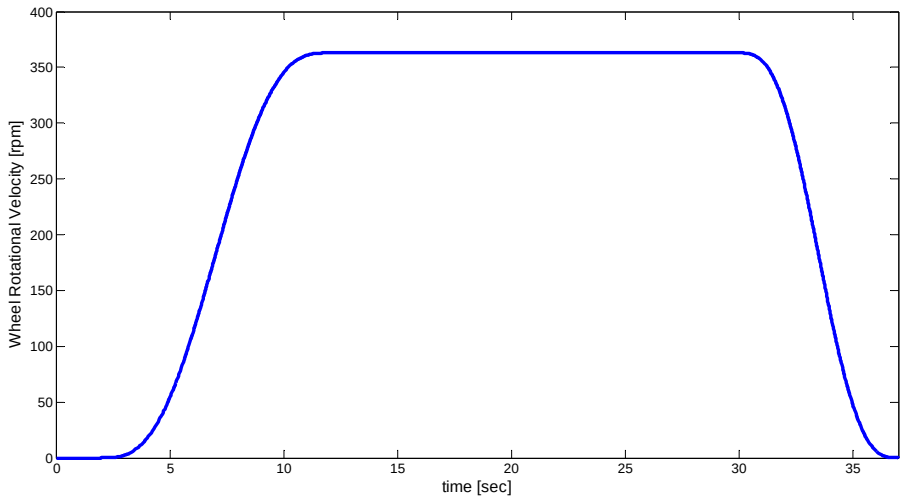

Figure 5.2: Wheel Rotational Velocity Input Profile

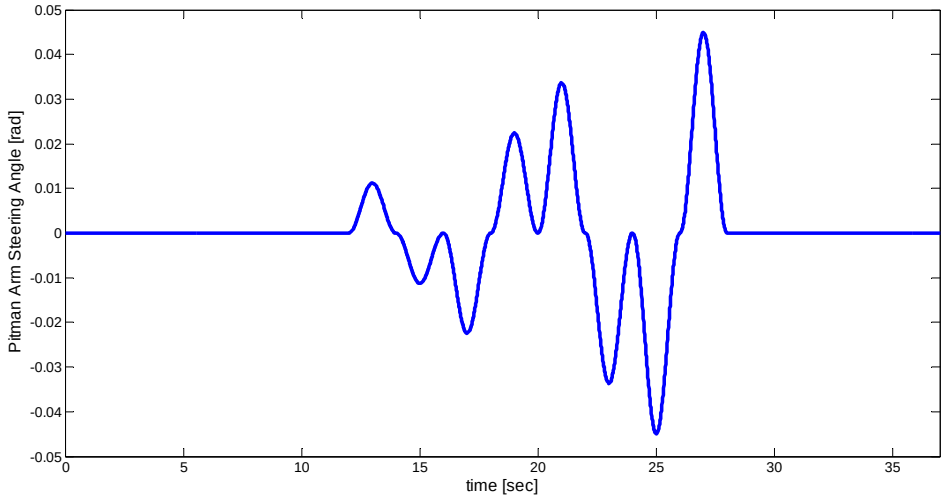

Figure 5.3: Pitman Arm Steering Angle Input

5.2 HMMWV SCALING LAWS

Despite a large number of states and parameters in the HMMWV model, one can group these variables into categories in the derivation of scaling laws. It turns out, for this

model, that these variable categories are either in the mechanical domain (force-velocity) or rotational domain (torque-rotational velocity).

In this chapter, the symbols in the first column of Table 5.2 are used to represent the corresponding sets of variables. For instance, the Mass category (M) contains all of the variables whose fundamental unit is [M]. This variable classification allows us to readily apply dimensional analysis and derive scaling laws of this rather complex system.

Variable Category	**Categorical Name**	**Fundamental Units**
M	Mass	[M]
x	Displacement	[L]
v	Linear Velocity	$[LT^{-1}]$
a	Acceleration	$[LT^{-2}]$
I	Inertia	$[ML^{2}]$
θ	Angle	[-]
ω	Angular Velocity	$[T^{-1}]$
K	Stiffness	$[MT^{-2}]$
B	Damping	$[MT^{-1}]$
t	Time	[T]
C_a	Tire Lateral Stiffness	$[MLT^{-2}]$

Table 5.2: Categories of variables in HMMWV model

All of the 11 variable categories in Table 5.2 can be measured in terms of 3 fundamental units. Therefore, by Buckingham's Pi Theorem, the corresponding number of dimensionless (Pi) parameter categories is 11-3 = 8. The choice of these Pi parameters is not unique, but one possible selection is given below:

$$\pi_1 = \frac{I}{Mx^2} \ , \ \pi_2 = \frac{aM}{xK} \ , \ \pi_3 = \frac{B}{m^{1/2}K^{1/2}} \ , \ \pi_4 = \frac{\omega M^{1/2}}{K^{1/2}}$$
$$\pi_5 = \frac{tK^{1/2}}{M^{1/2}} \ , \ \pi_6 = \frac{vM^{1/2}}{xK^{1/2}} \ , \ \pi_7 = \frac{C_a}{Kx} \ , \ \pi_8 = \theta \tag{5.1}$$

Next, as previously illustrated in Chapter 3, these dimensionless parameters result in the following scaling laws:

$$\lambda_I = \lambda_M \lambda_x^2 \ , \ \lambda_a \lambda_M = \lambda_x \lambda_K \ , \ \lambda_B = \lambda_M^{1/2} \lambda_K^{1/2} \ , \ \lambda_K = \lambda_M^{1/2} \lambda_\omega$$
$$\lambda_t = {\lambda_M^{1/2}}\Big/{\lambda_K^{1/2}} \ , \ \lambda_v = {\lambda_x \lambda_K^{1/2}}\Big/{\lambda_M^{1/2}} \ , \ \lambda_{C_a} = \lambda_x \lambda_K \ , \ \lambda_\theta = 1 \tag{5.2}$$

For the design scaling study of the HMMWV, it is assumed that we need to comply with the following specifications:

1) The vehicle follows the same speed profile and steering maneuver. This results in $\lambda_v = 1$ and $\lambda_\theta = 1$.
2) The time scale of the simulation does not change, i.e., $\lambda_t = 1$.

These assumptions simplify the scaling laws in Equation 5.2 into the following:

$$\lambda_{C_a} = \lambda_M = \lambda_B = \lambda_K = \lambda_I = S$$
$$\lambda_a = \lambda_v = \lambda_x = \lambda_\theta = 1 \tag{5.3}$$

where S denotes the scaling factor variable needed in the scaling. It is worth noting the scaling laws above imply, in similitude scaling, that all of the physical dimensions of the vehicle should remain the same. That is, for instance, the track width, wheel base, and suspension arm lengths can be left identical to those of the original design. It is interesting to see that the first set of the "categorical" scaling laws in Equation 5.3 is

quite similar to those obtained for the 2-DOF quarter-car system with the only difference being the presence of the lateral stiffness categorical scaling factor.

One can see from the scaling laws in Equation 5.3 that the possibility of scaling this vehicle design, while maintaining absolute dynamic similitude is very difficult to achieve practically. First of all, it is almost impractical to presume that the designer has the luxury of freely changing all inertial, compliance, and damping parameters. More specifically, our design specification requires an extra load added to the vehicle. This added load, in turn, changes the CG height of the vehicle, thereby making a violation of the last scaling law in Equation 5.3 inevitable. These observations clearly attest to the need to resort to the approximate similitude scaling technique developed in this dissertation. To this end, the components necessary to construct the approximate similitude formulation of this HMMWV study are described in the subsequent sections.

5.3 USING ACTIVITY ANALYSIS TO ASSESS RELATIVE IMPORTANCE OF SCALING LAWS

The researchers in [43] show that the selection of the time window over which activities are calculated depends on which behavior of the system is of our interest. As a result, because our design scaling study of the HMMWV focuses on the rollover aspect of the vehicle, the time window over which activities in the model are calculated is chosen to include only the period where the steering input is in use. This corresponds to the 12-28 second time interval in Figure 5.3.

It is also important to note that some of the parameters appearing in the system scaling laws do not hold a one-to-one relationship with the bond-graph elements in the model. The chassis mass parameter, for instance, is considered as part of the three inertial elements in the translational dynamics block of the chassis sub-model, while, the x-component chassis inertia appears in only one inertial element in the rotational dynamics block. Similar to the fuel cell air supply system considered in the previous chapters, to evaluate the importance of scaling laws, the values of elements' activities need to be "post processed" in order to associate them with the existing parameters. The methods employed for such post-processing are explained in Appendix D. The methods also assume that the right and left vehicle components are symmetric, e.g., the right and left spring rates are constrained to be identical. The ranking of the parameters whose activity indices collectively contribute to approximately 99 percent of the overall activity index is given in Table 5.3.

Parameter	Activity Index [%]
Body Mass (M_{Body})	37.896
CG Height (X_{CG})	19.087
Rear Tire Lateral Stiffness ($C_{a,R}$)	10.481
Front Tire Lateral Stiffness ($C_{a,F}$)	7.675
Rear Spring Rate ($K_{Susp,R}$)	5.103
Front Spring Rate ($K_{Susp,F}$)	3.322
Front Wheel Hub Mass ($M_{Hub,F}$)	0.871
Rear Wheel Hub Mass ($M_{Hub,R}$)	0.815
Front Wheel Mass ($M_{Wheel,F}$)	0.811
Front Lower Arm Mass ($M_{LA,F}$)	0.804
Rear Wheel Mass ($M_{Wheel,R}$)	0.77
Rear Lower Arm Mass ($M_{LA,R}$)	0.738
Rear Rollbar Stiffness ($K_{Rollbar,R}$)	0.598
Rear Tire Stiffness ($K_{Tire,R}$)	0.589
Front Rollbar Stiffness ($K_{Rollbar,F}$)	0.373
Z-axis Body Principal Moment of Inertia (I_{zz})	0.346
Y-axis Tire Principal Moment of Inertia ($I_{Tire,YY}$)	0.343
Front Tire Stiffness ($K_{Tire,F}$)	0.322
Front Upper Arm Mass ($M_{UA,F}$)	0.114
Rear Suspension Damping ($B_{Susp,R}$)	0.112
Rear Upper Arm Mass ($M_{UA,R}$)	0.105
Front Suspension Damping ($B_{Susp,F}$)	0.089
Rear Tire Damping ($B_{Tire,R}$)	0.018
Front Tire Damping ($B_{Tire,F}$)	0.0127
X-axis Body Principal Moment of Inertia (I_{xx})	0.012

Table 5.3: HMMWV parameter importance ranking

Since the last scaling law in Equation 5.3 suggests that the parameters associated with physical length dimensions (e.g., suspension arm lengths, wheel base) be kept at their original values to satisfy similitude. Then, it makes sense that in our scaling study that these parameters are not part of the design parameter set and, therefore, can be neglected from the similitude objective as well as the relative importance analysis.

5.4 FORMULATION OF SIMILITUDE AND DESIGN OBJECTIVES

In this HMMWV design scaling study, the design requirement is set up to reflect the situation in which an extra weight is added to the vehicle's roof. This specification yields the following design objective (F_d):

$$F_d = W(\lambda_{M_{Body}} - \lambda_{M_{Body,desired}})^2 \tag{5.4}$$

where W represents the importance weighting placed on the design objective to vary its importance with respect to the similitude objective, and $\lambda_{M_{Body,desired}}$ denotes the ratio of the desired chassis mass (including the weight of the added roof-top mass) over the nominal chassis mass. This desired added mass is assumed in our problem to be 15 percent (or approximately 530 kg) of the original chassis mass.

The categorical notion introduced earlier in Section 5.2, again, enables us to represent the similitude metric by using different summations of the activity-weighted deviations of the scaling laws as shown below:

$$\begin{aligned} F_S = {} & \sum_{i=1}^{k_M} A_{M_i}(\lambda_{M_i} - S)^2 + \sum_{j=1}^{k_B} A_{B_j}(\lambda_{B_j} - S)^2 + \sum_{l=1}^{k_K} A_{K_l}(\lambda_{K_l} - S)^2 + \\ & \sum_{m=1}^{k_m} A_{C_{a,m}}(\lambda_{C_{a,m}} - S)^2 + \sum_{n=1}^{k_n} A_{a_n}(\lambda_{a_n} - 1)^2 + \\ & \sum_{p=1}^{k_p} A_{v_p}(\lambda_{v_p} - 1)^2 + \sum_{q=1}^{k_q} A_{X_q}(\lambda_{X_q} - 1)^2 \end{aligned} \tag{5.5}$$

where, for instance, A_{M_i} and λ_{M_i} denote the activity relative importance and scaling law associated with the i[th] mass parameter respectively.

Note that, based on the findings in the previous chapters; an exclusion from the similitude metric of the unimportant scaling laws should not significantly penalizing

dynamic similitude and, therefore, will not affect much the accuracy of the similitude metric in Equation 5.5. It is for this reason that the similitude objective of this problem can be greatly simplified to account for only the important parameters and preclude those less important ones not appearing in Table 5.3.

Furthermore, the change in CG height of the vehicle and the amount of added roof-top load are coupled and constrained via the following relationship:

$$\Delta X_{CG} = \frac{X_{roof} M_{added}}{M_{Body,nom} + M_{added}} \tag{5.6}$$

where X_{roof} is the height at which the added load is placed with respect to the nominal CG and $M_{Body,nom}$ is the nominal mass of the vehicle. It is then assumed that the added load (M_{added}) does not significantly affect the value of z-axis principal inertia of the chassis (I_{zz}) and can be neglected, while its effect on the x-axis principal moment-of-inertia is constrained through the parallel-axis theorem [57] expressed as follows:

$$I_{xx,new} = I_{xx,nom} + M_{Body,nom}\Delta X_{CG}^2 + M_{added}(X_{roof} - \Delta X_{CG})^2 \tag{5.7}$$

Note that the change in I_{yy} is not accounted for because the activity associated with I_{yy} does not make the ranking as shown in Table 5.3. These two coupling constraints in Equations 5.6 and 5.7 again highlight the fact that similitude scaling of this vehicle system is not possible and, therefore, the approximate similitude framework should be of use in this study.

5.5 APPROXIMATE SIMILITUDE SCALING RESULTS

The formulations of the design and similitude objective functions allow us to utilize the multiobjective scaling tool previously developed in Chapter 4 to determine the trade-offs between approximate similitude and the competing design requirement. In particular, the four scaling design runs illustrated in Table 5.4 are considered where different components in the model are allowed to be modified to accommodate the scaling:

Components	Run 1	Run 2	Run 3	Run 4
Tires	Scalable	*Fixed at original*	Scalable	Scalable
Suspension spring rates and suspension dampers	*Fixed at original*	Scalable	Scalable	Scalable
Rollbar stiffnesses	*Fixed at original*	Scalable	Scalable	Scalable
Masses of suspension arms and wheels	*Fixed at original*	*Fixed at original*	*Fixed at original*	Scalable

Table 5.4: Scaling study scenarios

Further, one can see from Equations 5.2 and 5.3 that exact similitude scaling in this problem allows the designer to be able to preserve the quantities of which dimensions are angle, velocity, as well as acceleration. This ability becomes very valuable in this context because it maintains the time responses in roll angle, yaw rate and lateral acceleration of the original vehicle design. These responses are commonly known to be important factors in defining a vehicle's rollover stability [50, 58]. However, as explained earlier in Section 5.2, exact similitude scaling of this problem is not always feasible from a practical design point of view. To this end, the approximate similitude framework

(described by Equations 5.4 to 5.7 and Equation 4.3) is employed and the results are discussed as follows. By varying the importance weighting (W) in Equation 5.4, different Pareto optimal solutions [49] are obtained and the trade-offs between satisfying the design requirement and deviation from similitude are unveiled in Figures 5.4 – 5.6 below. As suggested by Equation 5.3, similitude in this context can be heuristically measured by the increases of the maximum roll angle, yaw rate, and lateral acceleration from their original values.

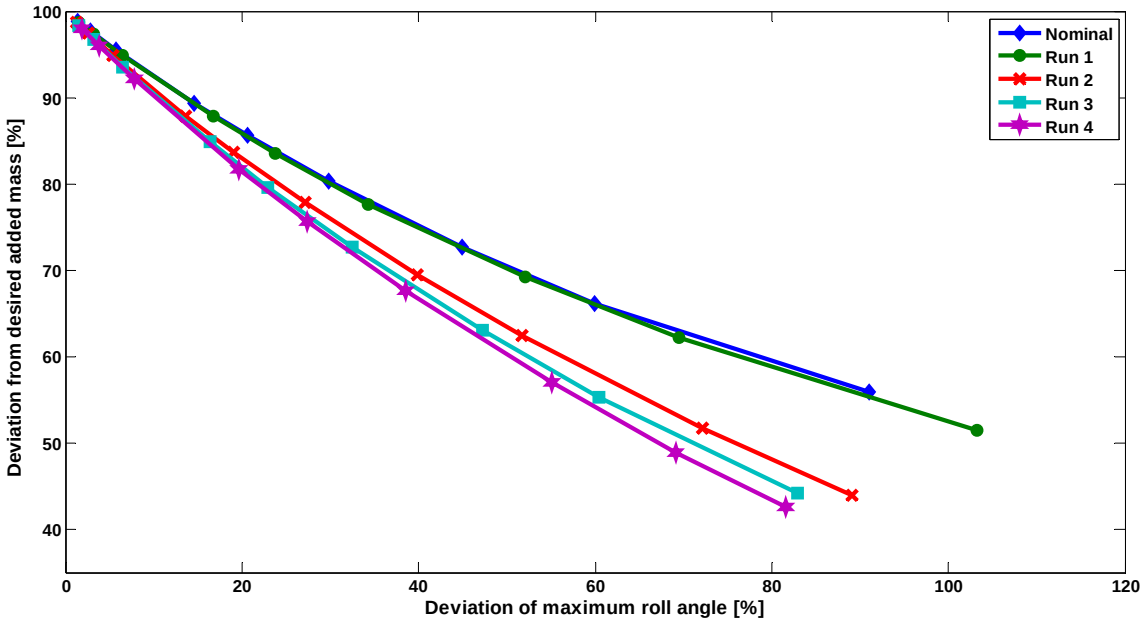

Figure 5.4: Trade-off between maximum roll angle and added mass

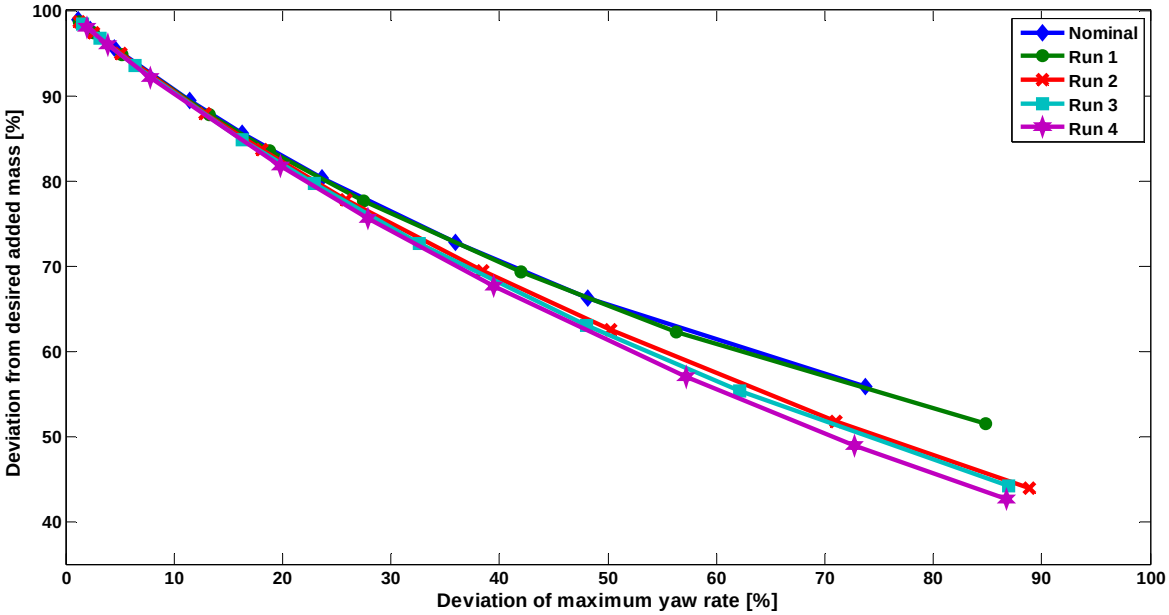

Figure 5.5: Trade-off between maximum yaw rate and added mass

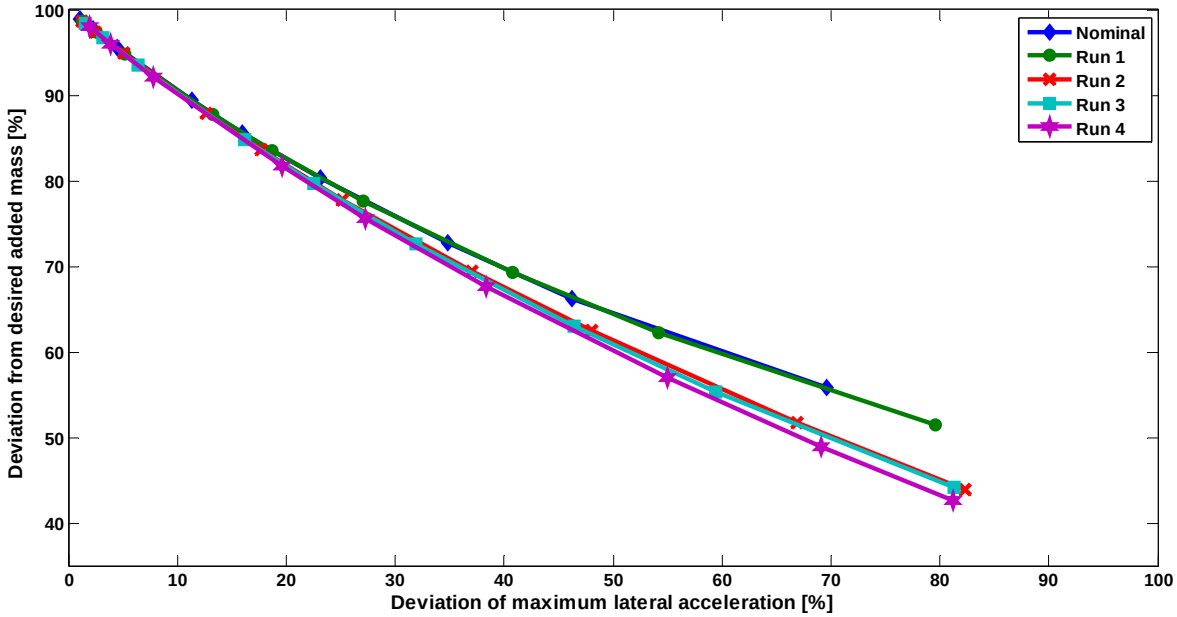

Figure 5.6: Trade-off between maximum lateral acceleration and added mass

In addition to the four design runs described in Table 5.4, the trade-offs of the nominal design where no component is allowed to scale are also appended to the above figures (denoted by "Nominal"). According to the concept of Pareto optima [49, 59], the design space on the right of each curve denotes the corresponding feasible design solutions which are dominated by the design solutions represented by the curve. Further, based on the notation used to present these trade-off curves above, one can see that any right-to-left shifting of the curves implies a smaller deviation of maximum roll angle (or yaw rate, or lateral acceleration) from the original value. This means that the vehicle's rollover safety is improved. With this in mind, some very interesting remarks which can be made from Figures 5.4 – 5.6 are:

1) Comparing Runs 3 and 4 indicates that the scaling of suspensions springs, dampers and anti-rollbars seems to offer us greater gains in terms of our ability to add the roof-top mass when compared to the scaling of unsprung masses.

2) The trade-off curves in these figures cannot "penetrate" further to the right because of the rollover constraint. That is, the right end point of every trade-off curve represents the vehicle design which is on the verge of rolling over and adding any more mass to the vehicle will cause it to rollover.

3) The setup in Run 2 can reflect the situation where the vehicle is equipped with active suspension and anti-rollbar equipment. The installation of such equipment enables the vehicle to operate along the Pareto curves when subject to different added weights.

4) An addition of more scaling components does not necessarily guarantee that the deviations in the critical rollover factors (as shown in Figures 5.4 – 5.6) are kept closer to the original values. This can be observed through the fact that all of the trade-off curves in Figures 5.4 – 5.6 shift only minimally from right to left when the nominal case is compared to Scenario 1. On the other hand, the curves seem to shift to a greater extent, when the suspension components are added to the scaling list.

These remarks are discussed as follows: The first remark can be explained by considering the importance ranking in Table 5.3 which indicates that the influence of the suspension springs, dampers, and rollbars are collectively greater than the unsprung masses. For this reason, one can expect to benefit more from the ability to scale these suspension components. The second remark highlights the fact that if one needs to better satisfy the design specification (i.e., adding a heavier mass to the roof) and avoid rolling-over, some extra components in the vehicle have to be made scalable. For example, the track width of the vehicle might have to be lengthened. The third remark features the advantage which one can gain from implementing active-safety equipments (i.e., active anti-rollbars and suspensions). Such information should become very useful when the designer needs to decide whether or not he/she should install these advanced and costly equipments.

The fourth remark highlights the fact that the change in the tire properties does not seem to have much of an effect on the rollover properties of the vehicle. This can be explained by first noting that the rollovers which are presented in Figures 5.4 -5.6 above are the type of rollover induced by an excessive chassis roll angle and lateral force which

normally happens with the vehicles with high CG heights (e.g., HMMWV, sport-utility vehicles) [50]. Since the tire characteristics do not directly affect the movement of the vehicle body and, therefore, any changes in its parameters can be considered secondary for this type of rollover. In addition, this finding also demonstrates that, under some circumstances, activity cannot be used to quantify the relative importance of scaling laws accurately. Recall that activity, by its nature, is a metric that quantifies the importance of each component toward the *overall* dynamics of the system. It does not, however, capture the dependence of each component on any particular behavior or output of the system. For these reasons, the tire lateral stiffnesses which can be regarded as an important factor in other types of instability studies (e.g., sideway skid) still appear very high in activity ranking of this HMMWV model but does not contribute to the rollover responses considered in this chapter.

Lastly, it is very interesting to note that the evaluation of the design and similitude objectives to obtain Pareto optimal solutions does not rely on the use of the simulation model. The simulation is run "offline" only to eventually check the rollover stability of each optimal design. On the other hand, if one were to set up a traditional design optimization problem to minimize, for example, the maximum roll angle; he/she would need to include the simulation model during each optimization iteration. This inclusion definitely renders the design problem at hand more computationally expensive. Therefore, the luxury of being able to run the simulation model offline should allow the designer to be able to use the similitude objective, in particular, as a very computationally efficient method to estimate the extent to which the redesigned vehicle's characteristics deviate from those of the original model. This again attests to the fact that our scaling

methodology, in many circumstances, has the potential to be a great aid to traditional design optimization techniques which are generally more computationally intensive.

5.6 CHAPTER SUMMARY

This chapter demonstrates the applicability of the scaling techniques developed in this dissertation to a complex nonlinear dynamic model. Despite the complexity, the application of the Pi theorem to derive scaling laws is made rather easy by systematically classifying the variables into different categories. The presence of the physical constraints due to the added mass highlights the need for us to resort to the approximate scaling framework. The use of the activity metric to identify the less important parameter proves to be very beneficial in reducing the number of parameters needed to be accounted for in the similitude metric.

The results of this case study also reveal limitations of the activity metric, when dealing with complex systems, in determining which components are more important under some specific circumstances. In particular, activity fails to recognize that the tires become less important when the scenario of interest is rollovers induced by excessive body roll movements. Nevertheless, this finding does not break down the framework that has been developed in this dissertation. Instead, this should be considered as a warning signal that a more sophisticated metric to quantify the relative importance of scaling laws may be needed which can more accurately capture such importance, but this new metric is very likely to be less computationally efficient compared to activity – yet another trade-off to be decided.

CHAPTER VI

SUMMARY, CONTRIBUTIONS, AND FUTURE WORK

6.1 SUMMARY

A new design scaling methodology is developed in this dissertation. This methodology takes a design and adapts it to meet new requirements or operate in a new environment. This scaling notion is potentially useful because it focuses mainly on retaining existing desirable characteristics of the original "tested" design as closely as possible through minimal design modifications. More specifically, the methodology is more efficient than the ones existing in the literature for the following reasons.

First, it furnishes the similitude-based scaling method with the activity metric to identify the importance of each system scaling law. Activity, a monotonically-increasing aggregate measure of power flows, was chosen because of its computational advantage and justification as a tractable importance metric. This innovative combination of the similitude and activity notions adds more flexibility in scaling by allowing the designer to neglect the scaling of the least important parameters.

Second, the next step is taken to consider the situation in which the components that have been identified to be more important by activity cannot be scaled as per the scaling laws. This situation creates a need for us to build a metric that continuously

quantifies the degree to which the scaled design is close to satisfying the discrete definition of exact similitude. In order to capture the relative importance of scaling laws, this metric, named the "approximate similitude" metric, also incorporates the information identified previously by activity in the first part of this work. The notion of similitude hypersurface is also introduced to facilitate in the development of the metric as well as to offer better mathematical insight. The validity of the approximate similitude metric is justified through the results obtained in various case studies. It has been observed through these studies that the similitude metric seems to correlate well with the deviations of invariant properties from their original values.

Third, the inability to scale the more important components according to the scaling laws implies that one cannot completely retain the desirable characteristics of the original design. With this in mind, one can take the approximate similitude metric and incorporate it into a multiobjective scaling framework which also accounts for other competing design requirements. This framework ultimately allows the designer to see the trade-offs between the ability to keep the desirable characteristics close to those of the original system versus the ability to satisfy the imposed design requirements.

Three different case studies are conducted to demonstrate how to use the methodology and framework developed as well as the important perspectives the results provide. The first case study is a simple single-domain two-degree-of-freedom quarter car system. The benefits gained from being able to neglect the least important scaling laws are clearly demonstrated through this case study. Additionally, despite its simplicity, this system plays an important role in illustrating the idea of approximate similitude metric as explained earlier in Chapter 4.

The second case study represents a simplified version of a fuel cell's air supply system which is a nonlinear multi-domain problem. The design goal of this case study is to increase the air flow rates going through the system. The physical constraints encountered in this problem motivate the need for developing the approximate similitude metric. Upon applying the approximate similitude framework, the corresponding similitude objective has an interesting aspect different from the quarter car system. That is, the similitude hypersurface in this case is two-dimensional. The results obtained in this problem show that the approximate similitude framework can help one trade off the ability to maintain a desirable characteristic demonstrated by blower operational efficiency against the ability to satisfy the desired flow rates.

The final case study represents a complex nonlinear multibody dynamic vehicle model. The objective of the scaling in this case is (i) to maintain the rollover behavior of the vehicle, while (ii) adding some extra load to the roof. The first part of the objective is captured by the similitude metric, while the second part is captured by the design objective. The formulation of this scaling study shows the usefulness of activity to reduce the number of parameter needed to be accounted for in the similitude metric. Furthermore, the use of the similitude objective in this problem offers an advantage over the traditional optimization approach in that it does not require the vehicle model to be simulated to obtain the trade-off solutions. This essentially alleviates the heavy computational cost that usually incurs from optimizing a very complex system.

6.2 LIMITATIONS AND ASSUMPTIONS

The method developed in this work, when applied to the model of a system, presumes that that model stays valid within the ranges of scaled parameters. In other words, the changes in the scaled parameters cannot violate any of the assumptions originally accounted for in the model. For instance, one can manipulate geometric parameters in a fuel cell stack system such that a flooding phenomenon occurs. The scaling technique will fail, in this case, if such a phenomenon is not captured originally by the model. One way to prevent this from happening is to assure that the scaled parameters are changed within the bounds over which our model does not lose its validity.

It is important to note that term "original" design which was used very often in the context of this dissertation is assumed to imply that this design has been developed until it possess the characteristics which are worthwhile to retain in scaling. However, the methodology in this work does not fail if this assumption does not hold. It only means that the scaled design that we obtain will probably not be of great value.

The continuous quantification of approximate similitude in this work is developed based on the premise that this quantity can be assessed using an activity-weighted distance from a design point to the similitude-hypersurface. Due to the characteristic of such a distance, an implicit assumption made here is that the degree of approximate similitude does not change dramatically in the vicinity of the similitude-hypersurface and, therefore, can be well approximated by such a distance.

Since the activity metric was limited to systems which can be modeled as discrete elements, our scaling methodology at its current stage is applicable only to such a model

classification. Nevertheless, the potential of adapting the method and making it applicable to systems described by partial differential equations definitely exists.

Even though the results from the HMMWV case study show that activity does not succeed in quantifying the influence of some components under the rollover scenario of interest, the formulation of the similitude metric as well as the multiobjective scaling framework are still valid and can, therefore, be readily improved if a more efficient metric is implemented to more accurately capture the influence of scaling laws.

6.3 CONTRIBUTIONS

The significant contributions to which this dissertation has made are summarized as follows:

More Efficient Method to Asses Importance of Scaling Laws

In contrast to sensitivity analysis, the use of activity to quantify the relative importance of scaling laws allows the designer to obtain such information from only one run of simulation. This advantage clearly helps mitigate the computational burden resulting from sensitivity analysis.

Quantitative Continuous Definition of Approximate Similitude

The definition of approximate similitude developed in this work makes it possible to evaluate the degree to which two designs are close to satisfying the existing discrete definition of exact dynamic similitude. This quantification can also be presented using a graphical notation, thereby facilitating the visualization of this similitude metric itself.

Multiobjective Scaling Framework

The development of the approximate similitude quantification consequently helps equip the designer with a tool to scale a system design whose desirable characteristics cannot be perfectly maintained via similitude alone. This also allows the designer to see the trade-off between the deviations of the desirable characteristics from their original values and the extent to which the design requirement is achieved. This trade-off information reveals the limitation of the system that one can achieve from scaling and therefore can be during the system redesign process. In addition, it is worthwhile to note that the evaluation of the approximate similitude metric does not entail the use of simulation model since the metric is expressed only in terms of the system parameters. As a result, the metric can become, in and of itself, an easy-to-evaluate method to get a quick estimate of how a scaled design candidate would perform in comparison to the original design. Alternatively stated, our approximate similitude metric allows for quick efficient benchmarking of different potential scaled designs.

6.4 FUTURE WORK

This work has not only developed new research ideas but also leveraged many tools which are either existing in the literature or commonly used in engineering. For this reason, it is hoped that this work can lead to many different exciting avenues briefly summarized as follows:

Applicability of the Approximate Similitude Metric in Physical Testing Paradigm

The principle of similitude has been a mainstay in helping the engineer to scale the test results of a scaled prototype back to its actual-sized counterpart. Such scaling is often subject to the same type of dilemma as considered in this work. That is, physical constraints can prevent perfect similitude to be achieved. For this reason, it would be interesting to see if the approximate similitude metric developed herein can help improve the results obtained from the non-similitude prototypes so that they better represent the actual-sized system.

Achieving a Better Degree of Similitude through Controls

It has been shown by other researchers that attainment of similitude, in linear systems theory, is equivalent to having the same open-loop pole and zero locations [32, 33, 37]. Based on this line of thoughts, there should be a possibility for one to implement a control strategy to help move the poles and zeros of the scaled design closer to those of the original design, thus achieving a better degree of similitude. In addition, the HMMWV scaling case study implies that if we have at our disposal an adaptive spring-damper-antirollbar system, then the scaled adaptive vehicle's behavior can trace along the trade-off curves (Figures 5.4 – 5.6), thereby minimizing the rollover propensity when the vehicle has to be subject to different values of roof-top loads. This motivates the idea that having an adaptive control system can potentially be very beneficial from a similitude-scaling standpoint.

Improving the Scaling Laws Relative Importance Metric

Even though activity is very computational efficient, it was not originally developed especially as a metric to quantify the overall importance of system components. Its limitations in pointing out the correct important components are clearly present in Chapter 5. To this very end, there has recently been work done in improving the ability of this metric to better quantify such importance [60]. Additionally, there also are other techniques in the literature that can also become candidates suitable for this task [61, 62]. Replacing activity with a better importance metric will certainly improve the accuracy of the methodology in identifying which components can be judiciously neglected in scaling. In addition, this replacement should also help one discover the designs which achieve better trade-offs than those obtained from the activity-based formulation.

APPENDICES

APPENDIX A

FORMAL STATEMENT OF BUCKINGHAM'S PI THEOREM AND A GENERLIZATION OF SIMILITUDE PRINCIPLE

A.1 FORMAL STATEMENT OF BUCKINGHAM'S PI THEOREM

Let $a_1, a_2, a_3, ..., a_n$ be physical quantities such that the p first ones are expressed in terms of different fundamental units, and the last $(n-p)$ quantities are referred to units derived from the p fundamental units. If among these n quantities there exists a relation

$$F(a_1, a_2, ..., a_n) = 0 \tag{A.1}$$

that holds for any choice of the fundamental units, this relation can be transformed into another with no more than $(n-p)$ parameters that are of zero dimensions, i.e.

$$f(x_1, x_2, ..., x_{n-p}) = 0 \tag{A.2}$$

The parameters $x_1, x_2, ..., x_{n-p}$ are monomial functions of $a_1, a_2, a_3, ..., a_n$ (for example, $x_1 = A a_1^{\alpha_1} a_2^{\alpha_2} ... a_n^{\alpha_n}$). The proof of this theorem can be found in Bridgman [12].

A.2 A GENERALIZATION OF SIMILITUDE PRINCIPLE

It is obvious from the above statement of Buckingham's Pi theorem that the notions of *fundamental dimensions* and *fundamental units* are central to the theorem. The theorem, however, does not designate how the fundamental units of a problem should be selected; neither does it indicate how many of them are needed. To answer these questions, Moran [44] has generalized the similarity concept into mathematical forms that do not require the *a priori* selection of fundamental dimensions. The forms were

developed based on element group theory, and this generalization's connections to traditional Buckingham's Pi theorem can be summarized as follows:

Suppose that a system by the following equation:

$$u_j = I_j(x_1, \dots, x_m)$$

where $x_1,\dots,x_m$ denote the inputs or design parameters of the system, and $u_1,\dots,u_n$ denote its outputs. Furthermore, consider the r-parameter groups of scale changes, S_r, G_r, defined as follows:

$$G_r: \begin{Bmatrix} S_r: \overline{x_i} = a_1^{b_{i1}} \dots a_r^{bir} x_i & (i = 1, \dots, m, m \geq 1) \\ \overline{u_j} = a_1^{c_{i1}} \dots a_r^{cir} u_j & (j = 1, \dots, n, n \geq 1) \end{Bmatrix}$$

Next, suppose that the systems' governing equation remains invariant under this group transformation, i.e., $\overline{u_j} = I_j(\overline{x_1}, \dots, \overline{x_m})$, and suppose that the matrix $[b_{i\alpha}]$ has rank $r < m$. Then r becomes the minimal number of "fundamental dimensions" needed to describe this system. Futhermore, one can derive $m - r$ "dimensionless" parameter which remain invariant with similitude-based scaling. In other words, fixing these dimensionless parameters allows one to scale this system without altering its desirable characteristics.

APPENDIX B

DERIVATION OF 2-DOF MASS-SPRING-DAMPER SYSTEM SCALING LAWS

This section provides a detailed procedure of how to derive the scaling laws of the quarter car system introduced in Chapter 3:

1) Identify the variables associated with the system:

$$\{M_s, M_{us}, K_s, B_s, K_t, B_t, F, x_1, x_2, t\} \tag{B.1}$$

2) Identify the dimensional formula of each variable above by using as many fundamental units as necessary, where

   - **A dimensional formula** is the relation that shows the fundamental units for a physical quantity raised to appropriate powers and enclosed in square brackets, e.g., Velocity = $[LT^{-1}]$. By Buckingham Pi's theorem, dimensional formulae are always in the form of the products of powers of the fundamental units

Dimensional formulae of the quarter system are given as follows:

$$\begin{aligned} &M_s, M_{us} = [M] \qquad K_s, K_t = [MT^{-2}] \quad B_s, B_t = [MT^{-1}] \\ &F = [MLT^{-2}] \qquad x_1, x_2 = [L] \qquad t = [T] \end{aligned} \tag{B.2}$$

3) By Buckingham's Pi theorem, the number of dimensionless Pi parameter is the number of variables (M = 10) subtracted the number of fundamental units needed (N = 3). This gives the number of pi parameters = M – N = 7.

4) Select a "core" group which consists of N = 3 variables, then form a set of product groups, assuming arbitrary exponents for each variable. By requiring each product group to be dimensionless, it is possible to solve for those

arbitrary exponents. In this case, we select x_1, M_s, K_s as the variables in the core group. This results in the following product groups:

$$\begin{aligned}
\pi_1 &= x_1^{\alpha_1} M_s^{\alpha_2} K_s^{\alpha_3} M_{us} \\
\pi_2 &= x_1^{\alpha_4} M_s^{\alpha_5} K_s^{\alpha_6} x_2 \\
\pi_3 &= x_1^{\alpha_7} M_s^{\alpha_8} K_s^{\alpha_9} K_t \\
\pi_4 &= x_1^{\alpha_{10}} M_s^{\alpha_{11}} K_s^{\alpha_{12}} B_s \\
\pi_5 &= x_1^{\alpha_{13}} M_s^{\alpha_{14}} K_s^{\alpha_{15}} B_t \\
\pi_6 &= x_1^{\alpha_{16}} M_s^{\alpha_{17}} K_s^{\alpha_{18}} F \\
\pi_7 &= x_1^{\alpha_{19}} M_s^{\alpha_{20}} K_s^{\alpha_{21}} t
\end{aligned} \tag{B.3}$$

For example, consider the first Pi group and substitute each variable's dimensional formula given in Equation B.2 into the product group:

$$M^0 L^0 T^0 = (L)^{\alpha_1} (M)^{\alpha_2} \left(\frac{M}{T^2}\right)^{\alpha_3} (M)^1 \tag{B.4}$$

Equating the exponents on both sides gives the following set of equations:

$$\begin{aligned}
0 &= \alpha_2 + \alpha_3 + 1 \\
0 &= \alpha_1 \\
0 &= -2\alpha_3
\end{aligned} \tag{B.5}$$

Solving the above equations simultaneously gives, α_1 = -1, α_2 = 0, and α_3 = 0. Therefore, the first Pi group becomes:

$$\pi_1 = \frac{M_{us}}{M_s} \tag{B.6}$$

Repeating the same procedure for the remaining dimensionless parameters gives:

$$\pi_2 = \frac{x_2}{x_1} \qquad \pi_3 = \frac{k_t}{k_s} \qquad \pi_4 = \frac{B_s}{M_s^{1/2} k_s^{1/2}}$$
$$\pi_5 = \frac{B_t}{M_s^{1/2} k_s^{1/2}} \qquad \pi_6 = \frac{F}{k_s x_1} \qquad \pi_4 = \frac{k_s^{1/2} t}{M_s^{1/2}} \tag{B.7}$$

5) Similitude requires that the Pi parameter value of the original and scaled designs have to be identical. Based on the definition of scale factor (λ_i) defined in Chapter 3, this requirement results in the following scaling laws:

$$\begin{aligned}
&\lambda_{M_s} = \lambda_{M_{us}} \\
&\lambda_{K_t} = \lambda_{K_s} \\
&\lambda_{M_s}^{1/2} \lambda_{K_s}^{1/2} = \lambda_{B_s} \\
&\lambda_{M_s}^{1/2} \lambda_{K_s}^{1/2} = \lambda_{B_t} \\
&\lambda_t \lambda_{K_s}^{1/2} = \lambda_{B_s} \\
&\lambda_{x_1} \lambda_{K_s} = \lambda_F \\
&\lambda_{x_1} = \lambda_{x_2}
\end{aligned} \tag{B.8}$$

It is worth noting that the set of Pi parameters in Equation B.7 is not unique since it depends on the selection of the core variables. On the other hand, the resulting set of scaling laws in Equation B.8 is unique regardless of which set of Pi parameters is used in the derivation.

APPENDIX C

AIR SUPPLY SYSTEM'S BLOWER DATA AND ORIGINAL DESIGN'S PARAMETERS

The following figures show the data corresponding to the blower which was selected to be used as the original baseline model in this dissertation. This represents a D1G133-DC13-52 centrifugal blower obtained from EBM industries [63].

		n [RPM]	P_1 [kW]	η_{EL} [%]	Lp_A [dBA]			n [RPM]	P_1 [kW]	η_{EL} [%]	Lp_A [dBA]
1	1	1700	145	–	65	1	6	1400	78	–	60
1	2	1930	133	38	62	1	6	1580	70	38	56
1	3	2290	122	41	59	1	7	1760	56	41	53
1	4	2700	99	32	61	1	8	2000	44	32	53
1	1	1580	118	–	64						
1	2	1790	107	38	61						
1	3	2100	95	41	57						
1	4	2410	73	32	58						

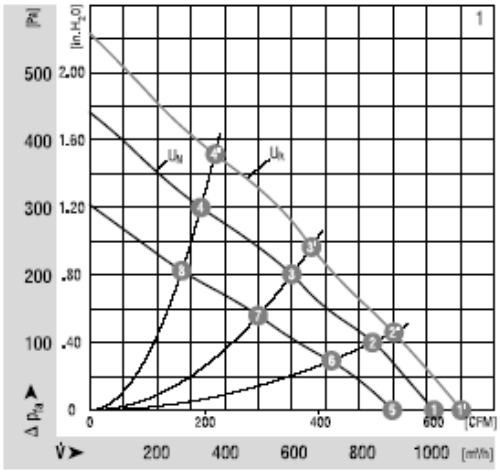

Figure C.1: Blower map and associated data

The values of the other parameters in the system corresponding to the original design which consumes the least amount of power in the blower to satisfy $\dot{m}_{steady}$ = 0.01 to 0.02 kg/s are given below. These values are obtained from [3, 46].

Parameter	Value
Supply Manifold Volume: V_{sm}	0.02 m^3
Return Manifold Volume: V_{rm}	0.005 m^3
First Nozzle Cross-sectional Area: $A_{t,1}$	0.03 m^2
Second Nozzle Cross-sectional Area: $A_{t,2}$	0.06 m^2
Multiple of Blower Size: D	1
Atmospheric Temperature: T_{atm}	298 K
Atmospheric Pressure: P_{atm}	101325 Pa
Return Manifold Temperature: T_{rm}	303 K
Original Blower Inertia: $I_{BW,original}$	0.05 $kg.m^2$

Table C.1: Air Supply System Original Design

The following plots show that the blower power consumption is monotonic with respect to the cross sectional areas of the first and second non-linear nozzles ($A_{t,1}$ and $At,2$).

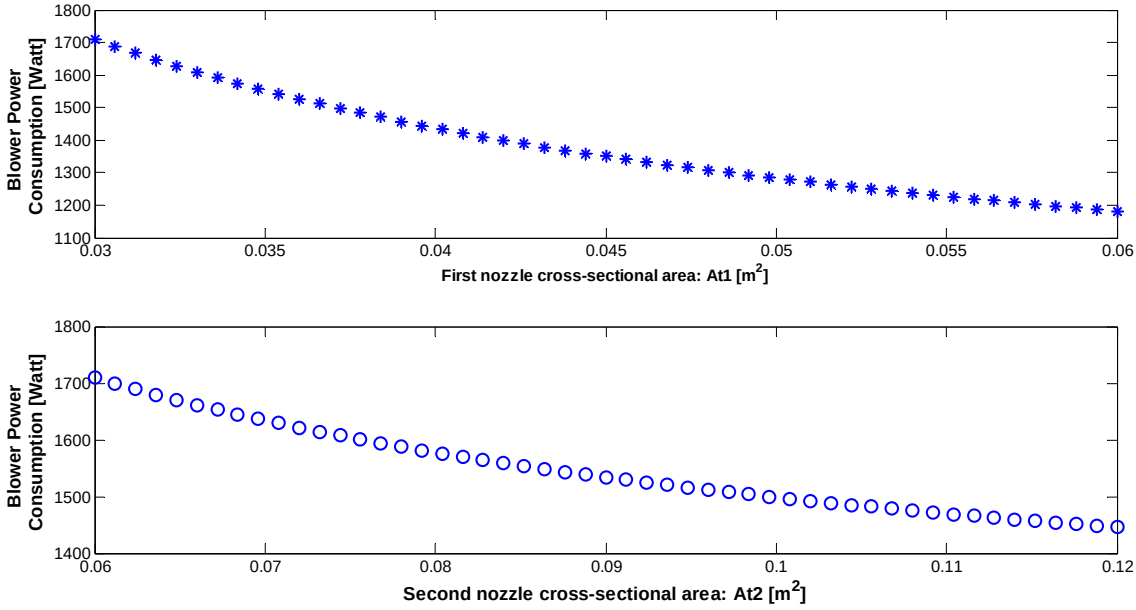

Figure C.2: Monotonicity in blower power consumption with respect to $A_{t,1}$ and $A_{t,2}$

APPENDIX D

DERIVATION OF QUARTER CAR'S NATURAL FREQUENCY AND DAMPING RATIO USING DIMENSIONLESS PARAMETERS AND THEIR CORRELATIONS WITH SIMILITUDE METRIC

The definitions of the sprung mass natural frequency ($\omega_{n\text{-}sprung}$) and damping ratio (ξ_s) of the quarter car system are given as:

$$\omega_{n-sprung} = \sqrt{\frac{K_s K_t}{M_s(K_s+K_t)}}$$
$$\xi_s = \frac{B_s}{\sqrt{4K_s M_s}} \tag{D.1}$$

Using the Pi parameters derived in Equation 3.3, the two expressions above can be simply arranged in terms of those Pi parameters as follows:

$$\omega_{n-sprung} = \frac{\pi_7}{t}\sqrt{\frac{\pi_3}{(\pi_3+1)}}$$
$$\xi_s = \frac{\pi_4}{\sqrt{4}} \tag{D.2}$$

It follows now that, if similitude is achieved (i.e., all of the Pi parameters retain their original values), then the damping ratio (ξ_s) has to remain invariant Further, since the time scale of the quarter system in scaling is assumed to be unchanged, the sprung mass natural frequency ($\omega_{n\text{-}sprung}$) remains invariant when similitude is achieved as well.

The following plots show the correlations between the quarter car problem's similitude metric (described by Equation 4.2) and the suspension damping ratio as well as first natural frequency. In this case, the most important parameter (i.e., K_s) is fixed at its original value and the scale variable (S) is fixed at one, then the rest of the variables by the same scaling factor (λ) with an increment of 0.05 ranging from 1 up to 2. These plots

attest to the validity of the similitude metric developed in this dissertation as a tool to quantify (or measure) the extent to which a design is "close" to satisfy similitude.

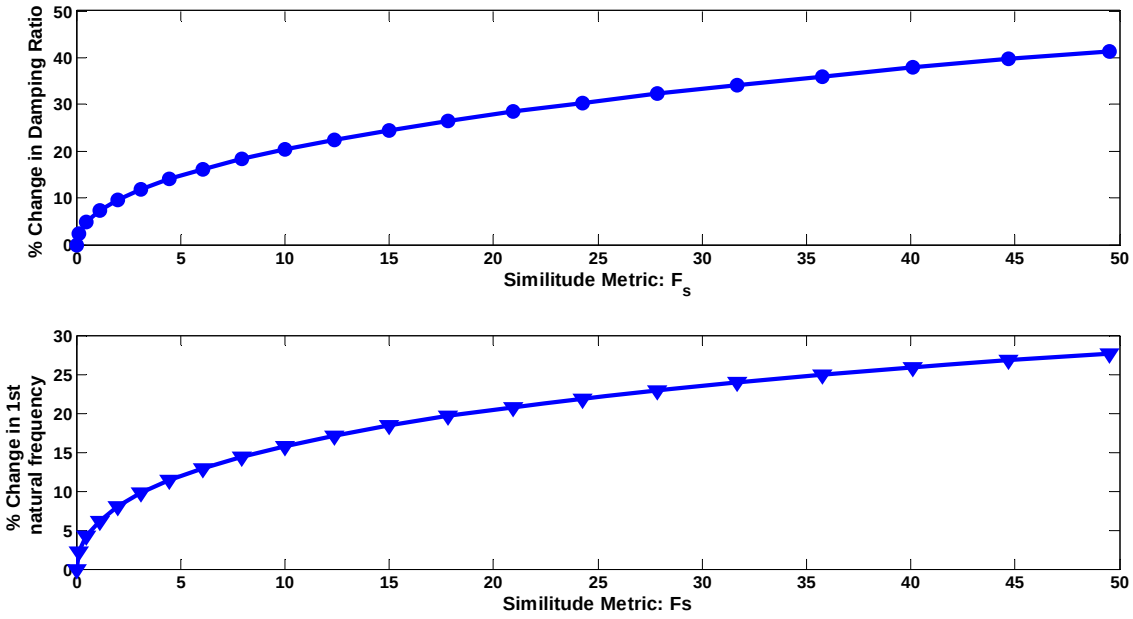

Figure D.1: Correlations between F_s vs. Damping Ratio and F_s vs. First Natural Frequency

APPENDIX E

MULTIBODY DYNAMIC HMMWV MODEL

The bond-graph multi-body dynamic HMMWV model is mainly comprised of the chassis, front suspension, rear suspension, tire, and steering sub-systems. The details of each of these sub-systems are explained below:

E.1 CHASSIS SUB-SYSTEM

The chassis sub-system as shown in Figure E.1 represents the body of the HMMWV vehicle which is modeled as a rigid body. The dynamics of this rigid body are described by Euler's equation and also rely on the use of coordinate transformations [10, 54]. The body has a total of ten attachment points connecting the chassis to the suspension and steering systems. The parameters describing properties of the chassis sub-system are given in Table E.1 below. Note that the distances of the attachment points shown in Table E.1 are calculated with respect to the CG of the body.

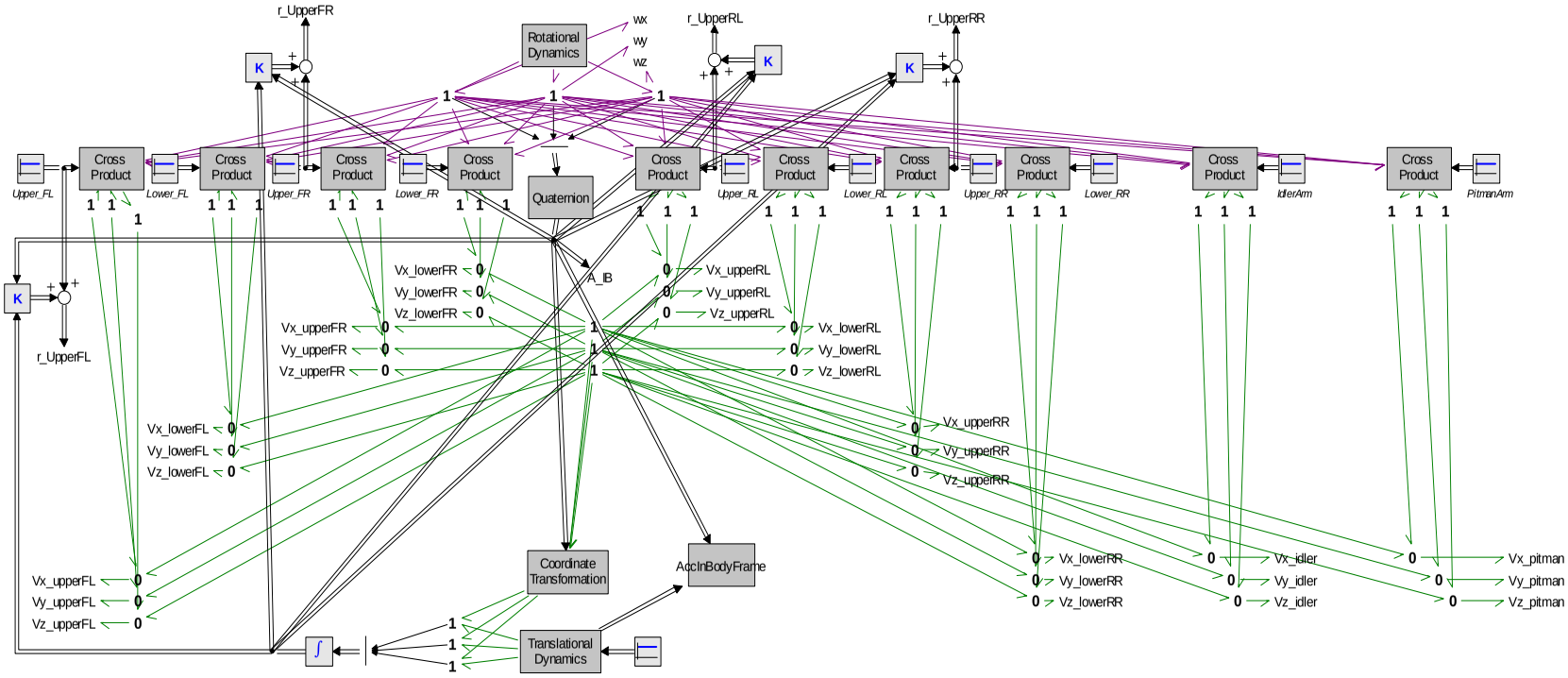

Figure E.2: Chassis sub-model

Parameters	Values	Units
Chassis\RotationalDynamics\H\Ixx	1695.6701	kg.m^2
Chassis\RotationalDynamics\H\Iyy	5950.4	kg.m^2
Chassis\RotationalDynamics\H\Izz	6357	kg.m^2
Chassis\TranslationalDynamics\Chassis_Mass	3840.3598	kg
Chassis\UpperArm_FR\X_AttachPoint	2.032	m
Chassis\UpperArm_FR\Y_AttachPoint	-0.4455	m
Chassis\UpperArm_FR\Z_AttachPoint	-0.69499	m
Chassis\UpperArm_RL\X_AttachPoint	-1.27	m
Chassis\UpperArm_RL\Y_AttachPoint	0.4455	m
Chassis\UpperArm_RL\Z_AttachPoint	-0.69499	m
Chassis\UpperArm_FL\X_AttachPoint	2.032	m
Chassis\UpperArm_FL\Y_AttachPoint	0.4455	m
Chassis\UpperArm_FL\Z_AttachPoint	-0.69499	m
Chassis\LowerArm_FL\X_AttachPoint	2.032	m
Chassis\LowerArm_FL\Y_AttachPoint	0.2275	m
Chassis\LowerArm_FL\Z_AttachPoint	-0.96499	m
Chassis\LowerArm_FR\X_AttachPoint	2.032	m
Chassis\LowerArm_FR\Y_AttachPoint	-0.2275	m
Chassis\LowerArm_FR\Z_AttachPoint	-0.96499	m
Chassis\LowerArm_RL\X_AttachPoint	-1.27	m
Chassis\LowerArm_RL\Y_AttachPoint	0.2275	m
Chassis\LowerArm_RL\Z_AttachPoint	-0.96499	m
Chassis\UpperArm_RR\X_AttachPoint	-1.27	m
Chassis\UpperArm_RR\Y_AttachPoint	-0.4455	m
Chassis\UpperArm_RR\Z_AttachPoint	-0.69499	m
Chassis\LowerArm_RR\X_AttachPoint	-1.27	m
Chassis\LowerArm_RR\Y_AttachPoint	-0.2275	m
Chassis\LowerArm_RR\Z_AttachPoint	-0.96499	m
Chassis\IdlerArm\X_AttachPoint	1.647	m
Chassis\IdlerArm\Y_AttachPoint	-0.28	m
Chassis\IdlerArm\Z_AttachPoint	-0.762	m
Chassis\PitmanArm\X_AttachPoint	1.647	m
Chassis\PitmanArm\Y_AttachPoint	0.25	m
Chassis\PitmanArm\Z_AttachPoint	-0.762	m

Table E.1: Chassis sub-system's parameters

E2. SUSPENSION SUB-SYSTEM

The suspension model is described by three rigid bodies representing the upper A-arm, lower A-arm and wheel hub. Each of these bodies is connected to one other body or the chassis through either a rotational joint or a spherical joint [10, 64]. These connections are illustrated in the figure showing the front suspension model below. The configuration of the front suspension only differs from the rear suspension in that both of the spherical joints (in Figure E.2) are replaced with rotational joints. The associated parameter values of are also given in Tables E.2 and E.3. Note the, due to symmetry of the left and right sides of the vehicle, only the parameters of the left sides of the front and rear suspensions are given in this appendix.

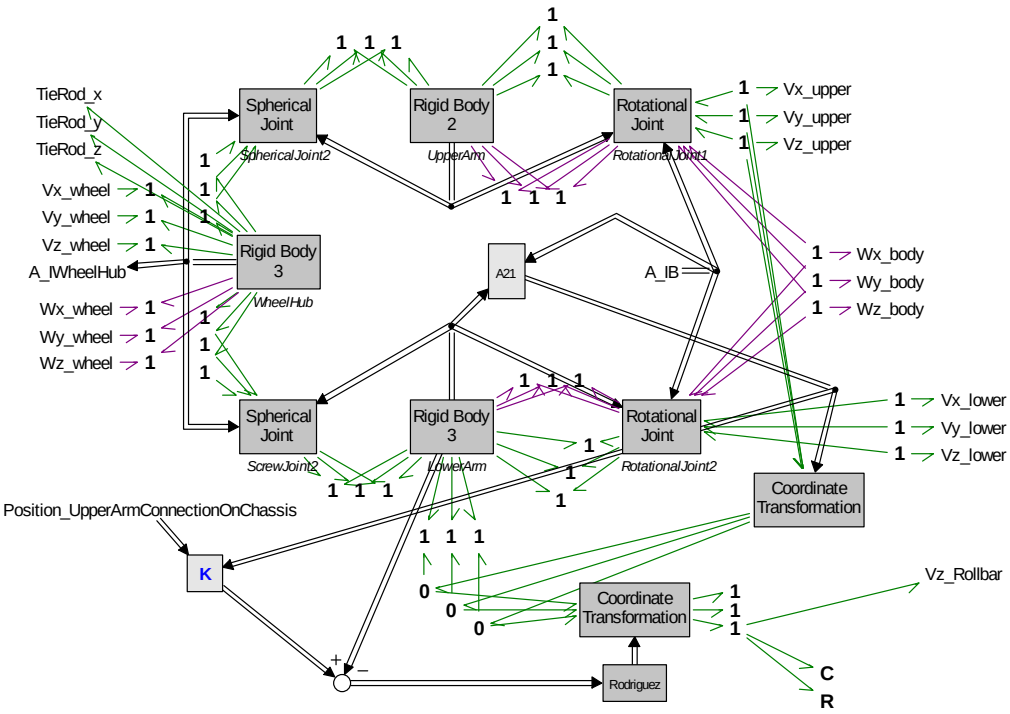

Figure E.2: Front suspension sub-model

Parameters	Values	Units
FrontLeft\UpperArm\RotationalDynamics\H\Ixx	0.0114	kg.m^2
FrontLeft\UpperArm\RotationalDynamics\H\Iyy	0.0104	kg.m^2
FrontLeft\UpperArm\RotationalDynamics\H\Izz	0.0205	kg.m^2
FrontLeft\UpperArm\TranslationalDynamics\Mass	4.704	kg
FrontLeft\UpperArm\ToChassis\X_AttachPoint	0	m
FrontLeft\UpperArm\ToChassis\Y_AttachPoint	-0.0777778	m
FrontLeft\UpperArm\ToChassis\Z_AttachPoint	0	m
FrontLeft\UpperArm\ToWheelHub\X_AttachPoint	0	m
FrontLeft\UpperArm\ToWheelHub\Y_AttachPoint	0.1222222	m
FrontLeft\UpperArm\ToWheelHub\Z_AttachPoint	-0.02	m
FrontLeft\LowerArm\RotationalDynamics\H\Ixx	0.1976	kg.m^2
FrontLeft\LowerArm\RotationalDynamics\H\Iyy	0.2158	kg.m^2
FrontLeft\LowerArm\RotationalDynamics\H\Izz	0.1106	kg.m^2
FrontLeft\LowerArm\TranslationalDynamics\Mass	34.351	kg
FrontLeft\LowerArm\ToWheelHub\X_AttachPoint	0	m
FrontLeft\LowerArm\ToWheelHub\Y_AttachPoint	0.2846305	m
FrontLeft\LowerArm\ToWheelHub\Z_AttachPoint	0.02	m
FrontLeft\LowerArm\ToStrut\X_AttachPoint	0	m
FrontLeft\LowerArm\ToStrut\Y_AttachPoint	0.0846305	m
FrontLeft\LowerArm\ToStrut\Z_AttachPoint	0	m
FrontLeft\LowerArm\ToChassis\X_AttachPoint	0	m
FrontLeft\LowerArm\ToChassis\Y_AttachPoint	-0.1703695	m
FrontLeft\LowerArm\ToChassis\Z_AttachPoint	0	m
FrontLeft\WheelHub\RotationalDynamics\H\Ixx	0.1976	kg.m^2
FrontLeft\WheelHub\RotationalDynamics\H\Iyy	0.2158	kg.m^2
FrontLeft\WheelHub\RotationalDynamics\H\Izz	0.1106	kg.m^2
FrontLeft\WheelHub\TranslationalDynamics\Mass	34.351	kg
FrontLeft\WheelHub\ToUpperArm\X_AttachPoint	0	m
FrontLeft\WheelHub\ToUpperArm\Y_AttachPoint	-0.0505	m
FrontLeft\WheelHub\ToUpperArm\Z_AttachPoint	0.115	m
FrontLeft\WheelHub\ToLowerArm\X_AttachPoint	0	m
FrontLeft\WheelHub\ToLowerArm\Y_AttachPoint	-0.0135	m
FrontLeft\WheelHub\ToLowerArm\Z_AttachPoint	-0.115	m
FrontLeft\WheelHub\ToWheel\X_AttachPoint	0	m
FrontLeft\WheelHub\ToWheel\Y_AttachPoint	0.0635	m
FrontLeft\WheelHub\ToWheel\Z_AttachPoint	0	m
FrontLeft\WheelHub\TieRod_position\X_AttachPoint	-0.1354	m
FrontLeft\WheelHub\TieRod_position\Y_AttachPoint	-0.0251	m

FrontLeft\WheelHub\TieRod_position\Z_AttachPoint	0	m
FrontLeft\SpringConstant	268726.8227	N/m
FrontLeft\SpringInitialLength	0.272523	m
FrontLeft\Damping	24142.3716	N.s/m

Table E.2: Front left suspension sub-system's parameters

Parameters	**Values**	**Units**
RearLeft\UpperArm\RotationalDynamics\H\Ixx	0.0114	kg.m^2
RearLeft\UpperArm\RotationalDynamics\H\Iyy	0.0104	kg.m^2
RearLeft\UpperArm\RotationalDynamics\H\Izz	0.0205	kg.m^2
RearLeft\UpperArm\TranslationalDynamics\mass	4.704	kg
RearLeft\UpperArm\ToChassis\X_AttachPoint	0	m
RearLeft\UpperArm\ToChassis\Y_AttachPoint	-0.0777778	m
RearLeft\UpperArm\ToChassis\Z_AttachPoint	0	m
RearLeft\UpperArm\ToWheelHub\X_AttachPoint	0	m
RearLeft\UpperArm\ToWheelHub\Y_AttachPoint	0.1222222	m
RearLeft\UpperArm\ToWheelHub\Z_AttachPoint	-0.02	m
RearLeft\LowerArm\RotationalDynamics\H\Ixx	0.1976	kg.m^2
RearLeft\LowerArm\RotationalDynamics\H\Iyy	0.2158	kg.m^2
RearLeft\LowerArm\RotationalDynamics\H\Izz	0.1106	kg.m^2
RearLeft\LowerArm\TranslationalDynamics\mass	34.351	kg
RearLeft\LowerArm\ToWheelHub\X_AttachPoint	0	m
RearLeft\LowerArm\ToWheelHub\Y_AttachPoint	0.2846305	m
RearLeft\LowerArm\ToWheelHub\Z_AttachPoint	0.02	m
RearLeft\LowerArm\ToStrut\X_AttachPoint	0	m
RearLeft\LowerArm\ToStrut\Y_AttachPoint	0.0846305	m
RearLeft\LowerArm\ToStrut\Z_AttachPoint	0	m
RearLeft\LowerArm\ToChassis\X_AttachPoint	0	m
RearLeft\LowerArm\ToChassis\Y_AttachPoint	-0.1703695	m
RearLeft\LowerArm\ToChassis\Z_AttachPoint	0	m
RearLeft\WheelHub\RotationalDynamics\H\Ixx	0.1976	kg.m^2
RearLeft\WheelHub\RotationalDynamics\H\Iyy	0.2158	kg.m^2
RearLeft\WheelHub\RotationalDynamics\H\Izz	0.1106	kg.m^2
RearLeft\WheelHub\TranslationalDynamics\mass	34.351	kg
RearLeft\WheelHub\ToUpperArm\X_AttachPoint	0	m
RearLeft\WheelHub\ToUpperArm\Y_AttachPoint	-0.0505	m
RearLeft\WheelHub\ToUpperArm\Z_AttachPoint	0.115	m
RearLeft\WheelHub\ToLowerArm\X_AttachPoint	0	m

RearLeft\WheelHub\ToLowerArm\Y_AttachPoint	-0.0135	m
RearLeft\WheelHub\ToLowerArm\Z_AttachPoint	-0.115	m
RearLeft\WheelHub\ToWheel\X_AttachPoint	0	m
RearLeft\WheelHub\ToWheel\Y_AttachPoint	0.0635	m
RearLeft\WheelHub\ToWheel\Z_AttachPoint	0	m
RearLeft\C2\SpringConstant	322470.9309	N/m
RearLeft\C2\SpringInitialLength	0.272523	m
RearLeft\R2\Damping	37648.4211	N.s/m

Table E.3: Rear left suspension sub-system's parameters

E.3 TIRE SUB-SYSTEM

The tire model is mainly composed of a rigid body representing the wheel and two slip models, one for the longitudinal slip and the other for the lateral slip. The governing equations in these slip models are obtained from the simulation software DADS [52] and shown in the Figures 4 and 5 below. The same configuration and parameters (given in Table E.4) are used for all the four tires.

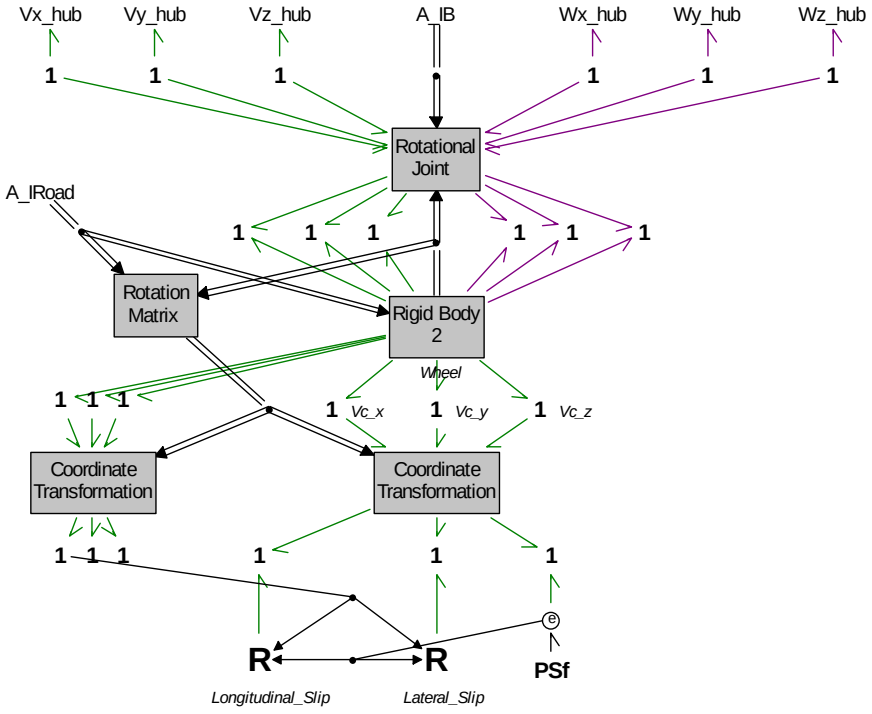

Figure E.4: Tire sub-model

Parameters	Values	Units
tireFL\Wheel\RotationalDynamics\H\Ixx	1	kg.m^2
tireFL\Wheel\RotationalDynamics\H\Iyy	1	kg.m^2
tireFL\Wheel\RotationalDynamics\H\Izz	1	kg.m^2
tireFL\Wheel\TranslationalDynamics\mass	30	kg
tireFL\Wheel\ToWheelHub\X_AttachPoint	0	m
tireFL\Wheel\ToWheelHub\Y_AttachPoint	-0.15	m
tireFL\Wheel\ToWheelHub\Z_AttachPoint	0	m
tireFL\Wheel\R_tire\TireDamping	200000	N.s/m
tireFL\Wheel\C_tire\TireStiffness	1000000	N/m
tireFL\Wheel\Rwheel\WheelRadius	0.461	m
tireFL\Wheel\ToGround\x	0	m
tireFL\Wheel\ToGround\y	0	m
tireFL\Longitudinal_Slip\mu	1.8	-
tireFL\Lateral_Slip\CorneringStiffness	100000	N/rad
tireFL\Lateral_Slip\mu	1.8	-

Table E.4: Front left tire sub-system's parameters

The following codes represent governing equations of the tire longitudinal and lateral slip models. These equations are written and implemented in 20-sim's SIDOPS language [65]:

```
variables
      real Fx,Vx_o,Vdiff,F_long;
      real Kappa,Slip,mu_f, signVx;
equations
// First, if Vx is small, it is kept at a small value to aviod singularity
signVx =       if (Vx ==0) then
                     1
               else
                     sign(Vx)
               end;
if (abs(Vx) < 0.0001) then
      Vx_o = signVx * 0.0001;
else
      Vx_o = Vx;
end;

// Calculate Slip (note p.f = Vx - W.R)
Vdiff = p.f;
Kappa = (-Vdiff/Vx_o); // that is Kappa = (W.R - Vx)/Vx
Slip = abs(Kappa);

// Calculate mu_f --> piecewise linear
mu_f = if Slip < 0.2 then
               (mu/0.2)*Slip
          else
               if Slip < 0.25 then
                     mu*Slip + 0.8*mu
               else
                     if Slip < 0.5 then
                           (-0.2*mu)*Slip + 1.1*mu
                     else
                           mu
                     end
               end
          end;
F_long = Fz*mu_f;

// Rectify the sign
if (Vdiff < 0) then
      Fx = F_long; // Traction
else
      Fx = -F_long; // Braking
end;
p.e = Fx;
```

Figure E.6: Longitudinal tire slip sub-model

```
variables
      real Fy,Vx_o,Vy;
      real aph_n, aph,slip,Fmax;
      real a1, a2, a3, Flat, Flat_check;

equations
// First, if Vx is small, it is kept at a small value to aviod singularity
if (abs(Vx) < 0.0001) then
      Vx_o =  0.0001;
else
      Vx_o = abs(Vx);
end;

// Calculate side slip angle
Vy = p.f;
aph = arctan(Vy/Vx_o);
//aph =         sign(Vy) * pi /2;
slip = abs(aph);
aph_n = 2.5*Fz/Ca;
Fmax =mu*Fz;
```

Figure E.7: Lateral tire slip sub-model

E.4 STEERING SUB-SYSTEM

The steering system is mainly comprised of the components as illustrated in Figure E.8 and its bond-graph model is shown in Figure E.9. The associated parameters implemented for this steering system model are given in Table E.5.

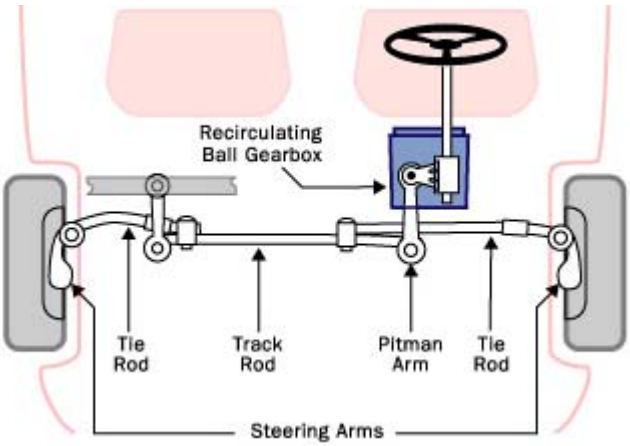

Figure E.8: HMMWV steering system components

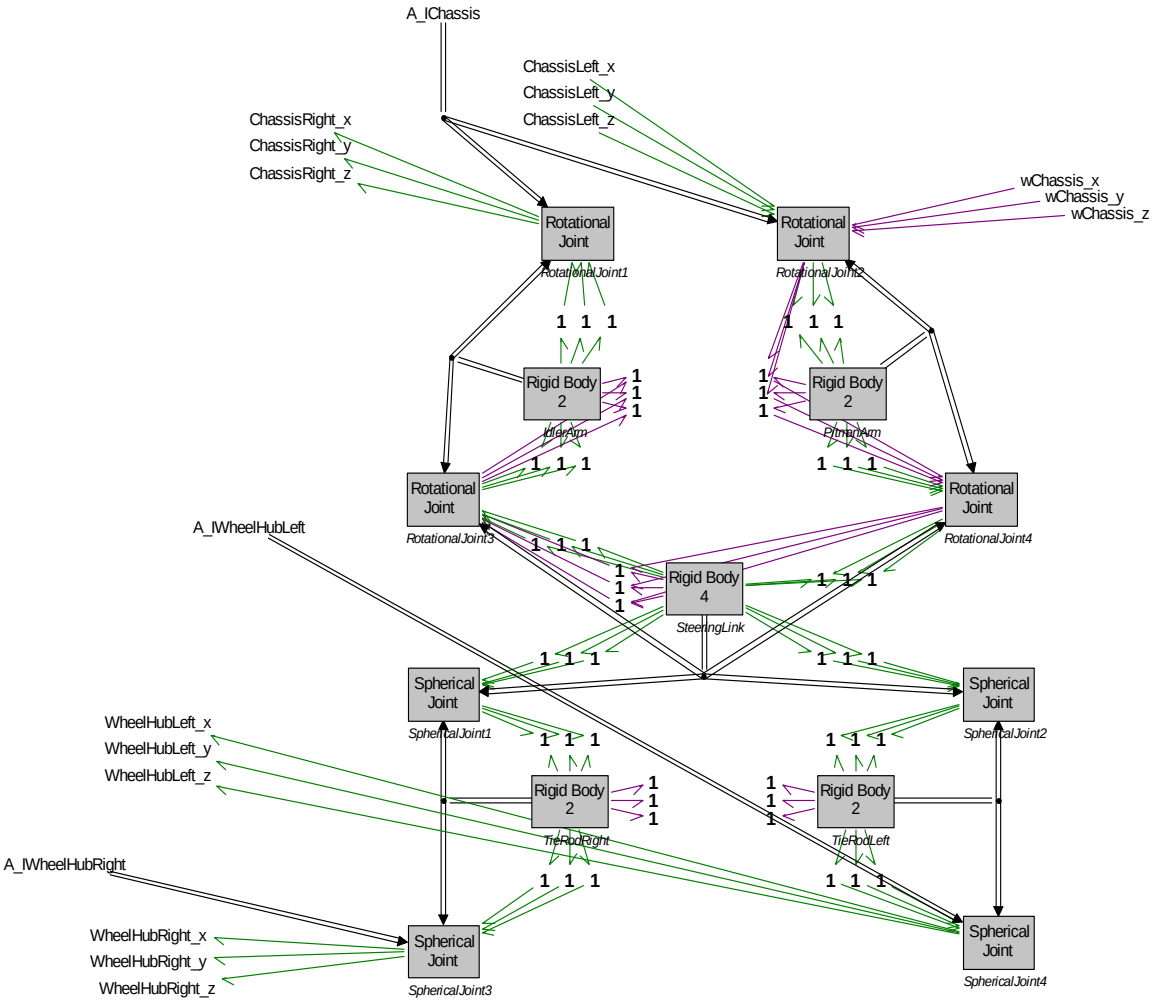

Figure E.9: Steering sub-model

Parameters	Values	Units
Steering\IdlerArm\RotationalDynamics\H\Ixx	0.000566	kg.m^2
Steering\IdlerArm\RotationalDynamics\H\Iyy	0.00188	kg.m^2
Steering\IdlerArm\RotationalDynamics\H\Izz	0.00215	kg.m^2
Steering\IdlerArm\TranslationalDynamics\Constant1\m	2	kg
Steering\IdlerArm\SteeringLink_Position\X_AttachPoint	0.051	m
Steering\IdlerArm\SteeringLink_Position\Y_AttachPoint	0	m
Steering\IdlerArm\SteeringLink_Position\Z_AttachPoint	0	m
Steering\IdlerArm\Chassis_Position\X_AttachPoint	-0.051	m
Steering\IdlerArm\Chassis_Position\Y_AttachPoint	0	m

Steering\IdlerArm\Chassis_Position\Z_AttachPoint	0	m
Steering\PitmanArm\RotationalDynamics\H\Ixx	0.000566	kg.m^2
Steering\PitmanArm\RotationalDynamics\H\Iyy	0.00188	kg.m^2
Steering\PitmanArm\RotationalDynamics\H\Izz	0.00215	kg.m^2
Steering\PitmanArm\TranslationalDynamics\Constant1\m	2	kg
Steering\PitmanArm\SteeringLink_Position\X_AttachPoint	0.051	m
Steering\PitmanArm\SteeringLink_Position\Y_AttachPoint	0	m
Steering\PitmanArm\SteeringLink_Position\Z_AttachPoint	0	m
Steering\PitmanArm\Chassis_Position\X_AttachPoint	-0.051	m
Steering\PitmanArm\Chassis_Position\Y_AttachPoint	0	m
Steering\PitmanArm\Chassis_Position\Z_AttachPoint	0	m
Steering\SteeringLink\RotationalDynamics\H\Ixx	0.204	kg.m^2
Steering\SteeringLink\RotationalDynamics\H\Iyy	0.000833	kg.m^2
Steering\SteeringLink\RotationalDynamics\H\Izz	0.205	kg.m^2
Steering\SteeringLink\TranslationalDynamics\Constant1\m	5	kg
Steering\SteeringLink\TieRodRight_Position\X_AttachPoint	0.0629	m
Steering\SteeringLink\TieRodRight_Position\Y_AttachPoint	-0.35	m
Steering\SteeringLink\TieRodRight_Position\Z_AttachPoint	0	m
Steering\SteeringLink\PitmanArm_Position\X_AttachPoint	-0.011	m
Steering\SteeringLink\PitmanArm_Position\Y_AttachPoint	0.25	m
Steering\SteeringLink\PitmanArm_Position\Z_AttachPoint	0	m
Steering\SteeringLink\IdlerArm_Position\X_AttachPoint	-0.011	m
Steering\SteeringLink\IdlerArm_Position\Y_AttachPoint	-0.28	m
Steering\SteeringLink\IdlerArm_Position\Z_AttachPoint	0	m
Steering\SteeringLink\TieRodLeft_Position\X_AttachPoint	0.0629	m
Steering\SteeringLink\TieRodLeft_Position\Y_AttachPoint	0.35	m
Steering\SteeringLink\TieRodLeft_Position\Z_AttachPoint	0	m
Steering\TieRodRight\RotationalDynamics\H\Ixx	0.0185	kg.m^2
Steering\TieRodRight\RotationalDynamics\H\Iyy	0.0008	kg.m^2
Steering\TieRodRight\RotationalDynamics\H\Izz	0.0185	kg.m^2
Steering\TieRodRight\TranslationalDynamics\Constant1\m	2	kg
Steering\TieRodRight\SteeringLink_Position\X_AttachPoint	0	m
Steering\TieRodRight\SteeringLink_Position\Y_AttachPoint	0.1605	m
Steering\TieRodRight\SteeringLink_Position\Z_AttachPoint	0	m
Steering\TieRodRight\WheelHub_Position\X_AttachPoint	0	m
Steering\TieRodRight\WheelHub_Position\Y_AttachPoint	-0.1605	m
Steering\TieRodRight\WheelHub_Position\Z_AttachPoint	0	m
Steering\TieRodLeft\RotationalDynamics\H\Ixx	0.0185	kg.m^2
Steering\TieRodLeft\RotationalDynamics\H\Iyy	0.0008	kg.m^2

Steering\TieRodLeft\RotationalDynamics\H\Izz	0.0185	kg.m^2
Steering\TieRodLeft\TranslationalDynamics\Constant1\m	2	kg
Steering\TieRodLeft\SteeringLink_Position\X_AttachPoint	0	m
Steering\TieRodLeft\SteeringLink_Position\Y_AttachPoint	-0.1605	m
Steering\TieRodLeft\SteeringLink_Position\Z_AttachPoint	0	m
Steering\TieRodLeft\WheelHub_Position\X_AttachPoint	0	m
Steering\TieRodLeft\WheelHub_Position\Y_AttachPoint	0.1605	m
Steering\TieRodLeft\WheelHub_Position\Z_AttachPoint	0	m

Table E.5: Steering sub-system's parameters

APPENDIX F

METHODS TO ASSOCIATE PARAMETERS WITH ELEMENT ACTIVITES

As discussed in the dissertation, the energetic elements of the fuel cell's air supply system as well as HMMWV system do not necessarily associate with only one parameter, or some parameters can affect more than one energetic element. This makes it less straightforward to assess the relative importance of these parameters' scaling laws. To address this issue, we use the following ad-hoc, but rather intuitive, approaches to find such relative importance.

F.1 FUEL CELL AIR SUPPLY SYSTEM

Parameter	Method to associate activity
First Nozzle: $A_{t,2}$	Sum of the activities of the four bonds of the first nozzle 4-port resistor
Second Nozzle: $A_{t,1}$	Sum of the activities of the four bonds of the second nozzle 4-port resistor
Blower: D	Sum of the activities of the four bonds of the blower 4-port transformer
Atmospheric Temperature: T_{atm}	Sum of the activities of the two T_{atm} effort sources
Power Input: P_e	Activity of the modulated blower torque effort source
Blower Inertia: I_{BW}	Activity of the blower inertia element
Atmospheric Pressure: P_{atm}	Sum of the activities of the two P_{atm} effort sources
Return Manifold Temperature: T_{rm}	Activity of the return manifold effort source
Supply Manifold Volume: V_{sm}	Sum of the activities of the two bonds of the supply manifold 2-port compliance element
Return Manifold Volume: V_{rm}	Activity of the return manifold volume compliance element

Table F.1: Methods to associate the fuel cell's air supply system parameter importance with element activities

F.2 HMMWV SYSTEM

The parameters that appear in Table D.2 below are only the ones accounted for in the similitude objective (F_s). Those not contributing to the objective are omitted:

Parameter	Method to associate activity
Chassis\TranslationalDynamics\Mass	Sum of activities of x,y and z component I-elements
TireRL\Lateral_Slip\Ca	Activity of the lateral slip R-element
TireRR\Lateral_Slip\Ca	Activity of the lateral slip R-element
TireFR\Lateral_Slip\Ca	Activity of the lateral slip R-element
Chassis\Lower_RL\SuspensionAttachmentPoint-Z	Sum of activities associated with corresponding MTF elements
Chassis\Lower_RR\SuspensionAttachmentPoint-Z	Sum of activities associated with corresponding MTF elements
TireFL\Lateral_Slip\Ca	Activity of the lateral slip R-element
RearRight\SpringRate	Activity of the suspension spring C-element
Chassis\Upper_RR\SuspensionAttachmentPoint-Z	Sum of activities associated with corresponding MTF elements
RearLeft\SpringRate	Activity of the suspension spring C-element
Chassis\Upper_RL\SuspensionAttachmentPoint-Z	Sum of activities associated with corresponding MTF elements
Chassis\Lower_FL\SuspensionAttachmentPoint-Z	Sum of activities associated with corresponding MTF elements
Chassis\Lower_FR\SuspensionAttachmentPoint-Z	Sum of activities associated with corresponding MTF elements
FrontRight\SpringRate	Activity of the suspension spring C-element
FrontLeft\SpringRate	Activity of the suspension spring C-element
Chassis\Upper_FR\SuspensionAttachmentPoint-Z	Sum of activities associated with corresponding MTF elements
Chassis\Upper_FL\SuspensionAttachmentPoint-Z	Sum of activities associated with corresponding MTF elements
Rollbar_Rear\Stiffness	Activity of the rollbar stiffness C-element
FrontRight\WheelHub\TranslationalDynamics\Mass	Sum of activities of x,y and z component I-elements
RearRight\WheelHub\TranslationalDynamics\Mass	Sum of activities of x,y and z component I-elements
TireFR\Wheel\TranslationalDynamics\Mass	Sum of activities of x,y and z component I-elements
FrontRight\LowerArm\TranslationalDynamics\Mass	Sum of activities of x,y and z component I-elements
FrontLeft\WheelHub\TranslationalDynamics\Mass	Sum of activities of x,y and z component I-elements
TireRR\Wheel\TranslationalDynamics\Mass	Sum of activities of x,y and z component I-elements
FrontLeft\LowerArm\TranslationalDynamics\Mass	Sum of activities of x,y and z component I-elements
RearLeft\WheelHub\TranslationalDynamics\Mass	Sum of activities of x,y and z component I-elements
TireFL\Wheel\TranslationalDynamics\Mass	Sum of activities of x,y and z component I-elements
RearRight\LowerArm\TranslationalDynamics\Mass	Sum of activities of x,y and z component I-elements
Rollbar_Front\Stiffness	Activity of the rollbar stiffness C-element
TireRL\Wheel\TranslationalDynamics\Mass	Sum of activities of x,y and z component I-elements
RearLeft\LowerArm\TranslationalDynamics\Mass	Sum of activities of x,y and z component I-elements
Chassis\RotationalDynamics\Izz	Activity of the corresponding I-element
TireRR\Wheel\TireVerticalStiffness	Acitivity of the Tire stiffness C-element
TireRL\Wheel\C_Tire\TireVerticalStiffness	Acitivity of the Tire stiffness C-element
TireRL\Wheel\RotationalDynamics\Iyy	Activity of the corresponding I-element
TireFR\Wheel\C_Tire\TireVerticalStiffness	Acitivity of the Tire stiffness C-element
TireRR\Wheel\RotationalDynamics\Iyy	Activity of the corresponding I-element
TireFL\Wheel\C_Tire\TireVerticalStiffness	Activity of the corresponding I-element
FrontRight\UpperArm\TranslationalDynamics\Mass	Sum of activities of x,y and z component I-elements
RearLeft\R2\SuspensionDamping	Activity of the suspension damping R-element
Steering\SteeringLink\TranslationalDynamics\Mass	Sum of activities of x,y and z component I-elements

RearRight\UpperArm\TranslationalDynamics\Mass	Sum of activities of x,y and z component I-elements
FrontLeft\UpperArm\TranslationalDynamics\Mass	Sum of activities of x,y and z component I-elements
RearRight\R2\SuspensionDamping	Activity of the suspension damping R-element
RearLeft\UpperArm\TranslationalDynamics\Mass	Sum of activities of x,y and z component I-elements
FrontRight\R2\SuspensionDamping	Activity of the suspension damping R-element
FrontLeft\R2\SuspensionDamping	Activity of the suspension damping R-element
Steering\TieRodRight\TranslationalDynamics\Mass	Sum of activities of x,y and z component I-elements
Steering\IdlerArm\TranslationalDynamics\Mass	Sum of activities of x,y and z component I-elements
Steering\TieRodLeft\TranslationalDynamics\Mass	Sum of activities of x,y and z component I-elements
Steering\PitmanArm\TranslationalDynamics\Mass	Sum of activities of x,y and z component I-elements
Chassis\RotationalDynamics\Ixx	Activity of the corresponding I-element
TireRL\Wheel\TireDamping	Activity of the Tire damping R-element
TireRR\Wheel\TireDamping	Activity of the Tire damping R-element
TireFR\Wheel\TireDamping	Activity of the Tire damping R-element
TireFL\Wheel\TireDamping	Activity of the Tire damping R-element
TireFL\Wheel\RotationalDynamics\Iyy	Activity of the corresponding I-element
TireFR\Wheel\RotationalDynamics\Iyy	Activity of the corresponding I-element
TireFL\Wheel\RotationalDynamics\Ixx	Activity of the corresponding I-element
TireFL\Wheel\RotationalDynamics\Izz	Activity of the corresponding I-element
TireFR\Wheel\RotationalDynamics\Ixx	Activity of the corresponding I-element
TireFR\Wheel\RotationalDynamics\Izz	Activity of the corresponding I-element
TireRL\Wheel\RotationalDynamics\Izz	Activity of the corresponding I-element
TireRL\Wheel\RotationalDynamics\Ixx	Activity of the corresponding I-element
TireRR\Wheel\RotationalDynamics\Ixx	Activity of the corresponding I-element
TireRR\Wheel\RotationalDynamics\Izz	Activity of the corresponding I-element
Chassis\RotationalDynamics\Iyy	Activity of the corresponding I-element
FrontLeft\WheelHub\RotationalDynamics\Ixx	Activity of the corresponding I-element
FrontLeft\LowerArm\RotationalDynamics\Izz	Activity of the corresponding I-element
FrontRight\LowerArm\RotationalDynamics\Izz	Activity of the corresponding I-element
FrontRight\WheelHub\RotationalDynamics\Izz	Activity of the corresponding I-element
RearLeft\LowerArm\RotationalDynamics\Izz	Activity of the corresponding I-element
RearLeft\WheelHub\RotationalDynamics\Izz	Activity of the corresponding I-element
RearRight\LowerArm\RotationalDynamics\Izz	Activity of the corresponding I-element
RearRight\WheelHub\RotationalDynamics\Izz	Activity of the corresponding I-element
FrontLeft\WheelHub\RotationalDynamics\Izz	Activity of the corresponding I-element
FrontRight\WheelHub\RotationalDynamics\Ixx	Activity of the corresponding I-element
RearLeft\WheelHub\RotationalDynamics\Ixx	Activity of the corresponding I-element
RearRight\WheelHub\RotationalDynamics\Ixx	Activity of the corresponding I-element
FrontRight\LowerArm\RotationalDynamics\Ixx	Activity of the corresponding I-element
FrontLeft\LowerArm\RotationalDynamics\Ixx	Activity of the corresponding I-element
FrontLeft\UpperArm\RotationalDynamics\Ixx	Activity of the corresponding I-element
FrontRight\UpperArm\RotationalDynamics\Ixx	Activity of the corresponding I-element
RearLeft\LowerArm\RotationalDynamics\Ixx	Activity of the corresponding I-element
RearRight\LowerArm\RotationalDynamics\Ixx	Activity of the corresponding I-element
RearLeft\UpperArm\RotationalDynamics\Ixx	Activity of the corresponding I-element
RearRight\UpperArm\RotationalDynamics\Ixx	Activity of the corresponding I-element
FrontLeft\UpperArm\RotationalDynamics\Izz	Activity of the corresponding I-element
FrontRight\UpperArm\RotationalDynamics\Izz	Activity of the corresponding I-element

RearLeft\UpperArm\RotationalDynamics\Izz	Activity of the corresponding I-element
RearRight\UpperArm\RotationalDynamics\Izz	Activity of the corresponding I-element
FrontLeft\WheelHub\RotationalDynamics\Iyy	Activity of the corresponding I-element
FrontLeft\UpperArm\RotationalDynamics\Iyy	Activity of the corresponding I-element
FrontLeft\LowerArm\RotationalDynamics\Iyy	Activity of the corresponding I-element
FrontRight\UpperArm\RotationalDynamics\Iyy	Activity of the corresponding I-element
FrontRight\LowerArm\RotationalDynamics\Iyy	Activity of the corresponding I-element
FrontRight\WheelHub\RotationalDynamics\Iyy	Activity of the corresponding I-element
RearLeft\UpperArm\RotationalDynamics\Iyy	Activity of the corresponding I-element
RearLeft\LowerArm\RotationalDynamics\Iyy	Activity of the corresponding I-element
RearLeft\WheelHub\RotationalDynamics\Iyy	Activity of the corresponding I-element
RearRight\UpperArm\RotationalDynamics\Iyy	Activity of the corresponding I-element
RearRight\LowerArm\RotationalDynamics\Iyy	Activity of the corresponding I-element
RearRight\WheelHub\RotationalDynamics\Iyy	Activity of the corresponding I-element

Table F.2: Methods to associate HMMWV parameter importance with element activities

BIBLIOGRAPHY

BIBLIOGRAPHY

1. Otto, K.N. and K.L. Wood, *Product Evolution: A Reverse Engineering and Redesign Methodology.* Research in Engineering Design, 1998. **10**(4): p. 226-243.

2. Fathy, H.K., R. Ahlawat, and J.L. Stein. *Proper powertrain modeling for engine-in-the-loop simulation*. in *2005 ASME International Mechanical Engineering Congress and Exposition, IMECE 2005, Nov 5-11 2005*. 2005. Orlando, FL, United States: American Society of Mechanical Engineers, New York, NY 10016-5990, United States.

3. Pukrushpan, J.T., A.G. Stefanopoulou, and P. Huei. *Modeling and control for PEM fuel cell stack system*. 2002. Anchorage, AK, USA: American Automatic Control Council.

4. Chen, L., A. Macwan, and S. Li, *Model-based rapid redesign using decomposition patterns.* Journal of Mechanical Design, Transactions of the ASME, 2007. **129**(3): p. 283-294.

5. Cho, Y.M. and R. Rajamani, *Identification and experimental validation of a scalable elevator vertical dynamic model.* Control Engineering Practice, 2001. **9**(2): p. 181-7.

6. Wei, X. and G. Rizzoni. *A scalable approach for energy converter modeling and supervisory control design*. in *2001 ASME International Mechanical Engineering Congress and Exposition, Nov 11-16 2001*. 2002. New York, NY, United States: American Society of Mechanical Engineers, New York, NY 10016-5990, United States.

7. Szirtes, T., *Applied dimensional analysis and modeling*. 1998, New York :: McGraw-Hill.

8. Yang-Tse, C. and C. Che-Min, *Scaling, dimensional analysis, and indentation measurements.* Materials Science & Engineering R: Reports, 2004. **R44**(4-5): p. 91-149.

9. Murphy, G., *Similitude in Engineering*. 1950: The Ronald Press Company.

10. Karnopp, D.C., Margolis, D.L., and Rosenberg, R.C., *System Dynamics: A Unified Appraoach*. Third edition ed. 1990: John Wiley & Sons, Inc., New York.

11. Macagno, E.O., *Historico-critical review of dimensional analysis.* Journal of the Franklin Institute, 1971. **292**(6): p. 391-402.

12. Bridgman, P.W., *Dimensional Analysis*. second ed. 1931: Yale University Press.

13. Schuring, D.J., *Scale Models in Engineering: Fundamentals and Applications*. 1977: Pergamon Press.

14. Vassalos, D., *Physical modelling and similitude of marine structures.* Ocean Engineering (Pergamon), 1999. **26**(2): p. 111-123.

15. Drazetic, P., et al., *Applying non-direct similitude technique to the dynamic bending collapse of rectangular section tubes.* International Journal of Impact Engineering, 1994. **15**(6): p. 797-814.

16. Oshiro, R.E. and M. Alves, *Scaling impacted structures.* Archive of Applied Mechanics, 2004. **74**(1-2): p. 130-45.

17. Soedel, W., *Similitude approximations for vibrating thin shells.* Journal of the Acoustical Society of America, 1971. **49**(5): p. 1535-41.

18. Cuddy, M.R. and K.B. Wipke, *Analysis of the fuel economy benefit of drivetrain hybridization.* Proceedings of the 1997 International Congress and Exposition, Feb 24-27 1997, SAE Special Publications, 1997. **1243**: p. 101-111.

19. Delagrammatikas, G.J. and D.N. Assanis, *Development of a neural network model of an advanced, turbocharged diesel engine for use in vehicle-level optimization studies.* Proceedings of the Institution of Mechanical Engineers, Part D (Journal of Automobile Engineering), 2004. **218**(D5): p. 521-33.

20. Delagrammatikas, G.J., *A Design Optimization Methodology for Advanced and Hybrid, Diesel-based, Automotive Powertrains*, in *Mechanical Engineering*. 2001, The University of Michigan.

21. Rizzoni, G., L. Guzzella, and B.M. Baumann, *Unified modeling of hybrid electric vehicle drivetrains.* IEEE/ASME Transactions on Mechatronics. **4**(3): p. 246-57.

22. Guzzella, L. and C.H. Onder, *Introduction to Modeling and Control of Internal Combustion Engine Systems*. 2004: Springer-Verlag.

23. Boettner, D.D., et al. *Component power sizing and limits of operation for Proton Exchange Membrane (PEM) fuel cell/battery hybrid automotive applications*. in *2001 ASME International Mechanical Engineering Congress and Exposition, Nov 11-16 2001*. 2001. New York, NY, United States: American Society of Mechanical Engineers.

24. Jeongwoo, H., M. Kokkolaras, and P. Papalambros. *Optimal design of hybrid fuel cell vehicles*. 2006. Irvine, CA, United States: American Society of Mechanical Engineers, New York, NY 10016-5990, United States.

25. Ohl, G.L., J.L. Stein, and G.E. Smith, *A dynamic model for the design of methanol to hydrogen steam reformers for transportation applications.* Journal of Energy Resources Technology, Transactions of the ASME, 2004. **126**(2): p. 149-158.

26. Moran, M.J., *A generalization of dimensional analysis.* Journal of the Franklin Institute, 1971. **292**(6): p. 423-432.

27. Tsung, Y.N. and A.G. Hansen, *Similarity analysis of differential equations by Lie group.* Journal of the Franklin Institute, 1971. **292**(6): p. 471-89.

28. Wu, J.-J., M.P. Cartmell, and A.R. Whittaker, *Prediction of the vibration characteristics of a full-size structure from those of a scale model.* Computers and Structures, 2002. **80**(18-19): p. 1461-1472.

29. Wu, J.-J., *The complete-similitude scale models for predicting the vibration characteristics of the elastically restrained flat plates subjected to dynamic loads.* Journal of Sound and Vibration, 2003. **268**(5): p. 1041-53.

30. Goldfarb, M., *Similarity and invariance in scaled bilateral telemanipulation.* Journal of Dynamic Systems, Measurement and Control, Transactions of the ASME, 1999. **121**(1): p. 79-87.

31. Poliey, M. and A.G. Alleyne. *Dimensionless analysis of tire characteristics for vehicle dynamics studies*. in *Proceedings of the 2004 American Control Conference (AAC), Jun 30-Jul 2 2004*. 2004. Boston, MA, United States: Institute of Electrical and Electronics Engineers Inc., Piscataway, NJ 08855-1331, United States.

32. Brennan, S. and A. Alleyne, *Using a scale testbed: Controller design and evaluation.* IEEE Control Systems Magazine, 2001. **21**(3): p. 15-26.

33. Brennan, S., *On Size and Control: The Use of Dimensional Analysis in Controller Design*, in *Mechanical Engineering*. 2002, University of Illinois at Urbana-Champaign.

34. Ghanekar, M., D.W.L. Wang, and G.R. Heppler. *Controller scaling laws for flexible link manipulators characterized by nondimensional Pi groups*. in *Proceedings of 1995 American Control Conference - ACC'95, 21-23 June 1995*. 1995. Seattle, WA, USA: American Autom Control Council.

35. Ghanekar, M., D.W.L. Wang, and G.R. Heppler, *Scaling laws for linear controllers of flexible link manipulators characterized by nondimensional groups.* IEEE Transactions on Robotics and Automation, 1997. **13**(1): p. 117-27.

36. Ghanekar, M., D.W.L. Wang, and G.R. Heppler. *Scaling laws for nonlinear controllers of dynamically equivalent rigid-link manipulators*. in *IEEE International Conference on Robotics and Automation, 16-20 May 1998*. 1998. Leuven, Belgium: IEEE.

37. Brennan, S. and A. Alleyne, *Robust scalable vehicle control via non-dimensional vehicle dynamics.* Vehicle System Dynamics, 2001. **36**(4-5): p. 255-77.

38. Ji-Huan, H. and H. Zhende, *A novel model for allometric scaling laws for different organs.* Chaos, Solitons and Fractals, 2006. **27**(4): p. 1108-14.

39. Kokshenev, V.B., *Observation of mammalian similarity through allometric scaling laws.* Physica A, 2003. **322**: p. 491-505.

40. McAlarney, M.E., *Use of the boundary element method for biological morphometrics.* Journal of Biomechanics, 1995. **28**(5): p. 609-16.

41. West, G.B. *The origin of universal scaling laws in biology*. 1999. Paris, France: Elsevier.

42. Rezaeepazhand, J. and G.J. Simitses. *Design of scaled down models for predicting shell vibration response*. in *Proceedings of the 36th AIAA/ASME/ASCE/AHS/ASC Structures, Structural Dynamics, and Materials Conference and AIAA/ASME Adaptive Structures Forum. Part 3 (of 5), Apr 10-13 1995*. 1995. New Orleans, LA, USA: AIAA, New York, NY, USA.

43. Louca, L.S., *An Energy-based Model Reduction Methodology for Automated Modeling*, in *Department of Mechanical Engineering*. 1998, University of Michigan.

44. Moran, M.J., *A Generalization of Dimensional Analysis.* Journal of the Franklin Institute, 1971. **292 (6)**: p. 423-432.

45. Rideout, D.G., *System Partitioning and Physical-domain Proper Modeling through Assesment of Power-conserving Model Structure*, in *Department of Mechanical Engineering*. 2004, University of Michigan.

46. Gelfi, S., et al. *Dynamics of low-pressure and high-pressure fuel cell air supply systems*. in *Proceedings of 2003 American Control Conference, 4-6 June 2003*. 2003. Denver, CO, USA: IEEE.

47. Dixon, S.L., *Fluid mechanics and thermodynamics of turbomachinery*. 1998, Boston :: Butterworth-Heinemann.

48. Wright, T., *Fluid Machinery: Performance, Analysis, and Design*. 1st ed. 1983: CRC Press LLC.

49. Papalambros, P.Y. and D.J. Wilde, *Principles of Optimal Design: Modeling and Computation*. 2nd ed. 2000: Cambridge University Press.

50. Gillespie, T.D., *Fundamentals of Vehicle Dynamics*. 1992: Society of Automotive Engineers, Inc.

51. Wong, J.Y., *Theory of Ground Vehicles*. Third ed. 2001: John Wiley & Sons, Inc.

52. *DADS: Dynamic Analysis and Design System---Reference Manual, Revision 9.0*.

53. Aardema, J., *Failure Analysis of the Lower Rear Ball Joint on the HMMWV*. 1998, U.S Army Tank-Automotive Command.

54. Pacejka, H.B., *MODELLING COMPLEX VEHICLE SYSTEMS USING BOND GRAPHS.* Journal of the Franklin Institute, 1985. **319**(1-2): p. 67-81.

55. Tiller, M., *Introduction to Physical Modeling with Modelica*. 2001: Kluwer Academic Publishers.

56. Mudaliar, N., D. LeBlanc, and P. Huei. *Linear estimator for road departure warning systems*. 2004. Boston, MA, USA: IEEE.

57. J.L. Meriam, L.G.K., *Dynamics*. Third ed. Engineering Mechanics. Vol. 2. 1993: John Wiley & Sons, Inc. .

58. Takano, S., et al. *Analysis of large vehicle dynamics for improving roll stability*. 2004. Kanagawa, Japan: Swets & Zeitlinger.

59. Sawaragi, M., H. Nakayama, and T. Tanino, *Theory of Multiobjective Optimization*. 1985: Academic Press, Inc. .

60. Ersal, T., H.K. Fathy, and J.L. Stein. *Realization-preserving Structure and Order Reduction of Nonlienar Energetic System Models Using Energy Trajectory Correlations*. in *Proceedings of 2007 IMECE*. 2007. Seattle, WA, USA.

61. Saltelli, A., K. Chan, and M.E. Scott, *Sensitivity Analysis*. 2000: John Wiley & Sons, Ltd.

62. Wu, J. and M. Hamada, *Experiments: Planning, Analysis, and Parameter Design Optimization*. 2000: John Wiley & Sons, Inc. .

63. http://www.ebmpapst.us/.

64. Zeid, A. and C. Chih-Hung, *Bond graph modeling of multibody systems: a library of three-dimensional joints.* Journal of the Franklin Institute, 1992. **329**(4): p. 605-36.

65. http://www.20sim.com/.